The Decays $\bar{B} \to \bar{K}^{(*)}\ell^+\ell^-$ at Low Recoil and their Constraints on New Physics

Dissertation

zur Erlangung des akademischen Grades

Dr. rer. nat.
im Fach Physik

eingereicht an der
Fakultät Physik
Technische Universität Dortmund

vorgelegt von
Danny van Dyk
aus Witten

Dortmund
Juli 2012

1. Gutachter: Prof. Dr. G. Hiller
2. Gutachter: Prof. Dr. H. Päs
Datum der mündlichen Prüfung: 28. Juni 2012
Vorsitzender des Promotionsausschusses: Prof. Dr. T. Weis

All work presented in this document is the author's own work, unless stated otherwise. This includes results which have been previously published (or will be published) in the following articles:

- Bobeth C., Hiller G. and van Dyk D. *The Benefits of $\bar{B} \to \bar{K}^* \ell^+ \ell^-$ Decays at Low Recoil*. JHEP **1007**, (2010), 098.
- Bobeth C., Hiller G. and van Dyk D. *More Benefits of Semileptonic Rare B Decays at Low Recoil: CP Violation*. JHEP **1107**, (2011), 067.
- Bobeth C., Hiller G., van Dyk D. and Wacker C. *The Decay $\bar{B} \to \bar{K} \ell^+ \ell^-$ at Low Hadronic Recoil and Model-Independent $\Delta B = 1$ Constraints*. JHEP **1201**, (2012), 107.
- Bobeth C., Hiller G. and van Dyk D. *General Analysis and Optimal Observables in $\bar{B} \to \bar{K}^* \ell^+ \ell^-$ Decays*. To appear.

Dedicated to the memory of my beloved grandfathers
Hans van Dyk and Günter Ortmann.

Abstract

In this thesis we test the validity of the Standard Model of particle physics by studying the exclusive rare decays $\bar{B} \to \bar{K}^{(*)}\ell^+\ell^-$. We calculate the angular distribution of the decay $\bar{B} \to \bar{K}^*\ell^+\ell^-$ in the most general basis of effective operators. We obtain results for the angular distribution in the kinematic region of low hadronic recoil. Based on our results for the angular distribution, we propose observables which exhibit no or only very weak dependence on hadronic matrix elements. Beyond CP-averaged observables, we also investigate direct and mixing induced CP asymmetries at low hadronic recoil. We conclude our investigation of exclusive decays by studying the decay $\bar{B} \to \bar{K}\ell^+\ell^-$, where we find a relation between the CP asymmetry of the rates of $\bar{B} \to \bar{K}^{(*)}\ell^+\ell^-$. Standard model results for a majority of our analytic results are given. Beyond that, we perform a model-independent analysis based on available experimental data and obtain constraints on the Wilson coefficients $\mathcal{C}_9$ and $\mathcal{C}_{10}$, as well as lower bounds on the zero-crossing in the $\bar{B} \to \bar{K}^*\ell^+\ell^-$ forward-backward asymmetry. Based on recent LHC data we find two disjoint solutions for the Wilson coefficients. One of the solutions is in good agreement with the Standard Model, but sizable deviations are still allowed.

Zusammenfassung

In der vorliegenden Dissertation überprüfen wie die Gültigkeit des Standardmodells der Teilchentheorie an Hand der exklusiven seltenen Zerfälle $\bar{B} \to \bar{K}^{(*)}\ell^+\ell^-$. Dazu betrachten wie die Winkelverteilung der Zerfallsrate des Zerfalls $\bar{B} \to \bar{K}^*\ell^+\ell^-$ unter Berücksichtigung der vollen Basis effektiver Operatoren. Weiterhin berechnen wir die Winkelverteilung für die kinematische Region mit großem hadronischen Rückstoß. Auf Basis der vorangegangenen Ergebnisse zur Winkelverteilung konstruieren wir neuen Observablen, welche nicht bzw. nur schwach von den hadronischen Matrixelementen abhängen. Zum Abschluss unserer Analyse exklusiver seltener Zerfälle studieren wir den Zerfalls $\bar{B} \to \bar{K}\ell^+\ell^-$, wobei wir Zusammenhänge zwischen den CP-Asymmetrien der Raten beider Zerfälle $\bar{B} \to \bar{K}^{(*)}\ell^+\ell^-$ aufzeigen. Zusätzlich präsentieren wir unsere numerischen Ergebnisse im Standardmodell für einen Teil der zuvor diskutierten Observablen. Über die analytische Arbeit hinaus untersuchen wir modellunabhängig die verfügbaren Experimentaldaten, um damit die Parameterbereiche der Wilsonkoeffizienten $\mathcal{C}_9$ und $\mathcal{C}_{10}$ einzuschränken. Auf Basis dieser Untersuchung berechnen wir eine untere Grenze für die Vorwärts-Rückwärts-Asymmetrie der Zerfallsrate von $\bar{B} \to \bar{K}^*\ell^+\ell^-$. Unter Berücksichtigung aktueller LHCb-Daten ergeben sich zwei disjunkte Lösungen für die Wilsonkoeffizienten. Eine der beiden Lösungen stimmt mit den Standardmodellervorhersagen gut überein, allerdings sind große Abweichungen immer noch erlaubt.

Contents

1. Introduction **1**

2. Theory of $b \to s\ell^+\ell^-$ Transitions **3**
2.1. Standard Model FCNCs . . . 3
2.2. Effective Field Theory . . . 8
2.3. From Partons to Hadrons . . . 12
2.4. Long-Distance Effects . . . 12

3. Phenomenology of $\bar{B} \to \bar{K}^{(*)}\ell^+\ell^-$ at Low Hadronic Recoil **15**
3.1. Kinematics and Notations . . . 15
3.2. Operator Product Expansion . . . 16
3.3. Form Factors and the Improved Isgur-Wise Relations . . . 18
3.4. The Decay $\bar{B} \to \bar{K}^*\ell^+\ell^-$ . . . 22
3.4.1. Angular Distribution . . . 22
3.4.2. Observables in the SM basis . . . 25
3.4.3. Low Recoil Observables in the SM Basis . . . 27
3.4.4. Including Chirality-Flipped Operators . . . 34
3.4.5. Including Scalar and Pseudo-Scalar Operators . . . 35
3.4.6. Including Tensor Operators . . . 36
3.4.7. Performance of Low Recoil Observables . . . 37
3.5. The Decay $\bar{B} \to \bar{K}\ell^+\ell^-$ . . . 41
3.5.1. Angular Distribution . . . 41
3.5.2. Observables . . . 42

4. Standard Model Results **45**

5. Model Independent Analysis **55**

6. Conclusion **61**

A. $\bar{B} \to \bar{K}^*(\to \bar{K}\pi)\,\ell^+\ell^-$ Matrix Element **63**

B. $\bar{B} \to \bar{K}^*$ Form Factors **65**

C. $\bar{B} \to \bar{K}$ Form Factors **69**

D. Introduction to EOS **73**
D.1. Use Cases . . . 73
D.2. Concepts and Implementation . . . 74
D.3. Development . . . 76

1. Introduction

Since the days of Rutherford the investigation of the fundamental interactions between elementary particles has been a driving force for Physics and physicists all over the world. We have come to an understanding that nature can be described by a set of four fundamental forces: gravity, electromagnetism, the weak nuclear force and the strong nuclear force. The latter three can be modeled on microscopic scales, or equivalently at high energies, by quantum field theories. However, a quantum theory that successfully models gravity has not yet been developed. Unification of electromagnetism and the weak force into a combined electroweak force was a major milestone on a road that is expected to lead to the unification of all four forces into one Grand Unified Theory. This road is paved with a multitude of models that aim to improve on our understanding of the current model, the Standard Model (SM) of particle physics. Although the SM has passed many experimental tests so far, such as the successful prediction [1] of the bottom quark [2] and the top quark [3, 4], we do know that it has also a number of shortcomings. Its failure to describe the fact that neutrinos do have nonvanishing masses and thus are capable to mix and oscillate [5] is certainly one of the vexing problems. The lack of a candidate particle that constitutes dark matter[6] is another. It is an ongoing scientific endeavor to formulate new models which encompass the predictive power of the SM while simultaneously explaining the differences between SM predictions and nature.

In a large number of the successful tests of the SM, experiment and theory compete to measure and predict observables to ever higher precision. This race towards precision physics is ongoing, and especially the parts that suffer from contributions by the strong interaction prove to be quite daunting and daring. Among these, weak decays that involve transitions from bottom (b) to strange (s) quarks are of special interest, since they arise only at the one-loop level in the SM. It is therefore expected that New Physics (NP) effects are easily noticeable, since they do not need to compete with leading SM terms. Here, the rare semileptonic decays $b \to s\ell^+\ell^-$ provide a particularly promising and rich phenomenology. The first observation of an exclusive $b \to s\ell^+\ell^-$ decay was reported by the Belle collaboration [7]. Over time, BaBar [8] and CDF [9] confirmed this observation, and more observables beyond the branching ratio were studied as well. With the advent of first results from the LHCb collaboration, one of the main experiments at CERN's Large Hadron Collider (LHC), we have the opportunity to go further down the road, towards finding hints of the SM's successor.

In this thesis, we investigate mainly the interesting class of exclusive semileptonic rare b decays. The theory description of exclusive decays involves non-perturbative hadronic matrix elements which describe the transition to the final state meson. Hence, their calculations are affected by a larger theory uncertainty than the calculations for inclusive decays which can be calculated perturbatively. Here, we understand inclusive decays as processes for which the final state strange hadron is not fully specified. The situation is the opposite from the experimental point of view, and as a matter of fact only experiments at e^+e^- colliders can measure inclusive processes at all. However, the first

generation of B factories KEKB and PEP-II (and their respective experiments Belle and BaBar) have already been shutdown. In the case of KEKB, an upgrade to a second generation B factory is ongoing since 2010, and first data taking with the upgraded Belle II detector is expected late in 2015 [10]. Therefore, theorists must make the best out of the available data, especially data on exclusive decays from experiments at hadron colliders. With the shutdown of the Tevatron and its experiments CDF and D0 late in 2011, LHCb is the only running experiment capable of measuring (exclusive) $b \to s\ell^+\ell^-$ decays. The results from LHCb's 2011 run alone yield the most powerful constraints on the effective couplings in $b \to s\ell^+\ell^-$ decays so far. Improving upon the theoretical handling of exclusive $b \to s\ell^+\ell^-$ decays to make full use of the available data is therefore an important endeavor.

The layout of this thesis is as follows. We begin in Chapter 2 by examining the underlying theory to model-independently describe $b \to s$ transitions, and how the parton level decays relate to the observable processes involving b hadrons. We continue in Chapter 3 with the phenomenology of the decays $\bar{B} \to \bar{K}^*\ell^+\ell^-$ and $\bar{B} \to \bar{K}\ell^+\ell^-$ in the kinematic region of low hadronic recoil. Here, we pay special attention to the construction of observables that strongly benefit from the characteristic properties of the aforementioned decays at low recoil. After that, we calculate and present numerical results for the these observables and their theory uncertainties within the SM in Chapter 4. In Chapter 5, a model-independent analysis of the effective short-distance couplings that govern $b \to s\ell^+\ell^-$ decays follows suit. We conclude in Chapter 6.

2. Theory of $b \to s\ell^+\ell^-$ Transitions

Within the SM, change of flavor is always associated with $W^\pm$ boson exchange, i.e., with a charged current. However, in the SM Flavor Changing Neutral Current (FCNC) mediated processes arise at the one-loop level [11]. In this chapter we review the theory of $|\Delta B| = 1$ FCNCs in the SM (Section 2.1) and within the framework of an effective field theory (Section 2.2). Following that, we discuss the transition from the partonic to the hadronic environment in Section 2.3. We conclude the chapter in Section 2.4 by considering the implications of long-distance Quantum Chromo Dynamics (QCD) effects in form of intermediate bound states – in particular the radial excitations of the $\bar{c}c$ bound states – on both the theoretical and experimental handling of semileptonic $b \to s\ell^+\ell^-$ transitions.

2.1. Standard Model FCNCs

The SM of particle physics is a renormalizable Quantum Field Theory with a local gauge symmetry based on the symmetry group

$$G_{\mathrm{SM}} = SU(3)_{\mathrm{C}} \times SU(2)_{\mathrm{L}} \times U(1)_{\mathrm{Y}} \,. \tag{2.1}$$

It can be described by the following Lagrangian density

$$\begin{aligned} \mathcal{L} = \bar{\psi} i \not{D} \psi - \frac{1}{4}\left[A^a_{\mu\nu}A^{\mu\nu}_a + B_{\mu\nu}B^{\mu\nu} + G^b_{\mu\nu}G^{\mu\nu}_b\right] \\ - \bar{\psi}_L \hat{Y} \phi \psi_R + (D_\mu \phi)^* (D^\mu \phi) - V(\phi) \,, \end{aligned} \tag{2.2}$$

where we omit gauge-fixing and ghost terms. We do no discuss these terms, as well as the technical points of field quantization since they are not relevant to the work presented in this thesis. For a detailed description we refer to the literature, cf. e.g.[12]. Within Eq. (2.2) we use the covariant derivative

$$D_\mu = \partial_\mu - ig' \frac{\sigma^a}{2} A^a_\mu - igY B_\mu - ig_s \frac{\lambda^A}{2} G^A_\mu \tag{2.3}$$

and the field strength tensors

$$A^a_{\mu\nu} = \partial_\mu A^a_\nu - \partial_\nu A^a_\mu - g' \varepsilon^{abc} A^b_\mu A^c_\nu \,, \qquad (\text{for the } SU(2)_{\mathrm{L}}) \tag{2.4}$$

$$B_{\mu\nu} = \partial_\mu B_\nu - \partial_\nu B_\mu \,, \qquad (\text{for the } U(1)_{\mathrm{Y}}) \tag{2.5}$$

$$G^A_{\mu\nu} = \partial_\mu G^A_\nu - \partial_\nu G^A_\mu - g_s f^{ABC} G^B_\mu G^C_\nu \,, \qquad (\text{for the } SU(3)_{\mathrm{C}}) \,. \tag{2.6}$$

The quantities g, g' and g_s are the coupling constants of $U(1)_{\mathrm{Y}}$, $SU(2)_{\mathrm{L}}$ and $SU(3)_{\mathrm{C}}$ in this order. The σ^a and λ^A denote the Pauli and Gell-Mann matrices, respectively, and ε^{abc} and f^{ABC} denote the structure constants of the nonabelian groups $SU(2)_{\mathrm{L}}$ and the

Name	Symbol	$\mathbf{SU(3)_C}$	$\mathbf{SU(2)_L}$	Y
Gauge Fields				
Gluons	G^A_μ, $A = 1, \ldots, 8$	**8**	**1**	0
$SU(2)_L$ Fields	A^a_μ, $a = 1, 2, 3$	**1**	**3**	0
Hypercharge Field	B_μ	**1**	**1**	0
Matter Fields				
Left-handed quarks	$Q_\mathrm{L} = (u_\mathrm{L}, d_\mathrm{L})$	**3**	**2**	$+1/3$
Right-handed up quarks	u_R	**3**	**1**	$+4/3$
Right-handed down quarks	d_R	**3**	**1**	$-2/3$
Left-handed leptons	$L_\mathrm{L} = (\nu_\mathrm{L}, e_\mathrm{L})$	**1**	**2**	-1
Right-handed charged leptons	e_R	**1**	**1**	-2
Symmetry Breaking Fields				
Higgs field	ϕ	**1**	**2**	$+1$

Table 2.1.: The field content of the SM. The columns $SU(3)_C$ and $SU(2)_L$ refer to the group representations in which the respective fields live, while the column Y lists the hypercharge of the respective fields. For the sake of readability we have suppressed the family indices of the matter fields.

$SU(3)_\mathrm{C}$, respectively. The nonvanishing structure constants give rise to self-interaction between the gauge fields associated with the respective groups. Moreover, the Dirac spinors ψ represent the matter fields – quarks and leptons – and we suppress any indication of multiplet or generation affiliation. The subscript L (R) denotes a left-chiral (right-chiral) projection of the spinor. The vector fields A^a_μ ($a = 1, 2, 3$), B_μ and G^b_μ ($A = 1, \ldots, 8$) represent the three $SU(2)_\mathrm{L}$ gauge fields, the hypercharge gauge field and the eight strong gauge fields, respectively. The hypercharge operator Y is related to the electric charge operator Q and the weak isospin operator I_3 via

$$\frac{Y}{2} = Q - I_3 \,. \tag{2.7}$$

The complex-valued scalar field ϕ and its potential

$$V(\phi) = -\mu^2 \left|\phi\right|^2 + \lambda \left|\phi\right|^4 \tag{2.8}$$

break the gauge symmetry spontaneously by means of the Higgs mechanism [13, 14, 15, 16].
The electroweak part of the SM was first proposed by Glashow and Weinberg[11] and Salam[1] in 1961 and 1967, respectively, and awarded with the Nobel Prize in Physics in 1979. Using data from their 2010/11 runs with an integrated luminosity of $\sim 5\mathrm{fb}^{-1}$, the LHC experiments ATLAS [18] and CMS [19] found indications of a Higgs mass peak around $123 - 125\,\mathrm{GeV}$. The most prevalent component of both their searches is

[1] There is no written record of A. Salam's contribution to the electroweak part of the SM. However, he discussed the workings of a $SU(2)\times U(1)$ gauge theory in a graduate course at Imperial College, London [17].

m_u	m_d	m_s	m_c	m_b	m_t
~ 0.003	~ 0.005	~ 0.1	~ 1.3	~ 4.2	~ 170

Table 2.2.: The approximate quark masses in GeV based on experimental measurements [22]. Due to the nature of the strong interaction, the definition of the quark masses inherently depends on the used renormalization scheme. We intend this table only to illustrate the large hierarchy between the masses, which spans five orders of magnitude between the top and the up quark.

the decay channel $h \to \gamma\gamma$, which is further backed up by searches in the channels $h \to ZZ^* \to \ell\bar{\ell}\ell'\bar{\ell}'$ and $h \to WW^* \to \ell\bar{\nu}\bar{\ell}'\nu'$. Besides these radiative and leptonic decay channels, CMS and the Tevatron experiments [20] CDF and D0 have taken into account decays into b jets. In combination with the LEP results [21], the experiments exclude a SM like Higgs for masses $\lesssim 600\,\mathrm{GeV}$ at 95%CL, with the exception of a small window around the aforementioned mass peak. No determination as to the nature of this apparent Higgs boson has been achieved yet. Both ATLAS and CMS hope to gather sufficient data in their 2012 runs, in order to find or exclude an SM-like Higgs boson with a significance of more than 5σ.

In principle, the theory as described above could be considered complete when using the aforementioned field content with just one generation of matter fields. However, experiments have shown conclusive evidence – e.g. discovery of the τ lepton [23] and discovery of Z decay into three types of neutrinos [24] – that the matter fields appear in at least three distinct families, i.e., three sets of matter fields with identical gauge properties but of different masses. We refer the reader to Tab. 2.1 for details of nomenclature and properties of the various gauge and matter fields. As a consequence, discrimination by mass is the only viable way to distinguish between these fields, and this gives rise to the concept of flavor. Disregarding the lepton sector, we switch from the basis with states $\tilde{u}$ and $\tilde{d}$ to the so-called mass basis by simultaneous orthogonalization of the quark mass terms

$$\mathcal{L} \supseteq v\left[\bar{\tilde{u}}_L \hat{Y}_u \tilde{u}_R + \bar{\tilde{d}}_L \hat{Y}_d \tilde{d}_R\right] \tag{2.9}$$

$$= v\left[\bar{\tilde{u}}_L U_u D_u V_u^\dagger \tilde{u}_R + \bar{\tilde{d}}_L U_d D_d V_d^\dagger \tilde{d}_R\right] \tag{2.10}$$

$$\equiv v\left[\bar{u}_L D_u u_R + \bar{d}_L D_d d_R\right\}\,, \tag{2.11}$$

with

$$vD_u = \mathrm{diag}(m_u, m_c, m_t)\,, \qquad vD_d = \mathrm{diag}(m_d, m_s, m_b)\,. \tag{2.12}$$

The quark masses are given in Tab. 2.2. Here the $\hat{Y}_{u,d}$ represent the 3×3 Yukawa matrices for up-type and down-type quarks, respectively, and v is the vacuum expectation value of the Higgs field ϕ. We denote the diagonalized Yukawa matrices by $D_{u,d}$, and the unitary orthogonalization matrices for left-chiral and right-chiral quarks by $U_{u,d}$ and $V_{u,d}$, respectively. We remark that two independent unitary matrices U_i and V_i arise when

diagonalizing $\hat{Y}_i$, since the latter are in general not Hermitian.

Within the framework of the SM, changes of flavor are realized by coupling of the $W^\pm$ gauge fields to a charged fermion current. We suppress charged currents in the lepton sector, which are not relevant to this work. For the quark sector and in the mass basis, charged currents are described in the Lagrangian by the term $\mathcal{L}_{\mathrm{cc}}$,

$$\mathcal{L} \supseteq \mathcal{L}_{\mathrm{cc}} = -\frac{g'}{\sqrt{2}} V_{ij} \bar{Q}_i \sigma^+ W_\mu^+ \gamma^\mu P_L Q_j + \mathrm{h.c.}\,, \tag{2.13}$$

with

$$W_\mu^\pm = \frac{A_\mu^1 \mp i A_\mu^2}{\sqrt{2}}\,, \qquad\qquad \sigma^\pm = \frac{\sigma^1 \pm i\sigma^2}{2}\,, \tag{2.14}$$

to which only the left-chiral doublets couple, while the right-chiral singlets do not. This discrimination based on chirality implies maximal parity violation in charged current decays. First considered in 1956 [25], parity violation was experimentally confirmed only one year later by Wu *et al.* [26]. Within $\mathcal{L}_{\mathrm{cc}}$, the relative coupling of a generation $j = 1,2,3$ down-type quark to a generation $i = 1,2,3$ up-type quark is given by the matrix element $V_{ij} = (U_u U_d^\dagger)_{ij}$. The matrix V is known as the Cabibbo-Kobayashi-Maskawa (CKM) matrix. The inverse process (up-type quark i to down-type quark j) is described by the Hermitian conjugate part within $\mathcal{L}_{\mathrm{cc}}$, and thus its coupling is given by V_{ij}^*. Since exactly one up-type quark index and one down-type quark index are relevant to selecting a CKM matrix element, we can rewrite the indices in terms of $i = u, c, t$ and $j = d, s, b$, and the CKM matrix then reads

$$V = \begin{pmatrix} V_{ud} & V_{us} & V_{ub} \\ V_{cd} & V_{cs} & V_{cb} \\ V_{td} & V_{ts} & V_{tb} \end{pmatrix}\,. \tag{2.15}$$

In 1983, Wolfenstein proposed [27] a parametrization in terms of four real-valued parameters A, λ, ρ, η. Of the former only A is of order one, and the remaining parameters $\lambda, \rho, \eta \ll 1$. Wolfenstein proposed an expansion in $\lambda \approx 0.22$, and to order λ^4 the CKM matrix reads

$$V = \begin{pmatrix} 1-\lambda^2/2 & \lambda & A\lambda^3(\bar{\rho} - i\bar{\eta}) \\ -\lambda & 1-\lambda^2/2 & A\lambda^2 \\ A\lambda^3(1-\bar{\rho}-i\bar{\eta}) & -A\lambda^2 & 1 \end{pmatrix} + \mathcal{O}\left(\lambda^4\right)\,. \tag{2.16}$$

Here we employ the barred quantities $\bar{\rho}, \bar{\eta}$, which are defined via

$$\rho + i\eta = \frac{(\bar{\rho} + i\bar{\eta})\sqrt{1 - A^2\lambda^4}}{\sqrt{1-\lambda^2}(1 - A^2\lambda^4(\bar{\rho} + i\bar{\eta}))}\,, \tag{2.17}$$

and using them instead of the original parameters ρ, η ensures that the expansion of the CKM matrix stays unitary to all orders in λ, cf. e.g.[28]. For the numerical values of the Wolfenstein parameters we refer to Tab. 4.2.

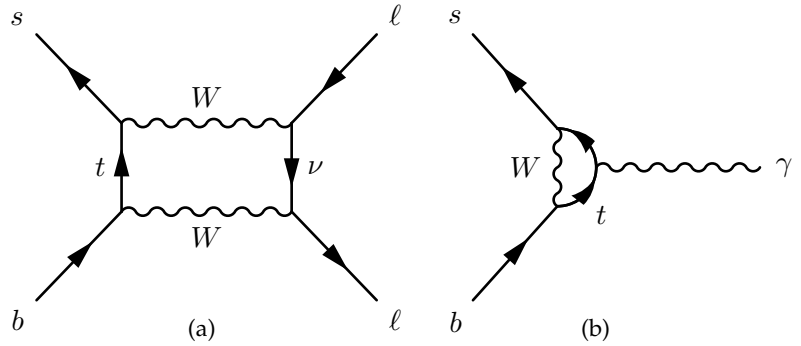

Figure 2.1.: Exemplary Feynman diagrams that describe contributions (a) to $b \to s\ell^+\ell^-$ decays and (b) to $b \to s\gamma$ decays.

In the SM there are no charge-neutral changes of flavor at tree-level. However, they can be realized by loop processes where a virtual W boson couples twice to a quark line, a process which is known as an FCNC. Amplitudes involving FCNCs exhibit the structure (here exemplary for $b \to s$ FCNCs),

$$\mathcal{A} = V_{ub}V_{us}^* f(\hat{m}_u^2) + V_{cb}V_{cs}^* f(\hat{m}_c^2) + V_{tb}V_{ts}^* f(\hat{m}_t^2)\,, \quad \hat{m}_q \equiv m_q/M_W\,, \tag{2.18}$$

where $f(\hat{m}^2)$ denotes an unspecified loop function which is process dependent. Examples for Feynman diagrams which contribute to $b \to s$ FCNC amplitudes are given in Fig. 2.1. Due to the Feynman rule for the evaluation of loops involving the $SU(2)_{\rm L}$ gauge fields, loop functions are usually suppressed by a factor of $(g'/4\pi)^2$. Amplitudes that emerge only at the one-loop level are therefore known to be *loop suppressed*. Moreover, we can apply the CKM unitarity relation

$$V_{cb}V_{cs}^* = -V_{tb}V_{ts}^* - V_{ub}V_{us}^* \tag{2.19}$$

to remove the CKM factors $V_{cb}V_{cs}^*$ from Eq. (2.18):

$$\mathcal{A} = V_{tb}V_{ts}^* \left[f(\hat{m}_t^2) - f(\hat{m}_c^2)\right] + V_{ub}V_{us}^* \left[f(\hat{m}_u^2) - f(\hat{m}_c^2)\right]\,. \tag{2.20}$$

The above amplitude is simultaneosuly suppressed by the CKM matrix elements and for degenerate quark masses. This mechanism of suppression is known as the Glashow-Iliopolus-Maiani (GIM) mechanism [11], and amplitudes that suffer from its suppression are known to be *GIM suppressed*. In the SM, one finds $V_{ub}V_{us}^*/V_{tb}V_{ts}^* \simeq (1+2i)\times 10^{-2}$. In addition, the loop function can be expanded around $\hat{m}_{c,u}^2 \ll 1$, and one obtains

$$\begin{aligned} f(\hat{m}_u^2) - f(\hat{m}_c^2) &= \left(\hat{m}_u^2 - \hat{m}_c^2\right) f'(0) + \mathcal{O}\left(\hat{m}_{c,u}^4\right) \\ &= \mathcal{O}\left(\hat{m}_c^2\right) = \mathcal{O}\left(10^{-4}\right)\,. \end{aligned} \tag{2.21}$$

On the other hand, the difference of loop functions $[f(\hat{m}_t^2) - f(\hat{m}_c^2)]$ is generically unsuppressed. One therefore finds that the terms $\propto V_{ub}V_{us}^*$ are suppressed in comparison to the leading terms by a factor of $\sim 10^{-6}$ and can safely be removed as long as CP conserving observables are considered. However, these contributions are essential when considering CP violating observables, cf. Eq. (3.95). In addition to the above loop and

GIM suppression, one further finds that $b \to s$ FCNCs in the SM suffer from mild *CKM suppression* due to the numerically small combination $V_{tb}V_{ts}^* \propto \lambda^2$. Taken together, one finds that in the SM the decays $b \to s\{\gamma, \ell^+\ell^-, g\}$ are very *rare decays*, with branching fractions of the order 10^{-4} (e.g.$B \to X_s\gamma$) down to 10^{-9} (e.g.$B_s \to \mu^+\mu^-$). While the branching ratios of these rare decays are very small and thus experimentally challenging, several of them have been discovered. On the other hand, FCNC decays of top quarks (t) have not yet been discovered. For them, the GIM suppression is worse then for b quarks. We show this explicitly for $t \to c$ FCNCs, where

$$\begin{aligned}
\mathcal{A}(t \to cX) &\sim V_{tb}^*V_{cb}f(\hat{m}_b^2) + V_{ts}^*V_{cs}f(\hat{m}_s^2) + V_{td}^*V_{cd}f(\hat{m}_d^2) && (2.22)\\
&= V_{tb}^*V_{cb}\left[f(\hat{m}_b^2) - f(\hat{m}_d^2)\right] + V_{ts}^*V_{cs}\left[f(\hat{m}_s^2) - f(\hat{m}_d^2)\right] && (2.23)\\
&= V_{tb}^*V_{cb}\hat{m}_b^2 f'(\hat{m}_b^2) + V_{ts}^*V_{cs}\hat{m}_s^2 f'(\hat{m}_s^2) + \mathcal{O}\left(\hat{m}_d^2\right) && (2.24)\\
&= \mathcal{O}\left(\lambda^2\hat{m}_b^2\right) \approx 10^{-4}\,. && (2.25)
\end{aligned}$$

Here the unitarity relation $V_{td}^*V_{cd} = -V_{tb}^*V_{cb} - V_{ts}^*V_{cs}$ has been used. It follows that in the SM the branching ratios are several orders of magnitude smaller than for $b \to s$ FCNCs, and they range from 5×10^{-12} for $\mathcal{B}(t \to cg)$ to 10^{-14} for $\mathcal{B}(t \to cZ)$ [29]. Even within extensions of the SM the t FCNCs remain rare, cf. e.g.[30] for a recent study within the Minimal Supersymmetric Standard Model where $\mathcal{B}(t \to cX) < 10^{-8}$ for $X = g, \gamma, Z$.

2.2. Effective Field Theory

Effective Field Theories, such as Chiral Perturbation Theory [31], Heavy Quark Effective Theory (HQET) [32] and Soft Collinear Effective Theory (SCET) [33], are widely used tools within the field of elementary particle theory, especially in cases where perturbative approaches to QCD face problems. Their common concept is the separation of different energy scales by means of a set of local field operators $\mathcal{O}_i$ and their associated scalar couplings $\mathcal{C}_i$, the so called Wilson coefficients. An effective Lagrangian can be constructed from both the local operators and Wilson coefficients. This effective Lagrangian is systematically expanded in some smallness parameter, e.g., $1/m_b$ in the case of HQET, and a soft momentum scale λ in the case of SCET. This expansion is known as an Operator Production Expansion (OPE). Effective theories are, however, not predictive theories in their own rights. In order to achieve predictive power, one has to calculate the a priori unknown Wilson coefficients. In the cases of HQET and SCET this can be achieved by comparing the results of the effective theory with those of the full theory in its perturbative regime, a process that is known as *matching*.

In the case of semileptonic $|\Delta B| = 1$ FCNCs, an OPE in $1/M_W^2$ is employed to arrive at the following effective Hamiltonian, see for instance [28],

$$\begin{aligned}
\mathcal{H}_{\text{eff}} = -\frac{4G_{\text{F}}}{\sqrt{2}}\left[V_{tb}V_{ts}^*\sum_{i\neq 1u,2u}\mathcal{C}_i\mathcal{O}_i + V_{ub}V_{us}^*\left(\mathcal{C}_1\left(\mathcal{O}_{1c} - \mathcal{O}_{1u}\right) + \mathcal{C}_2\left(\mathcal{O}_{2c} - \mathcal{O}_{2u}\right)\right)\right] \quad (2.26)\\
+ \cdots + \text{h.c.}\,.
\end{aligned}$$

Here $G_{\rm F}$ is the Fermi constant,

$$G_{\rm F} = \frac{\sqrt{2}(g')^2}{8M_W^2}\,, \tag{2.27}$$

and we suppress the dependence on the renormalization scale μ of both the local operators[2] $\mathcal{O}_i$ as well as their associated Wilson coefficients $\mathcal{C}_i$. The ellipses indicate terms of higher order in $1/M_W^2$ (or equivalently in $G_{\rm F}$), which are not taken into consideration within this work. The CKM structure of Eq. (2.26) is tailored toward the SM results. In particular, CKM unitarity has been employed by means of Eq. (2.19) to remove terms $\propto V_{cb}V_{cs}^*$.

In the paradigm of the performed OPE, we describe the light degrees of freedom, i.e., all fields with masses $m \leq \mu$, as part of the local operators $\mathcal{O}_i$, while the heavy degrees of freedom have been integrated out, i.e., their effects are completely described by the Wilson coefficients. Taking the SM as an example, the top quark and the heavy gauge bosons $W^\pm, Z^0$ are integrated out. We note here that by treating the Wilson coefficients as generalized couplings one can accommodate for the effects of Beyond the Standard Model (BSM) particles which are heavier than μ in a model-independent way. For non-hadronic $|\Delta B| = 1$ FCNCs, it is common to define the following *SM basis of operators*, which is the set of relevant operators whose Wilson coefficients are neither vanishing nor negligible within the SM. We do not consider the electroweak penguin operators. The SM basis reads

$$\begin{aligned}
\mathcal{O}_{1c} &= [\bar{s}\gamma_\mu T^a P_L c]\,[\bar{c}\gamma^\mu T^a P_L b]\,, & \mathcal{O}_{2c} &= [\bar{s}\gamma_\mu P_L c]\,[\bar{c}\gamma^\mu P_L b]\,, \\
\mathcal{O}_{1u} &= [\bar{s}\gamma_\mu T^a P_L u]\,[\bar{u}\gamma^\mu T^a P_L b]\,, & \mathcal{O}_{2u} &= [\bar{s}\gamma_\mu P_L u]\,[\bar{u}\gamma^\mu P_L b]\,, \\
\mathcal{O}_3 &= [\bar{s}\gamma_\mu P_L b]\textstyle\sum_q [\bar{q}\gamma^\mu P_L q]\,, & \mathcal{O}_5 &= [\bar{s}\gamma_\mu\gamma_\nu\gamma_\rho P_L b]\textstyle\sum_q [\bar{q}\gamma^\mu\gamma^\nu\gamma^\rho P_L q]\,, \\
\mathcal{O}_4 &= [\bar{s}\gamma_\mu T^a P_L b]\textstyle\sum_q [\bar{q}\gamma^\mu T^a P_L q]\,, & \mathcal{O}_6 &= [\bar{s}\gamma_\mu\gamma_\nu\gamma_\rho T^a P_L b]\textstyle\sum_q [\bar{q}\gamma^\mu\gamma^\nu\gamma^\rho T^a P_L q]\,, \\
\mathcal{O}_7 &= \frac{e}{(4\pi)^2} m_b\,[\bar{s}\sigma^{\mu\nu} P_R b]\,F_{\mu\nu}\,, & \mathcal{O}_9 &= \frac{e^2}{(4\pi)^2}\,[\bar{s}\gamma_\mu P_L b]\,\big[\bar{\ell}\gamma^\mu \ell\big]\,, \\
\mathcal{O}_8 &= \frac{g_s}{(4\pi)^2} m_b\,[\bar{s}\sigma^{\mu\nu} P_R T^a b]\,G^a_{\mu\nu}\,, & \mathcal{O}_{10} &= \frac{e^2}{(4\pi)^2}\,[\bar{s}\gamma_\mu P_L b]\,\big[\bar{\ell}\gamma^\mu\gamma_5 \ell\big]\,.
\end{aligned} \tag{2.28}$$

Here, the operators $\mathcal{O}_{1\ldots6}$ are defined as in [34]. For the operators $\mathcal{O}_{7\ldots10}$ we use the definitions of [35]. The chirality structure of the above operators reflects very well the maximal parity violation through coupling to W bosons in the SM, which arises from the vector/axial vector ($V-A$) nature of the weak interaction. The set of operators needs to be enlarged when we consider models beyond the SM, i.e., models in which there is no restriction to the $V-A$ structure. In this work we refer to the SM' basis as the union of the SM basis with the chirality-flipped operators $\mathcal{O}'_i$, $i = 7, 9, 10$. Here, the operators $\mathcal{O}'_i$ are obtained from the corresponding operators $\mathcal{O}_i$ by the exchange $P_L \leftrightarrow P_R$. Moreover, models beyond the SM can also accommodate for FCNCs of (pseudo-)scalar and (pseudo-)tensor nature. In order to handle such models, we define the SM'+

[2] While in general only the hadronic matrix elements of the operator $\mathcal{O}_i$ depend on the renormalization scale μ, in our choice of the basis Eq. (2.28) the operators $\mathcal{O}_{7,8}$ exhibit an explicit scale dependence through the $\overline{\rm MS}$ mass of the b quark.

basis which includes the operators

$$\mathcal{O}_S^{(\prime)} = \frac{e^2}{(4\pi)^2}\left[\bar{s}P_{R(L)}b\right]\left[\bar{\ell}\ell\right], \qquad \mathcal{O}_P^{(\prime)} = \frac{e^2}{(4\pi)^2}\left[\bar{s}P_{R(L)}b\right]\left[\bar{\ell}\gamma_5\ell\right], \tag{2.29}$$
$$\mathcal{O}_T = \frac{e^2}{(4\pi)^2}\left[\bar{s}\sigma_{\mu\nu}b\right]\left[\bar{\ell}\sigma^{\mu\nu}\ell\right], \qquad \mathcal{O}_{T5} = \frac{e^2}{(4\pi)^2}\frac{i\varepsilon^{\mu\nu\alpha\beta}}{2}\left[\bar{s}\sigma_{\mu\nu}b\right]\left[\bar{\ell}\sigma_{\alpha\beta}\ell\right],$$

in addition to those of the SM′ basis. The above definition of $\mathcal{O}_{T5}$ has been chosen to facilitate the calculation of amplitudes for exclusive decays, as both its hadronic and leptonic currents coincide with those that occur in $\mathcal{O}_T$. It coincides with the definitions used in [36, 37]. Furthermore, we find for $D = 4$ dimensions

$$\mathcal{O}_{T5} = \frac{e^2}{(4\pi)^2}\left[\bar{s}\sigma_{\mu\nu}b\right]\left[\bar{\ell}\sigma^{\mu\nu}\gamma_5\ell\right], \tag{2.30}$$

which agrees with the definition used in [38].

In order to calculate the amplitudes of $b \to s\ell^+\ell^-$ processes, one needs to evaluate both the matrix elements of the local operators and the Wilson coefficients at a common renormalization scale μ. As μ is an unphysical quantity, the result would not depend on the concrete value of μ if one worked to all orders in perturbation theory. However, as we can only work to fixed, finite order in the perturbative expansions we can observe a residual dependence on the value of the renormalization scale. Due to logarithmic terms of the form

$$L_{i,j}^W = \alpha_s^i \ln^j\left(\frac{\mu^2}{M_W^2}\right), \qquad L_{i,j}^b = \alpha_s^i \ln^j\left(\frac{\mu^2}{m_b^2}\right) \tag{2.31}$$

with $0 \leq j \leq i$, the convergence of the perturbative expansion is impaired for QCD corrections to the matrix elements of the local operators when $\mu \approx M_W$, and conversely for the calculation of the Wilson coefficients when $\mu \approx m_b$. This problem can be solved by resummation of the most relevant logarithmic terms. Here, one understands resummation of all logarithms $L_{i,i}$ as working to leading-logarithm, and resummation of all logarithms $L_{i,i\geq j\geq i-1}$ as working to next-to-leading-logarithm. In $|\Delta B| = 1$ FCNCs, resummation of large logarithms is accomplished by evolution of the Wilson coefficients from the high scale μ_0 to the low scale $\mu_b \approx m_b$ as governed by the Renormalization Group Equations (RGE). This technique is known as RGE-improved perturbation theory, and makes use of the μ dependence of the Wilson coefficients $\mathcal{C}_i$, which can be written as

$$\frac{\mathrm{d}\,\mathcal{C}_i}{\mathrm{d}\ln\mu} = \gamma_{ji}\,\mathcal{C}_j\,, \qquad \frac{\mathrm{d}\,g_s}{\mathrm{d}\ln\mu} = \beta(g_s). \tag{2.32}$$

with the solution [35]

$$\mathcal{C}_i(\mu_b) = U_{ij}(\mu_b,\mu_0)\,\mathcal{C}_j(\mu_0), \quad \mu_0 \geq \mu_b\,, \tag{2.33}$$
$$U_{ij}(\mu_b,\mu_0) = \exp\int_{g_s(\mu_0)}^{g_s(\mu_b)} \mathrm{d}g' \frac{\gamma_{ji}(g')}{\beta(g')}\,. \tag{2.34}$$

Here the anomalous mass dimension matrix of the operator basis γ and the beta function of QCD β are functions of the strong coupling g_s. We briefly derive the resummation of large logarithms to leading logarithm (LL) for a single operator $\mathcal{O}$ with anomalous dimension

$$\gamma_{\mathcal{O}} = \gamma^{(0)} \frac{g_s^2}{16\pi^2} + \mathcal{O}\left(g_s^4\right) , \tag{2.35}$$

and its associated Wilson coefficients $\mathcal{C}$. Our derivation of the resummation is based on Ref. [28], to which we refer the reader for an in-depth discussion of LL and NLL results in $b \to s$ FCNCs. Using the LO results for the QCD beta function

$$\frac{\mathrm{d}g_s}{\mathrm{d}\ln\mu} = \beta(g_s) = -\beta^{(0)} \frac{g_s^3}{16\pi^2} + \mathcal{O}\left(g_s^5\right) , \qquad \beta^{(0)} = 11 - \frac{2}{3} n_f , \tag{2.36}$$

where n_f is the number of active quark flavors, we can rewrite Eq. (2.32)

$$\frac{\mathrm{d}\mathcal{C}}{\mathrm{d}g_s} = \frac{\mathrm{d}\mathcal{C}}{\beta(g_s)\mathrm{d}\ln\mu} = \frac{\gamma(g_s)}{\beta(g_s)}\mathcal{C} . \tag{2.37}$$

Inserting the LO results for both β and γ yields

$$\frac{\mathrm{d}\mathcal{C}}{\mathrm{d}g_s} = -\frac{\gamma^{(0)}}{g_s\beta^{(0)}}\mathcal{C} . \tag{2.38}$$

The above differential equation can be solved by separation of $\mathrm{d}\mathcal{C}$ and $\mathrm{d}g_s$,

$$\frac{\mathrm{d}\mathcal{C}}{\mathcal{C}} = -\frac{\gamma^{(0)}}{\beta^{(0)}} \frac{\mathrm{d}g_s}{g_s} , \tag{2.39}$$

and subsequent integration. The solution reads

$$\mathcal{C}(\mu_b) = \eta^a \mathcal{C}(\mu_0), \qquad \text{with } \eta = \frac{\alpha_s(\mu_b)}{\alpha_s(\mu_0)},\ a = -\frac{\gamma^{(0)}}{2\beta^{(0)}} . \tag{2.40}$$

We can now use the LO results for the running strong coupling

$$\alpha_{\mathrm{s}}(\mu_b) = \frac{\alpha_{\mathrm{s}}(\mu_0)}{1 - \beta^{(0)} \frac{\alpha_{\mathrm{s}}}{4\pi} \ln \frac{\mu_b^2}{\mu_0^2}} \tag{2.41}$$

and find that the factor η resums all leading logarithms $\alpha_{\mathrm{s}}^i \ln^i(\mu_b^2/\mu_0^2)$:

$$\eta^a \simeq \left[1 - \beta^{(0)} \frac{\alpha_{\mathrm{s}}}{4\pi} \ln \frac{\mu_b^2}{\mu_0^2}\right]^{\frac{\gamma^{(0)}}{2\beta^{(0)}}} \tag{2.42}$$

$$= 1 - \frac{\gamma^{(0)}}{2} \frac{\alpha_{\mathrm{s}}}{4\pi} \ln \frac{\mu_b^2}{\mu_0^2} + \mathcal{O}\left(\alpha_{\mathrm{s}}^2 \ln^2 \frac{\mu_b^2}{\mu_0^2}\right) . \tag{2.43}$$

Within the SM, the Wilson coefficients $\mathcal{C}_i$ and the anomalous mass dimension matrix γ associated with the operators of the SM basis have been calculated to next-to-next-to-leading order (NNLO) in α_s [35]. In combination with the N^{3}LO-computation of the beta functions of QCD, this allows the resummation of large logarithms in the RGE up to next-to-next-to-leading logarithm (NNLL) [35].

2.3. From Partons to Hadrons

While the previous sections discuss the calculation of $b \to s$ FCNCs at the parton level, the more difficult question is how the latter relate to $|\Delta B| = 1$ decays of b hadrons. Since the remainder of this work concentrates on decays of B mesons, we will abstain from discussing baryonic processes.

We begin with the nomenclature of B mesons, where we stick to the Particle Data Group convention, and define the $\bar{B}_q$ mesons to contain as valence partons one b quark and one $q = u, d, s$ antiquark. The antipartner of the $\bar{B}_q$ is labeled B_q, where all valence partons are replaced by their respective antipartners. The theory of $\bar{B}_q$ decays is divided into two concepts of decays, which are known as *inclusive* and *exclusive* decays. In the former, the initial state and parts of the final state are fixed, while the remainder of the final state is understood to contain all hadronic states that fulfill a certain criterion. Exclusive decays, on the other hand, fully specify both the initial and the final state. As an example for an inclusive decay we consider $\bar{B}_d \to X_s\gamma$, which is understood as the radiative decays of the $\bar{B}_d$ to all hadronic final states that contain at least one s quark. Both $\bar{B}_d \to X_s\gamma$ and $\bar{B}_d \to X_s\ell^+\ell^-$ decays can be calculated with very small theory uncertainties to next-to-next-to-leading order (NNLO) in the strong coupling α_s [39, 35]. However, the experimental measurement of inclusive rare decays of the $\bar{B}_d$ is notoriously difficult and can so far only be achieved by experiments at electron-positron colliders such as Belle and BaBar. The advent of the Belle II [40] (and the planned Super-B [41]) experiment will improve on the measurements of the inclusive decays. SuperB states the aim of reducing the overall experimental error on $\mathcal{B}(\bar{B} \to X_s\ell^+\ell^-)$ from 23% down to 4% – 6% [41]. Conversely, exclusive decays are experimentally clean. In the absence of neutrinos in the final state, their properties can also be measured by experiments at hadron colliders. In point of fact, the LHCb experiment has so far provided the most precise measurements in the area of several exclusive rare b decays, such as $\bar{B} \to \bar{K}^*\ell^+\ell^-$ [42] and $\bar{B}_s \to J/\psi\phi$ [43]. Unfortunately, the theoretical calculation of exclusive B decays is hampered by the fact that the necessary hadronic matrix elements cannot be obtained from perturbative QCD calculations. For the semileptonic decays, several nonperturbative techniques, such as Light Cone Sum Rules (LCSR) and Lattice QCD (LQCD), provide mutually consistent results for these nonperturbative hadronic quantities. For a comparison of LCSR and (preliminary) LQCD results for the $B \to K^{(*)}$ matrix elements, cf. Appendices B and C, respectively. However, both techniques yield results which are affected by considerable uncertainties [44, 45]. In order to reliably extract information on the underlying short-distance physics, it is of paramount importance to construct observables of exclusive decays in which the hadronic uncertainties are partially or even completely removed. In the remainder of this work we will show that exclusive rare B decays at low recoil provide very clean observables, and are thus ideally suited as probes of $|\Delta B| = 1$ short-distance physics.

2.4. Long-Distance Effects

The theoretical description of semileptonic $|\Delta B| = 1$ decays – as reviewed in this chapter – suffers from pollution through long-distance contributions by the 4-quark operators $\mathcal{O}_{1\ldots6}$ and by the chromomagnetic operator $\mathcal{O}_8$. Specifically, they arise from intermedi-

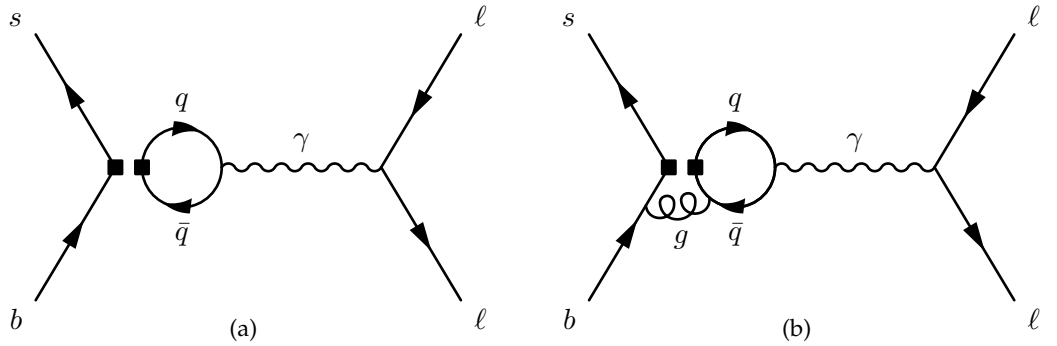

Figure 2.2.: Examples of loop diagrams which arise from intermediate quark-antiquark loops in the process $b \to s\ell^+\ell^-$. The black squares denote insertions of the local operators $\mathcal{O}_{1,2}$ ($q = c$) and $\mathcal{O}_{3\ldots6}$ ($q = u, d, s, c, b$).

Resonance	J/ψ(1S)	ψ'(2S)	$\psi(3770)$
M [MeV]	3096	3686	3772
Γ [MeV]	0.093 ± 0.003	0.304 ± 0.009	27.3 ± 1.0
$\mathcal{B}^{\ell\ell}$ [%]	5.93 ± 0.06	0.77 ± 0.08	$(9.7 \pm 0.7) \times 10^{-4}$

Resonance	$\psi(4040)$	$\psi(4160)$	$\psi(4415)$
M [MeV]	4039 ± 1	4153 ± 3	4421 ± 4
Γ [MeV]	80 ± 10	103 ± 8	62 ± 20
$\mathcal{B}^{\ell\ell}$ [%]	$(1.07 \pm 0.16) \times 10^{-3}$	$(8.1 \pm 0.9) \times 10^{-4}$	$(9.4 \pm 3.2) \times 10^{-4}$

Table 2.3.: Masses M, total decay widths Γ and branching ratios $\mathcal{B}^{\ell\ell}$ for the decay to $\ell^+\ell^-$ final states of the radially excited charmonia with $J^P = 1^-$. All values are taken from Ref. [22].

ate production of $\bar{q}q$ pairs, where $q = u, c$ for the current-current operators $\mathcal{O}_{1q,2q}$, and $q = u, d, s, c, b$ for the QCD penguin operators $\mathcal{O}_{3\ldots6}$. Exemplary Feynman diagrams of the emerging contributions to leading and next-to-leading order in α_s are depicted in Fig. 2.2(a) and Fig. 2.2(b), respectively.

The contributions from the current-current operators enter the $b \to s\ell^+\ell^-$ matrix elements with numerically large Wilson coefficients $\mathcal{C}_{1,2}$ and therefore need careful treatment. Especially for the production of $\bar{c}c$ pairs, one has to consider the resonant production of bound states with matching quantum numbers and quark contents, i.e., charmonia with $J^P = 1^-$. Their relevant properties are compiled in Tab. 2.3.

For the purpose of this thesis, we categorize these resonances as *narrow* ($J/\psi, \psi'$) and *wide* ($\psi(3770), \psi(4040), \psi(4160), \psi(4415)$), which can directly be inferred from their respective total decay widths. The narrow resonances are vetoed in the experimental results by means of phase space cuts. Currently, the collaborations Belle, CDF and LHCb

use identical cuts[3] [46, 47, 42] for the exclusion of both the J/ψ and the ψ' resonances: $8.68\,\mathrm{GeV}^2 \leq q^2 \leq 10.09\,\mathrm{GeV}^2$ and $12.86\,\mathrm{GeV}^2 \leq q^2 \leq 14.18\,\mathrm{GeV}^2$, respectively. However, the tails of these resonance peaks still affect the observables outside the experimental cuts. A recent study [48] finds for $q^2 \leq m^2_{\psi'}$ contributions to the amplitudes of up to 5% (20%) for $\bar{B} \to \bar{K}^{(*)}\ell^+\ell^-$ decays, which stem mainly from soft-gluon effects. We emphasize that these effects have not been taken into account in the present work.

In the region of large hadronic recoil, QCD Factorization (QCDF) can be employed to perturbatively compute long-distance effects from quark loops [49]. Although QCDF was originally employed to compute B decays into two light hadronic final states [50], it can be applied to the calculation of semileptonic rare B decays. The basic result of QCDF is the following (schematic) decomposition of the matrix element $\mathcal{M}(B \to hV)$

$$\mathcal{M}(B \to hV) = C \cdot \xi + \phi_B \otimes T \otimes \phi_h \,. \tag{2.44}$$

where h stands for the final state meson and V for either a photon or the electromagnetic coupling to a pair of charged leptons. Here C represents the factorizable contributions, multiplied by the $B \to h$ form factor ξ. Furthermore, the hard scattering kernel T contributes nonfactorizing terms that are convoluted with the Light Cone Distribution Amplitudes (LCDAs) ϕ_B and ϕ_h of both the initial and final state mesons. Both C and T can be calculated perturbatively. The region of validity for the application of QCDF is approximately $1\,\mathrm{GeV}^2 \leq q^2 \leq 6\,\mathrm{GeV}^2$, which effectively excludes narrow resonances that stem from either $\bar{u}u$ or $\bar{c}c$ loops. Results for $B \to \{K^*, \rho, \omega\}\,\ell^+\ell^-$ [49, 51] and $B \to K^*\gamma$ [52] have been obtained up to next-to-leading order (NLO) in the strong coupling α_s. Since within the virtual two-loop functions F_{ij} [53] the renormalization scheme of the quark masses is not fixed, one can choose the quark mass scheme for the intermediate quark loops. In Refs. [44, 45], the charm quark mass was taken in the $\overline{\mathrm{MS}}$ scheme, $m_c(m_c) = 1.27\,\mathrm{GeV}$. However, this choice leads to an early onset of the $\bar{c}c$ threshold effects at $q^2 = 4m_c^2 \simeq 6.5\,\mathrm{GeV}^2$, well below the mass square of the J/ψ, $m^2_{J/\psi} \simeq 9.6\,\mathrm{GeV}^2$. Instead, in this work we always use the pole mass scheme when computing observables by means of QCDF, with $m_c^\mathrm{pole} \simeq 1.59\,\mathrm{GeV}$. Here, the onset of threshold effects occurs only at $q^2 \simeq 10.1\,\mathrm{GeV}^2$, which matches the physical resonance much better.

For the low recoil region, the inclusion of quark-loop contributions is handled by means of an OPE, which is described in detail in Section 3.2.

[3] The inter resonance bin of LHCb differs by $0.04\,\mathrm{GeV}^2$ from the Belle and CDF bin. However, this deviation is irrelevant for this thesis, as the corresponding bin is not used in any of the presented analyses.

3. Phenomenology of $\bar{B} \to \bar{K}^{(*)}\ell^+\ell^-$ at Low Hadronic Recoil

Exclusive semileptonic $|\Delta B| = 1$ decays provide a large number of observables which can be measured both at (Super-)B factories and at the LHC. Previous works on the phenomenology of these decays focused on the kinematic region of large hadronic recoil [49, 51, 38, 54]. In contrast, in the course of this chapter we concentrate on the phenomenology of the exclusive decays $\bar{B} \to \bar{K}^{(*)}\ell^+\ell^-$ and $\bar{B}_s \to \phi\ell^+\ell^-$ in the kinematic region of low hadronic recoil, i.e., for small energy E_s of the final state meson, $E_s - m \lesssim \Lambda$. Here and throughout, we denote by Λ a smallness parameter for expansions in $1/m_b$, where $\Lambda = \mathcal{O}(\Lambda_{\rm QCD})$. First, we introduce the kinematics and common notations for both decays in Section 3.1. Next, we examine the low recoil framework as put forward in Ref. [55]. It consists of an OPE (discussed in Section 3.2) and a set of improved Isgur-Wise form factor relations for the individual decays (discussed in Section 3.3). Subsequently, we study the spectrum and phenomenological application of observables within the low recoil region for $\bar{B}_{d,s} \to \left\{\bar{K}^*, \phi\right\}\ell^+\ell^-$ and $\bar{B} \to \bar{K}\ell^+\ell^-$ decays in Section 3.4 and Section 3.5, respectively.

3.1. Kinematics and Notations

Before we turn to the individual decays $\bar{B} \to \bar{K}^*(\to \bar{K}\pi)\ell^+\ell^-$ and $\bar{B} \to \bar{K}\ell^+\ell^-$, we lay some groundwork by introducing notations and kinematics which are common to both decays. We begin by assigning the four-momenta $p, k, p_\pm$ and the polarization vector η to the participating particles,

$$\bar{B}(p) \to \bar{K}(k)\ell^+(p_+)\ell^-(p_-)\,, \qquad \bar{B}(p) \to \bar{K}^*(k,\eta)\ell^+(p_+)\ell^-(p_-)\,, \tag{3.1}$$

and introduce the four-momentum q of the lepton pair, which reads $q = p_+ + p_- = p - k$. For both the vector and the pseudoscalar decay channel, we follow the literature [38] and define θ_ℓ as the angle between the negatively charged lepton and the $\bar{B}$ meson in the dilepton rest frame. It is usual to use q^2, the invariant mass of the lepton pair, as a further kinematic variable. For the decay $\bar{B} \to \bar{K}\ell^+\ell^-$, which is a $1 \to 3$ decay, the two kinematic variables q^2 and θ_ℓ suffice. On the other hand, $\bar{B} \to \bar{K}^*(\to \bar{K}\pi)\ell^+\ell^-$ is a $1 \to 4$ decay. For its description three additional variables are needed. Following the literature [57] we choose θ_{K^*}, the angle between the final state kaon and $\bar{B}$ meson in the $\bar{K}^*$ rest frame, ϕ, the angle between the decay planes of the $\bar{K}$-π system and the lepton pair in the $\bar{B}$ rest frame, and finally k^2, the invariant mass of the $\bar{K}$-π system. The angles are schematically presented in Fig. 3.1. The full kinematically-accessible phase space is given by

$$4m_\ell^2 \leqslant q^2 \leqslant (M_B - M_K)^2\,, \qquad -1 \leqslant \cos\theta_\ell \leqslant 1 \tag{3.2}$$

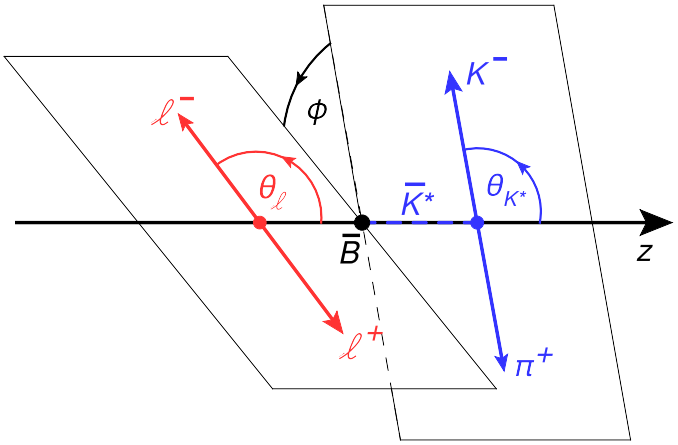

Figure 3.1.: Schematic of the kinematic angles within $\bar{B} \to \bar{K}^*(\to \bar{K}\pi)\ell^+\ell^-$ decays. Figure taken from Ref. [56].

for $\bar{B} \to \bar{K}\ell^+\ell^-$ decays, and by

$$4m_\ell^2 \leqslant q^2 \leqslant (M_B - M_{K^*})^2\,, \qquad -1 \leqslant \cos\theta_\ell \leqslant 1\,, \tag{3.3}$$

$$-1 \leqslant \cos\theta_{K^*} \leqslant 1\,, \qquad 0 \leqslant \phi \leqslant 2\pi \tag{3.4}$$

for $\bar{B} \to \bar{K}^*\ell^+\ell$ decays. No bounds on k^2 are given since we consider the K^* meson to decay on-shell, cf. also the details on the small width approximation in Section 3.4.1. In both cases, m_ℓ and M_B denote the mass of the charged leptons and the B meson, respectively. We further introduce the kinematic function

$$\lambda(a,b,c) \equiv a^2 + b^2 + c^2 - 2(ab + ac + bc)\,, \tag{3.5}$$

which is used to calculate spatial components of the used four-momenta. Furthermore, we use

$$\beta_\ell = \sqrt{1 - 4m_\ell^2/q^2} \tag{3.6}$$

to denote the lepton velocity in the dilepton rest frame.

3.2. Operator Product Expansion

As previously discussed in Section 2.4, the theory predictions for exclusive $b \to s\ell^+\ell^-$ processes suffer from pollution through intermediate quark loops, especially charm loops, which contribute via nonlocal electromagnetic coupling to the lepton current $j_\mu^{\text{e.m.}} \equiv -ie\bar{\ell}\gamma_\mu\ell$. Grinstein and Pirjol first noticed [55] that for low hadronic recoil this nonlocal contribution can be handled approximately like the inclusive production process $e^+e^- \to hadrons$, where an OPE applies for large center of mass energy [58]. In particular, they consider the four-momentum q^μ that flows through the intermediate

charm loop correlator. For a sufficiently slow moving final state hadron, $E_s - m \lesssim \Lambda$, which corresponds to a hard momentum q^μ, they find that the nonlocal contributions

$$\mathcal{T}_\mu^{(i)} = i \int \mathrm{d}^4x e^{iq\cdot x} \left\langle \bar{K}^* \right| T\left\{\mathcal{O}_i(0), j_\mu^{\mathrm{e.m.}}(x)\right\} \left|\bar{B}\right\rangle, \quad i = 1,\dots,6,8\,, \tag{3.7}$$

can be expanded simultaneously in the bottom quark mass m_b and the invariant dilepton mass $\sqrt{q^2}$ by means of the expansion

$$\mathcal{T}_\mu^{(i)}(q^2) = \sum_{k\geq -2}\sum_j C_{i,j}^{(k)}(q^2/m_b^2,\mu)\left\langle \mathcal{O}_j^{(k)}(\mu)\right\rangle_\mu . \tag{3.8}$$

Here, the effective operators $\mathcal{O}_j^{(k)}$ are power-suppressed by $1/Q^k$, where $Q = m_b, \sqrt{q^2}$, and the $C_{i,j}^{(k)}$ are the corresponding Wilson coefficients[1]. They find that contributions at leading order and power-suppressed terms of order m_c^2/Q^2 rely on the same hadronic matrix elements as the leading contributions from $\mathcal{O}_{7,9,10}$, which is in agreement with a later study [59]. Furthermore, all Λ/Q corrections that arise in the OPE are suppressed by an additional factor of α_s. The long-distance contributions up to $\mathcal{O}(\alpha_\mathrm{s}\Lambda/Q, \Lambda^2/Q^2)$ can therefore be absorbed into *effective Wilson coefficients* $\mathcal{C}_{7,9}^{\mathrm{eff}}$. In the notation of Ref. [60], these read

$$\begin{aligned}
\mathcal{C}_7^{\mathrm{eff}} &= \mathcal{C}_7 - \frac{1}{3}\left[\mathcal{C}_3 + \frac{4}{3}\mathcal{C}_4 + 20\,\mathcal{C}_5 + \frac{80}{3}\mathcal{C}_6\right] \\
&\quad + \frac{\alpha_s}{4\pi}\left[\left(\mathcal{C}_1 - 6\,\mathcal{C}_2\right)A(q^2) - \mathcal{C}_8 F_8^{(7)}(q^2)\right], \qquad (3.9)\\
\mathcal{C}_9^{\mathrm{eff}} &= \mathcal{C}_9 + h(0,q^2)\left[\frac{4}{3}\mathcal{C}_1 + \mathcal{C}_2 + \frac{11}{2}\mathcal{C}_3 - \frac{2}{3}\mathcal{C}_4 + 52\,\mathcal{C}_5 - \frac{32}{3}\mathcal{C}_6\right] \\
&\quad - \frac{1}{2}h(m_b,q^2)\left[7\,\mathcal{C}_3 + \frac{4}{3}\mathcal{C}_4 + 76\,\mathcal{C}_5 + \frac{64}{3}\mathcal{C}_6\right] + \frac{4}{3}\left[\mathcal{C}_3 + \frac{16}{3}\mathcal{C}_5 + \frac{16}{9}\mathcal{C}_6\right] \\
&\quad + \frac{\alpha_s}{4\pi}\left[\mathcal{C}_1\left(B(q^2) + 4\,C(q^2)\right) - 3\,\mathcal{C}_2\left(2\,B(q^2) - C(q^2)\right) - \mathcal{C}_8 F_8^{(9)}(q^2)\right] \qquad (3.10)\\
&\quad + 8\,\frac{m_c^2}{q^2}\left[\left(\frac{4}{9}\mathcal{C}_1 + \frac{1}{3}\mathcal{C}_2\right)(1+\hat{\lambda}_u) + 2\,\mathcal{C}_3 + 20\,\mathcal{C}_5\right]
\end{aligned}$$

and include the NLO QCD matching corrections and doubly Cabibbo-suppressed contributions [60] $\propto \hat{\lambda}_u = V_{ub}V_{us}^*/(V_{tb}V_{ts}^*)$. The latter give rise to CP violation in $b \to s\ell^+\ell^-$ transitions in the SM, which is tiny.

In the development of the OPE, Grinstein and Pirjol primarily use HQET [55]. Only in the final step, they reformulate their results in terms of QCD currents, which are obtained by reversing the NLO matching relations between QCD and HQET. Conversely, the study by Beylich *et al.* [59] formulates the expansion completely in terms of QCD currents. There, operators that involve covariant derivatives are removed by applying the QCD equations of motion. Furthermore, they explicitly compute some of the power-suppressed contributions, and find that isospin breaking effects arise only at the

[1] For details of the calculation, we refer the reader to Ref. [55]

$\mathcal{O}(\Lambda^3/Q^3)$ level and are thus negligible at the present level of both theoretical and experimental accuracy.

As mentioned above, the OPE is assumed to be valid for low hadronic recoil $E_s - m \lesssim \Lambda$ and up to duality violating effects. The latter are originally estimated [55] to be power corrections of the order Λ/Q. Beylich *et al.* studied the effects of local duality violation by applying a resonance model [61] to the nonlocal charm quark correlator that arises from Eq. (3.7). Their ansatz exhibits the well known effect of oscillating and exponentially decreasing contributions that is known from the behavior of the R factor [58],

$$R(q^2) = \frac{\mathrm{d}\sigma\left(e^+e^- \to \bar{q}q\right)/\mathrm{d}q^2}{\mathrm{d}\sigma\left(e^+e^- \to \mu^+\mu^-\right)/\mathrm{d}q^2}\,. \tag{3.11}$$

They conclude that integration over a sufficiently large part of the low recoil phase space smooths out most of the effects of local duality violation. As a lower bound $q^2 \geq 15\ \mathrm{GeV}^2$ is proposed, which excludes the $\psi(3770)$ resonance and lies above the threshold for open charm production [59]. Furthermore, they estimate the global duality violation (i.e., duality violation after integration) to be of the order of 2% [59].

However, the performance of the OPE can ultimately only be tested through experimental measurement. In Section 3.4 we therefore propose new observables $H_T^{(1,\ldots,5)}$, one of which ($H_T^{(1)}$) is designed to test the magnitude of local duality violation in the low recoil region.

3.3. Form Factors and the Improved Isgur-Wise Relations

The calculation of matrix elements for processes which involve quarks is complicated by the fact that QCD is only asymptotically free at large scales $\mu \gtrsim m_b$. Hadronization, however, is a process for which the typical scales are of the order Λ_{QCD}. Therefore, hadronization effects cannot be calculated in perturbative QCD. In order to cope with this problem in exclusive processes, one parametrizes the hadronic matrix elements of the various local currents in terms of so-called form factors. The hadronic matrix elements must fulfill a number of exact and approximate symmetries of QCD, such as symmetry under discrete Lorentz transformations or heavy quark symmetry, which can be used to reduce the number of independent form factors. By using symmetry under parity transformation and transversity of massive vector mesons, it is possible to restrict the set of independent hadronic matrix elements and parametrize them in terms of the hadronic momenta and polarization vectors. In this thesis, we only consider semileptonic decays of the form

$$\bar{B} \to \bar{K}\ell^+\ell^-\,, \qquad\qquad \bar{B} \to \bar{K}^*\ell^+\ell^-\,. \tag{3.12}$$

In the case of pseudoscalar mesons we can parametrize all nonvanishing hadronic matrix elements as [62]

$$\left\langle \bar{K}(k)\right| \bar{s}b \left|\bar{B}(p)\right\rangle = \frac{M_B^2 - M_K^2}{m_b + m_s} f_0^{BK}(q^2)\,, \tag{3.13}$$

$$\left\langle \bar{K}(k)\right| \bar{s}\gamma_\mu b \left|\bar{B}(p)\right\rangle = f_+^{BK}(q^2)(p+k)_\mu + \left[f_0^{BK}(q^2) - f_+^{BK}(q^2)\right] \frac{M_B^2 - M_K^2}{q^2} q_\mu\,, \tag{3.14}$$

$$\left\langle \bar{K}(k)\right| \bar{s}\sigma_{\mu\nu} b \left|\bar{B}(p)\right\rangle = i\frac{f_T^{BK}(q^2)}{M_B + M_K}\left[(p+k)_\mu q_\nu - q_\mu (p+k)_\nu\right]\,. \tag{3.15}$$

with independent form factors functions $f_i^{BK}(q^2)$. The QCD equation of motion for the quark fields,

$$i\not{D} q(x) = m_q q(x)\,, \tag{3.16}$$

provides an exact relation between the scalar current in Eq. (3.13) and the vector current in Eq. (3.14), thereby reducing the number of independent form-factors to three. Similarly, one obtains for pseudoscalar-to-vector transitions [63], such as in $\bar{B} \to \bar{K}^*$ and $\bar{B}_s \to \phi$, the parametrization

$$\langle V(k,\eta)|\, \bar{q}\gamma_5 b\, |B(p)\rangle = \frac{2iM_V}{m_s - m_b}(\eta^*\cdot q) A_0(q^2)\,, \tag{3.17}$$

$$\langle V(k,\eta)|\, \bar{q}\gamma_\mu b\, |B(p)\rangle = \frac{2V(q^2)}{M_B + M_V}\varepsilon_{\mu\rho\sigma\tau}\eta^{*\rho} p^\sigma k^\tau\,, \tag{3.18}$$

$$\begin{aligned}\langle V(k,\eta)|\, \bar{q}\gamma_\mu\gamma_5 b\, |B(p)\rangle = i\eta^{*\rho}\Bigg[&2M_V A_0(q^2)\frac{q_\mu q_\rho}{q^2} \\ &+ (M_B + M_V) A_1(q^2)\left(g_{\mu\rho} - \frac{q_\mu q_\rho}{q^2}\right) \\ &- A_2(q^2)\frac{q_\rho}{M_B + M_V}\left((p+k)_\mu - \frac{M_B^2 - M_V^2}{q^2}(p-k)_\mu\right)\Bigg]\,,\end{aligned} \tag{3.19}$$

$$\langle V(k,\eta)|\, \bar{q} i\sigma_{\mu\nu} q^\nu b\, |B(p)\rangle = -2T_1(q^2)\varepsilon_{\mu\rho\sigma\tau}\eta^{*\rho} p^\sigma k^\tau\,, \tag{3.20}$$

$$\begin{aligned}\langle V(k,\eta)|\, \bar{q} i\sigma_{\mu\nu}\gamma_5 q^\nu b\, |B(p)\rangle = {}& iT_2(q^2)\left(\eta_\mu^*(M_B^2 - M_V^2) - (\eta^*\cdot q)(p+k)_\mu\right) \\ &+ iT_3(q^2)\,(\eta^*\cdot q)\left(q_\mu - \frac{q^2}{M_B^2 - M_V^2}(p+k)_\mu\right)\,.\end{aligned} \tag{3.21}$$

Here Eq. (3.16) has, again, been used to express the hadronic matrix element of the pseudoscalar current in terms of the form factor A_0, which also contributes to the hadronic matrix element of the axial vector current. Note that by parity invariance the hadronic matrix element $\langle V(k,\eta)|\, \bar{q} b\, |B(p)\rangle = 0$. For large hadronic recoil, one can apply both an expansion in $1/M_B$ and use Large Energy Effective Theory [64], thereby reducing the number of independent hadronic matrix elements further from seven to two *universal soft form factors*, cf. Appendix B. The validity of these relations is given, as long as q^2 is not too close to the zero-recoil point. Unfortunately, the latter condition renders them unusable for studying the low recoil region.

In order to find further relations between the individual form factor functions for both decays, we employ the operator identity

$$i\partial^\nu(\bar{s}i\sigma_{\mu\nu}b) = -m_b\bar{s}\gamma_\mu b + i\partial_\mu(\bar{s}b) - 2\bar{s}i\overleftarrow{D}_\mu b\,, \tag{3.22}$$

with m_b, the $\overline{\text{MS}}$ mass of the b quark, and where we neglect terms proportional to m_s, the strange quark mass. Eq. (3.22) follows directly from Eq. (3.16). By taking the hadronic matrix elements of both sides of Eq. (3.22) in the case of $\bar{B} \to \bar{K}^*$ ($\bar{B} \to \bar{K}$) transitions, one obtains an exact relation [55, 44, 45] between the dipole form factors T_1, T_2, T_3 (f_T), the axial vector and vector form factors V, A_1, A_2 (f_+, f_0) and the matrix elements of the dimension-4 current $\bar{s}\overleftarrow{D}_\mu b$. In a further step, the relations are expanded simultaneously in $1/Q$, $Q = m_b, \sqrt{q^2}$. For $\bar{B} \to \bar{K}^*$ transitions, the results for the improved Isgur-Wise relations of the dipole form factors read [44]

$$\begin{aligned} T_1(q^2) &= \kappa V(q^2) + \mathcal{O}\left(\frac{\Lambda}{Q}\right), \qquad & T_2(q^2) &= \kappa A_1(q^2) + \mathcal{O}\left(\frac{\Lambda}{Q}\right), \\ T_3(q^2) &= \kappa A_2(q^2)\frac{M_B^2}{q^2} + \mathcal{O}\left(\frac{\Lambda}{Q}\right), \end{aligned} \tag{3.23}$$

in agreement with previous works [55]. We note here that the kinematical factor M_B^2/q^2 in the results for T_3 is of order one in the expansion in $1/Q$ and therefore kept. However, preliminary results from LQCD [65] suggest that large corrections for T_3 can arise, cf. Appendix B. Furthermore, for $\bar{B} \to \bar{K}$ transitions the dipole form factor reads [45]

$$f_T^{BK}(q^2,\mu) = \frac{M_B\,(M_B + M_K)}{q^2}\left[\kappa(\mu)\, f_+^{BK}(q^2) + \mathcal{O}\left(\frac{\Lambda}{m_b}\right)\right], \tag{3.24}$$

which agrees with the result in [66]. We remark that in Eq. (3.23) and Eq. (3.24) we neglect the mass of the strange quark m_s and HQET form factors that are subleading in the expansion in $1/Q$. We use further a common scale-dependent factor

$$\kappa(\mu) = \left(1 + 2\,\frac{D_0^{(v)}(\mu)}{C_0^{(v)}(\mu)}\right)\frac{m_b(\mu)}{M_B}\,, \tag{3.25}$$

which reflects the renormalization scale dependence of the dipole form factors. Here, we employ the HQET Wilson coefficients $C_0^{(v)}, D_0^{(v)}$ [55]

$$\bar{s}\gamma_\mu b = C_0^{(v)}\bar{s}\gamma_\mu h_v + C_1^{(v)}\bar{s}v_\mu h_v + \mathcal{O}\left(1/m_b\right), \tag{3.26}$$

$$\bar{s}i\overleftarrow{D}_\mu b = D_0^{(v)} m_b\bar{s}\gamma_\mu h_v + D_1^{(v)} m_b\bar{q}v_\mu h_v + \bar{q}i\overleftarrow{D}_\mu h_v + \mathcal{O}\left(1/m_b\right), \tag{3.27}$$

which can be calculated perturbatively. Using their perturbative results to NLO in α_s [55, 32], we obtain

$$\kappa = 1 - 2\,\frac{\alpha_s}{3\pi}\ln\left(\frac{\mu}{m_b}\right). \tag{3.28}$$

The performance of the improved Isgur-Wise relations given in Eq. (3.23) and Eq. (3.24) is subject to a detailed analysis in the Appendices B and C, respectively, where the relations are confronted with theory inputs from both LCSR and LQCD.

For $B \to K^*$ at low recoil, we find that the application of the improved Isgur-Wise relations drastically simplifies the structure of the hadronic matrix elements. In particular, it leaves only dependences on the following combinations of hadronic form factors

$$f_\perp(q^2) = \frac{\sqrt{2\lambda}}{M_B + M_K^*} V(q^2)\,, \tag{3.29}$$

$$f_\parallel(q^2) = \sqrt{2}(M_B + M_{K^*}) A_1(q^2)\,, \tag{3.30}$$

$$f_0(q^2) = \frac{(M_B^2 - M_{K^*}^2 - q^2)(M_B + M_{K^*})^2 A_1(q^2) - \lambda A_2(q^2)}{2M_{K^*}(M_B + M_{K^*})\sqrt{q^2}}\,, \tag{3.31}$$

which are further used in Section 3.4.1, and where $\lambda \equiv \lambda(M_B^2, M_{K^{(*)}}^2, q^2)$. The indices 0, $\perp$ and $\parallel$ here indicate that the dilepton pair the final state vector meson are in a state of angular momentum $J = 0, 1, 2$, respectively, and correspond to the indices of the transversity basis, cf. also Appendix A. Therefore, these combinations also arise when expressing $B_{d,s} \to \{K^*, \phi, \rho\}$ form factors in the helicity basis [67].

3.4. The Decay $\bar{B} \to \bar{K}^*\ell^+\ell^-$

We continue by studying the angular distribution of $\bar{B} \to \bar{K}^*\ell^+\ell^-$ decays in Section 3.4.1, and subsequently use it in the examination of existing observables (Section 3.4.2). After that, we turn to the construction and study of new observables in the low recoil region, within the SM (Section 3.4.3) and beyond (Sections 3.4.4-3.4.6). We conclude our studies on the phenomenology of $\bar{B} \to \bar{K}^*\ell^+\ell^-$ decays by examining the sensitivity of the low recoil observables towards small NP effects in Section 3.4.7.

3.4.1. Angular Distribution

We calculate the decay amplitude for the resonant production of an intermediate (real) $\bar{K}^*$ meson[2], and thus parametrize the propagator of the K^* as

$$D^{\mu\nu}_{K^*} = \frac{-i\left(g^{\mu\nu} - \frac{k^\mu k^\nu}{k^2}\right)}{k^2 - M^2_{K^*} + iM_{K^*}\Gamma_{K^*}}\,, \tag{3.32}$$

where we employ Γ_{K^*}, the decay width of $K^* \to K\pi$,

$$\Gamma_{K^*} = \frac{g^2_{K^*K\pi}}{6\pi} M_{K^*} |\vec{p}_K|^3 \tag{3.33}$$

as given, e.g., in Ref. [69], with the the effective coupling $g_{K^*K\pi}$, and the momentum of the kaon in the K^* rest frame $|\vec{p}_K|$ as given in Eq. (A.3). Then, we apply the small-width approximation

$$\frac{1}{(k^2 - M^2_{K^*})^2 + M^2_{K^*}\Gamma^2_{K^*}} \mapsto \frac{1}{M_{K^*}\Gamma_{K^*}} \delta\left(k^2 - M^2_{K^*}\right) \tag{3.34}$$

to the square of the matrix element, thereby removing the dependence on $g_{K^*K\pi}$ and restricting k^2 to $M^2_{K^*}$, the mass square of the $K^*(892)$ vector meson. We arrive at the complete differential decay width

$$\frac{\mathrm{d}^4\Gamma}{\mathrm{d}q^2 \mathrm{d}\cos\theta_\ell \mathrm{d}\cos\theta_{K^*} \mathrm{d}\phi} = \frac{3}{8\pi} J(q^2, \cos\theta_\ell, \cos\theta_{K^*}, \phi), \tag{3.35}$$

The dependence of the decay distribution in Eq. (3.35) on the angles θ_ℓ, θ_{K^*} and ϕ can be made explicit as

$$\begin{aligned} J(q^2, \theta_\ell, \theta_{K^*}, \phi) = {} & J_{1s}\sin^2\theta_{K^*} + J_{1c}\cos^2\theta_{K^*} + (J_{2s}\sin^2\theta_{K^*} + J_{2c}\cos^2\theta_{K^*})\cos 2\theta_\ell \\ & + J_3 \sin^2\theta_{K^*}\sin^2\theta_\ell \cos 2\phi + J_4 \sin 2\theta_{K^*}\sin 2\theta_\ell \cos\phi \\ & + J_5 \sin 2\theta_{K^*}\sin\theta_\ell \cos\phi + J_{6s}\sin^2\theta_{K^*}\cos\theta_\ell + J_{6c}\cos^2\theta_{K^*}\cos\theta_\ell \\ & + J_7 \sin 2\theta_{K^*}\sin\theta_\ell \sin\phi + J_8 \sin 2\theta_{K^*}\sin 2\theta_\ell \sin\phi \\ & + J_9 \sin^2\theta_{K^*}\sin^2\theta_\ell \sin 2\phi, \end{aligned} \tag{3.36}$$

where the angular coefficients $J_{i(a)} \equiv J_{i(a)}(q^2)$ for $i = 1, \ldots, 9$ and $a = s, c$ are functions of the dilepton mass.

[2] For nonresonant decays $\bar{B} \to \bar{K}_J(\to \bar{K}^-\pi^+)\ell^+\ell^-$, cf. Ref. [68]

When considering contributions from all operators within the SM' basis, we derive the following structure of the angular coefficients:

$$\begin{aligned}\frac{4}{3}J_{1s} &= \frac{2+\beta_\ell^2}{4}\left[|A_\perp^L|^2+|A_\parallel^L|^2+(L\leftrightarrow R)\right]+\frac{4m_\ell^2}{q^2}\,\mathrm{Re}\Big\{A_\perp^L A_\perp^{R*}+A_\parallel^L A_\parallel^{R*}\Big\}\\ &\quad+4\beta_\ell^2\left(|A_{0\perp}|^2+|A_{0\parallel}|^2\right)+(16-12\beta_\ell^2)\left(|A_{t\perp}|^2+|A_{t\parallel}|^2\right)\\ &\quad+8m_\ell\sqrt{\frac{2}{q^2}}\,\mathrm{Re}\Big\{\left(A_\parallel^L+A_\parallel^R\right)A_{t\parallel}^*-\left(A_\perp^L+A_\perp^R\right)A_{t\perp}^*\Big\}\end{aligned} \tag{3.37}$$

$$\begin{aligned}\frac{4}{3}J_{1c} &= |A_0^L|^2+|A_0^R|^2+\frac{4m_\ell^2}{q^2}\left[|A_t|^2+2\,\mathrm{Re}\{A_0^L A_0^{R*}\}\right]+\beta_\ell^2|A_S|^2\\ &\quad+(16-8\beta_\ell^2)|A_{t0}|^2+8\beta_\ell^2|A_{\parallel\perp}|^2+16\frac{m_\ell}{\sqrt{q^2}}\mathrm{Re}\{(A_0^L+A_0^R)A_{t0}^*\}\end{aligned} \tag{3.38}$$

$$\frac{4}{3}J_{2s} = \frac{\beta_\ell^2}{4}\Big[|A_\perp^L|^2+|A_\parallel^L|^2+(L\leftrightarrow R)-16\left(|A_{t\perp}|^2+|A_{t\parallel}|^2+|A_{0\perp}|^2+|A_{0\parallel}|^2\right)\Big] \tag{3.39}$$

$$\frac{4}{3}J_{2c} = -\beta_\ell^2\left[|A_0^L|^2+|A_0^R|^2-8\left(|A_{t0}|^2+|A_{\parallel\perp}|^2\right)\right] \tag{3.40}$$

$$\frac{4}{3}J_3 = \frac{\beta_\ell^2}{2}\Big[|A_\perp^L|^2-|A_\parallel^L|^2+(L\leftrightarrow R)+16\left(|A_{t\parallel}|^2-|A_{t\perp}|^2+|A_{0\parallel}|^2-|A_{0\perp}|^2\right)\Big] \tag{3.41}$$

$$\frac{4}{3}J_4 = \frac{\beta_\ell^2}{\sqrt{2}}\,\mathrm{Re}\Big\{A_0^L A_\parallel^{L*}+(L\leftrightarrow R)-8\sqrt{2}\left(A_{t0}A_{t\parallel}^*\right)+A_{\parallel\perp}A_{0\parallel}^*\Big\} \tag{3.42}$$

$$\begin{aligned}\frac{4}{3}J_5 &= \sqrt{2}\beta_\ell\,\mathrm{Re}\Big\{A_0^L A_\perp^{L*}-(L\leftrightarrow R)-2\sqrt{2}A_{t\parallel}A_S^*\\ &\quad-\frac{m_\ell}{\sqrt{q^2}}\Big[\left(A_\parallel^L+A_\parallel^R\right)A_S^*+4\sqrt{2}A_{0\parallel}A_t^*+4\sqrt{2}\left(A_0^L-A_0^R\right)A_{t\perp}^*-4\left(A_\perp^L-A_\perp^R\right)A_{t0}^*\Big]\Big\}\end{aligned} \tag{3.43}$$

$$\begin{aligned}\frac{4}{3}J_{6s} &= 2\beta_\ell\,\mathrm{Re}\Big\{A_\parallel^L A_\perp^{L*}-(L\leftrightarrow R)\\ &\quad+4m_\ell\sqrt{\frac{2}{q^2}}\left[\left(A_\perp^L-A_\perp^R\right)A_{t\parallel}^*-\left(A_\parallel^L-A_\parallel^R\right)A_{t\perp}^*\right]\Big\}\end{aligned} \tag{3.44}$$

$$\frac{4}{3}J_{6c} = 4\beta_\ell\,\mathrm{Re}\left\{2A_{t0}A_S^*+\frac{m_\ell}{\sqrt{q^2}}\left[\left(A_0^L+A_0^R\right)A_S^*+4A_{\parallel\perp}A_t^*\right]\right\} \tag{3.45}$$

$$\begin{aligned}\frac{4}{3}J_7 &= \sqrt{2}\beta_\ell\,\mathrm{Im}\Big\{A_0^L A_\parallel^{L*}-(L\leftrightarrow R)-2\sqrt{2}A_{t\perp}A_S^*\\ &\quad+\frac{m_\ell}{\sqrt{q^2}}\Big[\left(A_\perp^L+A_\perp^R\right)A_S^*+4\sqrt{2}A_{0\perp}A_t^*+4\sqrt{2}\left(A_0^L-A_0^R\right)A_{t\parallel}^*-4\left(A_\parallel^L-A_\parallel^R\right)A_{t0}^*\Big]\Big\}\end{aligned} \tag{3.46}$$

$$\frac{4}{3}J_8 = \frac{\beta_\ell^2}{\sqrt{2}}\,\mathrm{Im}\Big\{A_0^L A_\perp^{L*}+(L\leftrightarrow R)+8\sqrt{2}\left[A_{0,\perp}A_{\parallel\perp}^*-A_{t\perp}A_{t0}^*\right]\Big\} \tag{3.47}$$

$$\frac{4}{3}J_9 = \beta_\ell^2\,\mathrm{Im}\Big\{A_\perp^L A_\parallel^{L*}+(L\leftrightarrow R)+16\left(A_{t\perp}A_{t\parallel}^*-A_{0\perp}A_{0\parallel}^*\right)\Big\}\,. \tag{3.48}$$

Within Eqs. (3.37)-(3.48) we express the $\bar{B}\to\bar{K}^*(\to\bar{K}\pi)\ell^+\ell^-$ matrix element in terms

of the well-known transversity amplitudes [57]

$$A_\perp^{L,R} = \sqrt{2}N\sqrt{\lambda}\left\{\left[\left(\mathcal{C}_9+\mathcal{C}_9'\right) \mp \left(\mathcal{C}_{10}+\mathcal{C}_{10}'\right)\right]\frac{V}{M_B+M_{K^*}} + \frac{2M_b}{q^2}\left(\mathcal{C}_7+\mathcal{C}_7'\right)T_1\right\} \tag{3.49}$$

$$\begin{aligned} A_\parallel^{L,R} &= -N\sqrt{2}(M_B^2-M_{K^*}^2) \\ &\quad\times\left\{\left[\left(\mathcal{C}_9-\mathcal{C}_9'\right) \mp \left(\mathcal{C}_{10}-\mathcal{C}_{10}'\right)\right]\frac{A_1}{M_B-M_{K^*}} + \frac{2m_b}{q^2}\left(\mathcal{C}_7-\mathcal{C}_7'\right)T_2\right\}, \end{aligned} \tag{3.50}$$

$$\begin{aligned} A_0^{L,R} &= -\frac{N}{2M_{K^*}^2\sqrt{q^2}}\Big\{\left[\left(\mathcal{C}_9-\mathcal{C}_9'\right) \mp \left(\mathcal{C}_{10}-\mathcal{C}_{10}'\right)\right] \\ &\quad\times\left[(M_B^2-M_{K^*}^2-q^2)(M_B+M_{K^*})A_1 - \frac{\lambda}{M_B+M_{K^*}}A_2\right] \\ &\quad+\frac{2m_b}{q^2}\left(\mathcal{C}_7-\mathcal{C}_7'\right)\left[\left(M_B^2+3M_{K^*}^2-q^2\right)T_2 - \frac{\lambda}{M_B^2-M_{K^*}^2}T_3\right]\Big\}, \end{aligned} \tag{3.51}$$

$$A_t = N\left[2\left(\mathcal{C}_{10}-\mathcal{C}_{10}'\right) + \frac{q^2}{m_\ell\left(m_b+m_s\right)}\left(\mathcal{C}_P-\mathcal{C}_P'\right)\right]\sqrt{\frac{\lambda}{q^2}}A_0\,, \tag{3.52}$$

which are obtained by assuming factorization. Results for both the large recoil and the low recoil region can be found by replacing $\mathcal{C}_{7,9}$ with the respective effective Wilson coefficients $\mathcal{C}_{7,9}^{\text{eff}}$. Additionally, we use the scalar amplitude

$$A_S = -2N\left(\mathcal{C}_S-\mathcal{C}_S'\right)\frac{\sqrt{\lambda}}{m_b+m_s}A_0\,, \tag{3.53}$$

which was introduced in [69]. Their recent erratum[3] agrees with our result. Moreover, we introduce [70] the tensorial transversity amplitudes

$$A_{0\perp\,(t\perp)} = 2N\mathcal{C}_{T(T5)}\sqrt{\frac{\lambda}{q^2}}T_1\,, \tag{3.54}$$

$$A_{0\parallel\,(t\parallel)} = 2N\mathcal{C}_{T(T5)}\frac{M_B^2-M_{K^*}^2}{\sqrt{q^2}}T_2\,, \tag{3.55}$$

$$A_{\parallel\perp\,(t0)} = N\mathcal{C}_{T(T5)}\frac{1}{M_{K^*}}\left[\left(M_B^2+3M_{K^*}^2-q^2\right)T_2 - \frac{\lambda}{M_B^2-M_{K^*}^2}T_3\right], \tag{3.56}$$

which arise only after introducing the operators $\mathcal{O}_{T,T5}$. Here, the two indices denote the transversity state of the two polarization vectors which comprise the rank-two polarization tensor used in the calculation. The individual transversity states combine to angular momenta $J = 0, 1, 2$ for the indices $(\parallel\perp, t0)$, $(0\ \perp, t\ \perp)$ and $(0\ \parallel, t\ \parallel)$, respectively. For the definition of the tensorial amplitudes, cf. also Eq. (A.1). The normalization factor N that is used in all of the above amplitudes reads

$$N = G_{\text{F}}\alpha_e V_{tb}V_{ts}^*\sqrt{\frac{\beta_\ell q^2\sqrt{\lambda}}{3\cdot 2^{10}\pi^5 M_B^3}}\,. \tag{3.57}$$

[3] We refer here to revision v5 or later of the arXiv eprint.

For details on our parametrization of the hadronic matrix element in terms of the transversity amplitudes, especially regarding the newly introduced tensorial amplitudes, we refer the reader to Appendix A.

In order to further study the behavior at low recoil, we now apply the improved Isgur-Wise form factor relations Eq. (3.23) to the transversity amplitudes. By doing so, we reduce the dependence on hadronic matrix elements from seven to four independent form factors, up to corrections of order Λ/Q. From this we obtain the transversity amplitudes at low recoil

$$A_0^{L(R)} = -NC_-^{L(R)} f_0 \,, \tag{3.58}$$

$$A_\parallel^{L(R)} = -NC_-^{L(R)} f_\parallel \,, \tag{3.59}$$

$$A_\perp^{L(R)} = +NC_+^{L(R)} f_\perp \,, \tag{3.60}$$

with the short-distance coefficients

$$C_-^{L(R)} = \left(\left(\mathcal{C}_9^{\text{eff}} - \mathcal{C}_9' \right) + \kappa \frac{2 m_b M_B}{q^2} \left(\mathcal{C}_7^{\text{eff}} - \mathcal{C}_7' \right) \right) \mp \left(\mathcal{C}_{10} - \mathcal{C}_{10}' \right) \,, \tag{3.61}$$

$$C_+^{L(R)} = \left(\left(\mathcal{C}_9^{\text{eff}} + \mathcal{C}_9' \right) + \kappa \frac{2 m_b M_B}{q^2} \left(\mathcal{C}_7^{\text{eff}} + \mathcal{C}_7' \right) \right) \mp \left(\mathcal{C}_{10} + \mathcal{C}_{10}' \right) \,. \tag{3.62}$$

Here, we also make use of the low recoil OPE and replace $\mathcal{C}_{7,9} \mapsto \mathcal{C}_{7,9}^{\text{eff}}$. For the tensorial transversity amplitudes, we obtain

$$A_{0\perp\,(t\perp)} = \sqrt{2} N \kappa \mathcal{C}_{T(T5)} \frac{M_B + M_{K^*}}{\sqrt{q^2}} f_\perp \,, \tag{3.63}$$

$$A_{0\parallel\,(t\parallel)} = \sqrt{2} N \kappa \mathcal{C}_{T(T5)} \frac{M_B - M_{K^*}}{\sqrt{q^2}} f_\parallel \,, \tag{3.64}$$

$$A_{\parallel\perp\,(t0)} = 2 N \kappa \mathcal{C}_{T(T5)} \frac{M_B + M_{K^*}}{\sqrt{q^2}} f_0 \,. \tag{3.65}$$

The amplitudes A_t and A_S depend only on the form factor A_0 and remain the same as in Eq. (3.52) and Eq. (3.53), respectively.

3.4.2. Observables in the SM basis

While the angular decomposition of the $\bar{B} \to \bar{K}^* \ell^+ \ell^-$ decay rate provides with the J_i a set of well-defined observables in their own right, their theory predictions suffer strongly from the uncertainties of the hadronic form factors, the partially unknown subleading contributions of order Λ/M_B, and the uncertainties of the Wolfenstein parameters of the CKM matrix. Much effort has therefore been dedicated toward finding more sophisticated observables which are theoretically cleaner [69, 71]. As far as spin-averaged measurements are concerned, all of these observables can be expressed as functions of the J_i, whereby the aforementioned dominant theoretical uncertainties may cancel in parts or even completely.

We start with the single-differential decay rate $\mathrm{d}\Gamma/\mathrm{d}q^2$, which can be written as

$$\mathrm{d}\Gamma/\mathrm{d}q^2 = 2J_{1s} + J_{1c} - \frac{2J_{2s} + J_{2c}}{3} \,. \tag{3.66}$$

No cancellations between uncertainties occur, and thus the decay rate suffers from the same theoretical problems as the J_i themselves. However, there are further observables, two of which are inspired by the double-differential decay rates

$$\frac{\mathrm{d}\Gamma}{\mathrm{d}\cos\theta_l \mathrm{d}q^2} = \frac{1}{2}\Big(2J_{1s} + J_{1c} + \big[2J_{6s} + J_{6c}\big]\cos\theta_l + \big[2J_{2s} + J_{2c}\big]\cos 2\theta_l\Big), \tag{3.67}$$

$$\frac{\mathrm{d}\Gamma}{\mathrm{d}\cos\theta_{K^*} \mathrm{d}q^2} = \frac{3}{2}\Big(\Big[J_{1s} - \frac{1}{3}J_{2s}\Big]\sin^2\theta_{K^*} + \Big[J_{1c} - \frac{1}{3}J_{2c}\Big]\cos^2\theta_{K^*}\Big). \tag{3.68}$$

From Eq. (3.67) one can infer the observable

$$A_{\mathrm{FB}}(q^2) \equiv \frac{1}{\mathrm{d}\Gamma/\mathrm{d}q^2}\left[\int_{-1}^{0} - \int_{0}^{+1}\right]\mathrm{d}\cos\theta_\ell \frac{\mathrm{d}\Gamma}{\mathrm{d}\cos\theta_l \mathrm{d}q^2} = \frac{J_{6s} + \frac{1}{2}J_{6c}}{\mathrm{d}\Gamma/\mathrm{d}q^2}\,, \tag{3.69}$$

which denotes the forward-backward asymmetry of the negatively charged lepton with regard to the B meson direction within the dilepton center of mass frame. Furthermore, within Eq. (3.68) the term $\propto \cos^2\theta_{K^*}$ collects all contributions that stem from longitudinally polarized $\bar{K}^*$ states. This can be readily inferred from Eqs. (A.4)-(A.7) where the amplitudes $A_S, A_t, A_0^{L(R)}$, $A_{\parallel\perp}$ and A_{t0} only enter in combination with a factor of $\cos\theta_{K^*}$. One can therefore model-independently define two observables, see Eq. (3.68), which read

$$F_L \equiv \frac{J_{1c} - \frac{1}{3}J_{2c}}{\mathrm{d}\Gamma/\mathrm{d}q^2}\,, \qquad F_T \equiv \frac{1}{2}\frac{J_{1s} - \frac{1}{3}J_{2s}}{\mathrm{d}\Gamma/\mathrm{d}q^2}\,, \qquad F_L + F_T = 1\,, \tag{3.70}$$

which are the fraction of longitudinally (transversally) polarized $\bar{K}^*$ mesons. Hence,

$$\frac{1}{\mathrm{d}\Gamma/\mathrm{d}q^2}\frac{\mathrm{d}\Gamma}{\mathrm{d}\cos\theta_{K^*}\,\mathrm{d}q^2} = \frac{3}{2}F_L\cos^2\theta_{K^*} + \frac{3}{4}(1 - F_L)\sin^2\theta_{K^*}\,. \tag{3.71}$$

When further assuming $m_\ell = 0$ and within the SM′ basis of operators, one finds $J_{1s} = 3J_{2s}$ and $J_{1c} = -J_{2c}$, and we can therefore write

$$\frac{1}{\mathrm{d}\Gamma/\mathrm{d}q^2}\frac{\mathrm{d}\Gamma}{\mathrm{d}\cos\theta_l\,\mathrm{d}q^2} = \frac{3}{4}F_L(1 - \cos^2\theta_l) + \frac{3}{8}(1 - F_L)(1 + \cos^2\theta_l) + A_{\mathrm{FB}}\cos\theta_l\,. \tag{3.72}$$

This parametrization is used in the most recent experimental studies by BaBar [72], Belle [46], CDF [47] and LHCb [42]. Using the same assumption, we find that the triple-differential decay rate

$$\begin{aligned}\frac{1}{\mathrm{d}\Gamma/\mathrm{d}q^2}\frac{\mathrm{d}^3\Gamma}{\mathrm{d}\cos\theta_\ell\,\mathrm{d}\cos\theta_{K^*}\,\mathrm{d}q^2} = \frac{3}{4}\Big\{&(J_{1s} + J_{6s}\cos\theta_\ell + J_{2s}\cos 2\theta_\ell)\sin^2\theta_{K^*} \\ &+ (J_{1c} + J_{6c}\cos\theta_\ell + J_{2c}\cos 2\theta_\ell)\cos^2\theta_{K^*}\Big\}\end{aligned} \tag{3.73}$$

can also be expressed in terms of $F_L, F_T, A_{\mathrm{FB}}$,

$$\begin{aligned}\frac{1}{\mathrm{d}\Gamma/\mathrm{d}q^2}\frac{\mathrm{d}^2\Gamma}{\mathrm{d}\cos\theta_l\,\mathrm{d}\cos\theta_K\,\mathrm{d}q^2} = \frac{3}{4}\Big\{&\frac{3}{4}F_L(1 - \cos 2\theta_l)\cos^2\theta_K \\ &+ \left(\frac{3}{16}F_T(3 + \cos 2\theta_l) + A_{\mathrm{FB}}\cos\theta_l\right)\sin^2\theta_K\Big\}\,.\end{aligned} \tag{3.74}$$

In addition, so called transverse asymmetries $A_T^{(i)}$, $i = 2, \ldots, 5$ have been constructed for the large recoil region [71] in order to probe right-handed currents. Their definition in terms of the transversity amplitudes[4] reads

$$A_T^{(2)} \equiv \frac{|A_\perp^L|^2 + |A_\perp^R|^2 - |A_\parallel^L|^2 - |A_\parallel^R|^2}{|A_\perp^L|^2 + |A_\perp^R|^2 + |A_\parallel^L|^2 + |A_\parallel^R|^2} = \frac{1}{2}\frac{J_3}{J_{2s}}\,, \tag{3.75}$$

$$A_T^{(3)} \equiv \frac{|A_0^L A_\parallel^{L*} + A_0^{R*} A_\parallel^R|}{\sqrt{\left(|A_0^L|^2 + |A_0^R|^2\right)\left(|A_\perp^L|^2 + |A_\perp^R|^2\right)}} = \sqrt{\frac{4J_4^2 + \beta_l^2 J_7^2}{-2J_{2c}(2J_{2s} + J_3)}}\,, \tag{3.76}$$

$$A_T^{(4)} \equiv \frac{|A_0^L A_\perp^{L*} - A_0^{R*} A_\perp^R|}{|A_0^{L*} A_\parallel^L + A_0^R A_\parallel^{R*}|} = \sqrt{\frac{\beta_l^2 J_5^2 + 4J_8^2}{4J_4^2 + \beta_l^2 J_7^2}}\,, \tag{3.77}$$

$$A_T^{(5)} \equiv \frac{|A_\perp^L A_\parallel^{L*} - A_\perp^{R*} A_\parallel^L|}{|A_\perp^L|^2 + |A_\perp^R|^2 + |A_\parallel^L|^2 + |A_\parallel^R|^2} = \frac{\sqrt{16J_{1s}^2 - 9J_{6s}^2 - 36\left(J_3^2 + J_9^2\right)}}{8J_{1s}}\,. \tag{3.78}$$

The representation of the transverse asymmetries as functions of the J_i holds only approximately, i.e., it holds for $m_\ell = 0$ and within the SM' basis of operators. These observables benefit from strongly reduced uncertainties at large hadronic recoil [71] and essentially encode short-distance information only. Furthermore, they exhibit a large sensitivity to NP effects from right-handed currents. However, when turning to the low recoil end of the spectrum, we find a distinctively different behavior which will be discussed in the following section.

3.4.3. Low Recoil Observables in the SM Basis

As shown in Eqs. (3.58)-(3.60), at low recoil and in the SM' basis the transversity amplitudes $A_{\parallel,\perp,0}^{L(R)}$ factorize into common short-distance factors $C_\pm^{L,R}$, which depend on the leptons' helicities, and functions f_i, which depend on the hadronic matrix element and kinematic quantities. In the SM basis, the short-distance factors further unify $C_\pm^{L(R)} \overset{\mathcal{C}_i' \to 0}{\to} C^{L(R)}$, where

$$C^{L,R} = \left(\mathcal{C}_9^{\text{eff}} + \kappa \frac{2\,m_b^2}{q^2}\mathcal{C}_7^{\text{eff}}\right) \mp \mathcal{C}_{10}\,. \tag{3.79}$$

Since the J_i parametrize the rate of the spin-averaged decay, it follows that only two combinations of the $C^{L,R}$ can occur. These are

$$|C^L|^2 + |C^R|^2 \equiv 2\rho_1\,, \tag{3.80}$$

$$|C^L|^2 - |C^R|^2 \equiv 4\rho_2\,, \tag{3.81}$$

[4] The transverse asymmetry $A_T^{(1)}$ will not be discussed in this work, since its definition relies on the measurement of the lepton helicities. Therefore it cannot be expressed in terms of the J_i at all, since the latter parametrize the spin-averaged decay rate.

which in turn yield for the angular observables

$$\frac{4}{3\beta_\ell^2}(2J_2^s + J_3) = 2\rho_1 f_\perp^2\,, \qquad \frac{4\sqrt{2}}{3\beta_\ell^2}J_4 = 2\rho_1 f_0 f_\parallel\,, \qquad J_7 = 0\,, \tag{3.82}$$

$$\frac{4}{3\beta_\ell^2}(2J_2^s - J_3) = 2\rho_1 f_\parallel^2\,, \qquad \frac{2\sqrt{2}}{3\beta_\ell}J_5 = 2\rho_2 f_0 f_\perp\,, \qquad J_8 = 0\,, \tag{3.83}$$

$$-\frac{4}{3\beta_\ell^2}J_2^c = 2\rho_1 f_0^2\,, \qquad \frac{2}{3\beta_\ell}J_6^s = 4\rho_2 f_\parallel f_\perp \qquad J_9 = 0\,. \tag{3.84}$$

When plugging these results into Eqs. (3.75)-(3.78), we obtain for $A_{\rm FB}$ and F_L

$$A_{\rm FB} = 3\frac{\rho_2}{\rho_1} \times (f_0^2 + f_\perp^2 + f_\parallel^2)\,, \qquad F_L = \frac{f_0^2}{f_0^2 + f_\perp^2 + f_\parallel^2}\,, \tag{3.85}$$

and for the transverse asymmetries

$$A_T^{(2)} = \frac{f_\perp^2 - f_\parallel^2}{f_\perp^2 + f_\parallel^2}\,, \qquad A_T^{(3)} = \frac{f_\parallel}{f_\perp}\,, \tag{3.86}$$

$$A_T^{(4)} = 2\frac{\rho_2}{\rho_1} \times \frac{f_\perp}{f_\parallel}\,, \qquad A_T^{(5)} = \sqrt{1 - 4\frac{\rho_2^2}{\rho_1^2}} \times \frac{f_\parallel f_\perp}{f_\parallel^2 + f_\perp^2}\,. \tag{3.87}$$

At low recoil none of the above observables is free of hadronic uncertainties. Interestingly, $A_T^{(2,3)}$ as well as F_L do not exhibit any dependence on the short-distance coefficients to $\mathcal{O}(\Lambda/Q)$. We remark here that the latter fact makes $A_T^{(2,3)}$ and F_L ideal probes to test theory predictions of the hadronic form factors, be it extrapolations of LCSR results at small q^2 or results of lattice QCD calculations at large q^2 [44]. A recent study [73] extracts ratios of the form factor parameters from available data, and the authors find good agreement between data and theory predictions. On the other hand, the short-distance free observables can also be included in a global analysis of the available data on exclusive $b \to s\ell^+\ell^-$ processes. Here a Bayesian analysis can be employed, by which we can simultaneously constrain the form factor parameters and reduce the allowed ranges for the parameters of interest [74]. However, with regard to extracting short-distance information, the remaining transverse asymmetries $A_T^{(4,5)}$ are at low recoil only marginally better suited than the decay rate, and rather on par with the forward-backward asymmetry $A_{\rm FB}$.

In order to fully exploit the structure of the transversity amplitudes at low recoil, we define [44]

$$H_T^{(1)} \equiv \frac{\sqrt{2}J_4}{\sqrt{-J_{2c}\,(2J_{2s} - J_3)}} = \frac{\mathrm{Re}(A_0^L A_\parallel^{L*} + A_0^{R*} A_\parallel^R)}{\sqrt{\left(|A_0^L|^2 + |A_0^R|^2\right)\left(|A_\parallel^L|^2 + |A_\parallel^R|^2\right)}}\,, \tag{3.88}$$

$$H_T^{(2)} \equiv \frac{\beta_l J_5}{\sqrt{-2J_{2c}\,(2J_{2s} + J_3)}} = \frac{\mathrm{Re}(A_0^L A_\perp^{L*} - A_0^{R*} A_\perp^R)}{\sqrt{\left(|A_0^L|^2 + |A_0^R|^2\right)\left(|A_\perp^L|^2 + |A_\perp^R|^2\right)}}\,, \tag{3.89}$$

$$H_T^{(3)} \equiv \frac{\beta_l J_6}{2\sqrt{(2J_{2s})^2 - J_3^2}} = \frac{\mathrm{Re}(A_\parallel^L A_\perp^{L*} - A_\parallel^{R*} A_\perp^R)}{\sqrt{\left(|A_\parallel^L|^2 + |A_\parallel^R|^2\right)\left(|A_\perp^L|^2 + |A_\perp^R|^2\right)}}\,. \tag{3.90}$$

Contrary to the transverse asymmetries $A_T^{(i)}$ in Eqs. (3.75)-(3.78), we define the $H_T^{(i)}$ in terms of the angular coefficients J_i in order to account for amplitudes beyond $A_{\perp,\parallel,0}^{L,R}$. Within the SM basis of operators we find that[5]

$$H_T^{(1)} = \operatorname{sgn} f_0\,, \qquad H_T^{(2)} = 2\frac{\rho_2}{\rho_1}\,, \qquad H_T^{(3)} = 2\frac{\rho_2}{\rho_1}\,. \tag{3.91}$$

With these results the low recoil region provides two important phenomenological qualities. First, the relations $|H_T^{(1)}| = 1$ and $H_T^{(2)} = H_T^{(3)}$ provide an important test of the low recoil framework itself, chiefly to test the performance of the OPE. Sizable deviations from this relation would signal either increased deviation from the OPE or possible contributions from operators beyond the SM basis. The latter is studied in depth in the following sections. Second, the observables $H_T^{(2,3)}$ are free of hadronic inputs to $\mathcal{O}\left(\alpha_s\Lambda/M_B, \mathcal{C}_7\Lambda/\mathcal{C}_9 M_B\right)$, which makes them ideal probes of short-distance physics. In point of fact, both $H_T^{(2,3)}$ provide theoretically cleaner access than the forward-backward asymmetry $A_{\rm FB}$ to the very same short-distance information. In addition to accessing the short-distance information, the low recoil region also provides clean access to information on the hadronic physics involved. In particular, we can form ratios of observables that do not exhibit dependence on the short-distance couplings, thereby probing ratios of form factors $f_{0,\perp,\parallel}$ similar to the results for F_L and $A_T^{(2,3)}$, cf. Eq. (3.85) and Eq. (3.86). We find that

$$\frac{f_0}{f_\parallel} = \sqrt{\frac{-J_{2c}}{2J_{2s} - J_3}} = \frac{-J_{2c}}{\sqrt{2}J_4} = \frac{\sqrt{2}J_4}{2J_{2s} - J_3} = \frac{\sqrt{2}J_5}{J_6}\,, \tag{3.92}$$

$$\frac{f_0}{f_\perp} = \sqrt{\frac{-J_{2c}}{2J_{2s} + J_3}}\,, \tag{3.93}$$

$$\frac{f_\perp}{f_\parallel} = \sqrt{\frac{2J_{2s} + J_3}{2J_{2s} - J_3}} = \sqrt{\frac{-J_{2c}\left(2J_{2s} + J_3\right)}{\sqrt{2}J_4}}\,. \tag{3.94}$$

Since the short-distance information only cancels in ratios of the angular observables, the hadronic form factors $f_{0,\perp,\parallel}$ can only be extracted in the above ratios and not on their own.

In addition to the above observables, which are defined for the decay $\bar{B} \to \bar{K}^* \ell^+ \ell^-$, we can also turn to CP asymmetries of the decay. For this we employ the additional short-distance combinations $\bar{\rho}_1$, $\bar{\rho}_2$, which are obtained from ρ_1, ρ_2 by complex conjugation of the weak phases, i.e., the Wilson coefficients and the CKM factor $\hat{\lambda}_u$. Any CP violating quantities can therefore be parameterized in terms of the following building blocks

$$\begin{aligned}
\Delta\rho_1 &\equiv \rho_1 - \bar{\rho}_1 = 4\,\mathrm{Im}\{Y\}\;\mathrm{Im}\left\{\mathcal{C}_9 + \kappa\frac{2m_b M_B}{q^2}\mathcal{C}_7 + \hat{\lambda}_u Y_9^{(u)}\right\}\,, \\
\Delta\rho_2 &\equiv \rho_2 - \bar{\rho}_2 = 2\,\mathrm{Im}\{Y\}\;\mathrm{Im}\{\mathcal{C}_{10}\}\,,
\end{aligned} \tag{3.95}$$

[5] Here, the sign of the form factor term f_0 is $+1$ for the central values of the form factor extrapolations from both Ref. [63] and Ref. [48]. However, when varying the form factors A_1 and A_2 within their theory uncertainties, one finds that f_0 may flip its sign.

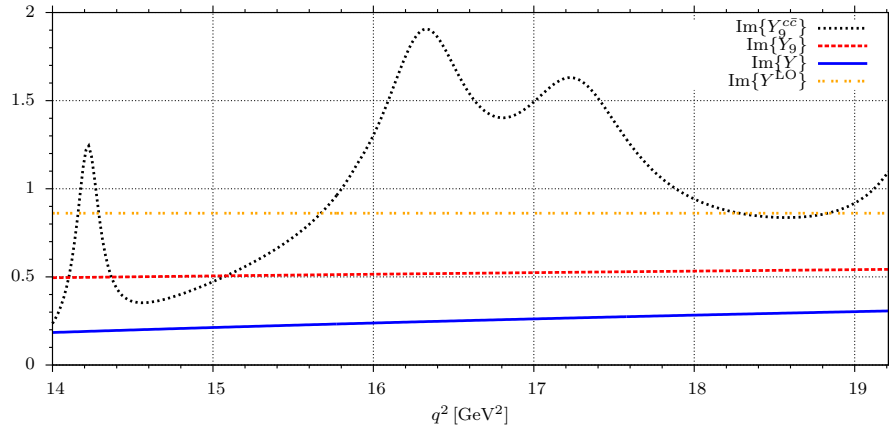

Figure 3.2.: The imaginary parts of Y (solid, blue) and Y_9 (dashed, red) in the OPE [55] including NLO α_s-corrections as functions of q^2 in the low recoil region. The LO result, where $\mathrm{Im}\, Y = \mathrm{Im}\, Y_9$, is given by the dashed-dotted (orange) curve. The $c\bar{c}$-resonance curve (dotted, black) based on the data in Tab. 2.3 shows the imaginary part of Y_9 from $e^+e^- \to hadrons$ data [75, 22]. Figure taken from [60].

where the complex-valued term

$$Y \equiv Y_9 + \kappa \frac{2m_b M_B}{q^2} Y_7 \tag{3.96}$$

emerges from the QCD long-distance contributions within the effective Wilson coefficients (Eq. (3.9), Eq. (3.10)). We decompose the latter as

$$\mathcal{C}_7^{\text{eff}} = \mathcal{C}_7 + Y_7\,, \qquad\qquad \mathcal{C}_9^{\text{eff}} = \mathcal{C}_9 + Y_9 + \hat{\lambda}_u Y_9^{(u)}\,. \tag{3.97}$$

Here, we suppress the q^2 dependence of the effective Wilson coefficients and the Y_i. Since the absorptive parts $\mathrm{Im}\{Y_i\} \propto \sin\delta_s$, with the strong phase δ_s, drive the magnitude of $\Delta\rho_{1,2}$, we pay closer attention to the Y_i. Their q^2 dependence is shown in Fig. 3.2. Note that $Y_9^{(u)}$ is real-valued. At leading order in the perturbative calculation, we can infer from Eq. (3.9) that $\mathrm{Im}\{Y_7\}$ vanishes while $\mathrm{Im}\{Y_9\}$ is governed by the one-loop function $h(m_q = 0, q^2)$ and the numerically large Wilson coefficients $\mathcal{C}_{1,2}$. When taking the NLO matching corrections into account, $\mathrm{Im}\{Y_9\}$ experiences strong suppression by about 50%, and $\mathrm{Im}\{Y\}$ is reduced by about one order of magnitude. As an alternative to the perturbative calculation, one can assume factorization of the correlator $\mathcal{T}_\mu$ (Eq. (3.7)) and fit a Breit-Wigner ansatz [75] to the available data on the charmonium peaks of J/ψ, ψ' within $e^+e^- \to hadrons$ measurements. Here, previous studies [76] found sizable discrepancies between the the measurement of $\mathcal{B}(B \to K^* J/\psi(\to \ell^+\ell^-))$ and the theory results based on the aforementioned ansatz. Assuming naive factorization [76], the amplitude for $B \to K^* \{J/\psi, \psi'\} (\to \ell^+\ell^-)$ decays is proportional to the short-distance coefficient

$$\mathcal{C}^{(0)} = \frac{4}{3}\mathcal{C}_1 + \mathcal{C}_2 + 6\mathcal{C}_3 + 60\mathcal{C}_5 \tag{3.98}$$

and a sum which collects the individual Breit-Wigner functions

$$\sum_n^{J/\psi,\ldots,\psi(4415)} \frac{\Gamma_n \mathcal{B}_n^{\ell\ell} M_n}{q^2 - M_n^2 + i\Gamma_n M_n} \tag{3.99}$$

where M_n, Γ_n and $\mathcal{B}_n^{\ell\ell}$ can be obtained from Tab. 2.3. This discrepancy was cured by the ad-hoc introduction of a *fudge factor* [76] ζ via

$$\mathcal{C}^{(0)} \mapsto \zeta \mathcal{C}^{(0)} \,. \tag{3.100}$$

However, contemporary data on $\mathcal{B}(B \to K^* J/\psi(\to \ell^+\ell^-))$ [22] and the NNLL results at the low scale $\mathcal{C}^{(0)}(\mu_b) = 0.590$ (cf. Tab. 4.1) do match very well. We therefore compute $\mathrm{Im}\{Y^{\bar{c}c}\}$ from the aforementioned Breit-Wigner ansatz and without any fudge factor. The result is shown in Fig. 3.2. We find that, after integration over the complete low recoil phase space, the LO and the resonance result agree quite well, while the NLO result deviates from the resonance result approximately by a factor of three [60]. We therefore conclude that the CP violating quantities $\Delta\rho_{1,2}$ are affected by considerable model-dependent uncertainties.

From the $\rho_{1,2}$, $\bar{\rho}_{1,2}$ we can construct two independent CP asymmetries,

$$a_{\mathrm{CP}}^{(1)} = \frac{\rho_1 - \bar{\rho}_1}{\rho_1 + \bar{\rho}_1} \,, \qquad a_{\mathrm{CP}}^{(2)} = \frac{\frac{\rho_2}{\rho_1} - \frac{\bar{\rho}_2}{\bar{\rho}_1}}{\frac{\rho_2}{\rho_1} + \frac{\bar{\rho}_2}{\bar{\rho}_1}} \,, \tag{3.101}$$

where in the SM basis $a_{\mathrm{CP}}^{(1)}$ can be obtained [60] from the decay rate $\mathrm{d}\Gamma/\mathrm{d}q^2$, and $a_{\mathrm{CP}}^{(2)}$ is identical to the CP asymmetry of the forward-backward asymmetry A_{FB}. No further independent ratios of the building blocks $\rho_{1,2}, \bar{\rho}_{1,2}$ can be formed at low recoil. However, we find that the denominator of $a_{\mathrm{CP}}^{(2)}$ is not positive definite for a generic BSM scenario, thus tainting this observable for model-independent analyses. We therefore propose a further observable to test $\Delta\rho_2$,

$$a_{\mathrm{CP}}^{(3)} = \frac{\rho_2 - \bar{\rho}_2}{\rho_1 + \bar{\rho}_1} \,, \tag{3.102}$$

which is finite in BSM scenarios, but not independent of $a_{\mathrm{CP}}^{(1,2)}$. Moreover, $a_{\mathrm{CP}}^{(3)}$ can be obtained from untagged measurements of the previously introduced observables $H_T^{(2,3)}$, and in terms of the angular observables J_i it reads

$$a_{\mathrm{CP}}^{(3)} = \begin{cases} \frac{J_5 - \bar{J}_5}{\sqrt{-2(J_{2c} + \bar{J}_{2c})[2(J_{2s} + \bar{J}_{2s}) + (J_3 + \bar{J}_3)]}} & \text{for } H_T^{(2)} \\ \frac{J_{6s} - \bar{J}_{6s}}{2\sqrt{4(J_{2s} + \bar{J}_{2s})^2 - (J_3 + \bar{J}_3)^2}} & \text{for } H_T^{(3)} \end{cases} . \tag{3.103}$$

Beyond the decay $\bar{B}^0 \to \bar{K}^*(\to \bar{K}\pi)\ell^+\ell^-$, we can additionally consider the $SU(3)_{\mathrm{F}}$ related decay $B_s, \bar{B}_s \to \phi(\to K^+K^-)\ell^+\ell^-$. Within the latter, the final state is a CP eigenstate with CP eigenvalues $\eta_{0,\parallel} = +1$ for the transversity amplitudes $A_{0,\parallel}$ and $\eta_\perp = -1$ for $A_\perp$. We account for mixing of the two possible initial states $B_s, \bar{B}_s$ through explicitly time-dependent transversity amplitudes

$$\begin{aligned} A_a^{L/R}(t) &\equiv A^{L/R}(\bar{B}_s(t) \to \phi\,(\to K^+K^-)_a l^+ l^-) \,, \\ \bar{A}_a^{L/R}(t) &\equiv A^{L/R}(B_s(t) \to \phi\,(\to K^+K^-)_a l^+ l^-) \,. \end{aligned} \tag{3.104}$$

Here $A_a^{L/R}(t)(\bar{A}_a^{L/R}(t))$ denotes the amplitude for a $\bar{B}_s$ (B_s) at the origin $t = 0$, which decays through the transversity state $a = \perp, \parallel, 0$ at a later point t of its eigentime. For later use, we define

$$\xi_a^{L/R} = e^{-i\Phi_M} \frac{A_a^{L/R}(0)}{A_a^{L/R}(0)[\delta_W \to -\delta_W]}\,, \tag{3.105}$$

where $[\delta_W \to -\delta_W]$ implies the conjugation of all weak phases in the denominator. This can easily be accommodated for by the replacement prescription for CP conjugation of $\rho_{1,2}$ earlier in this section. Moreover, Φ_M denotes the B_s–$\bar{B}_s$ mixing phase whose SM value $\Phi_M^{\rm SM} = 2\arg(V_{ts}^* V_{tb}) = \mathcal{O}\left(\lambda^2\right)$ is very small. According to Ref. [77] we can now express the untagged, CP averaged partial rates as

$$\mathrm{d}\Gamma(t) + \mathrm{d}\bar{\Gamma}(t) \sim \sum_{a,b=0,\perp,\parallel} \bar{A}_a(t)\bar{A}_b^*(t) + A_a(t)A_b^*(t) \tag{3.106}$$

with the time dependent building blocks

$$\begin{aligned}\bar{A}_a(t)\bar{A}_b^*(t) + A_a(t)A_b^*(t) = \frac{1}{2}\bar{A}_a(0)\,\bar{A}_b^*(0) \\ \times \left[(1 + \eta_a\eta_b\,\xi_a\xi_b^*)\left(e^{-\Gamma_L t} + e^{-\Gamma_H t}\right) + (\eta_a\xi_a + \eta_b\xi_b^*)\left(e^{-\Gamma_L t} - e^{-\Gamma_H t}\right)\right]\,.\end{aligned} \tag{3.107}$$

Here the chirality indices L, R are suppressed for brevity, and $\Gamma_{L(H)}$ denotes the width of the lighter (heavier) mass eigenstate of the B_s system. We do not consider CP violation via mixing, since it is constrained by measurements of the semileptonic, flavor-specific CP asymmetry $|A_{\rm SL}^s| \lesssim \mathcal{O}(10^{-2})$ [78]. After time integration of Eq. (3.107) we obtain

$$\int_0^\infty \mathrm{d}t\left[\bar{A}_a(t)\bar{A}_b^*(t) + A_a(t)A_b^*(t)\right] = \frac{\bar{A}_a(0)\,\bar{A}_b^*(0)}{\Gamma(1-y^2)}\left[1 + \eta_a\eta_b\,\xi_a\xi_b^* - y\,(\eta_a\xi_a + \eta_b\xi_b^*)\right], \tag{3.108}$$

where $\Gamma = (\Gamma_L + \Gamma_H)/2$ and $\Delta\Gamma = \Gamma_L - \Gamma_H$ denote the average width and the width difference of the B_s system, respectively, and $y = \Delta\Gamma/(2\,\Gamma)$ is the reduced width difference. The structure of the transversity amplitudes at low recoil, in particular the factorization into hadronic and short-distance terms, implies that the previously defined factors $\xi_a^{L(R)}$ simplify

$$\xi_a^{L(R)} \mapsto \xi_{L(R)} \equiv e^{-i\Phi_M}\frac{\mathcal{C}_9 \mp \mathcal{C}_{10} + \kappa\frac{2\hat{m}_b}{\hat{s}}\,\mathcal{C}_7 + Y + \hat{\lambda}_u Y_9^{(u)}}{\mathcal{C}_9^* \mp \mathcal{C}_{10}^* + \kappa\frac{2\hat{m}_b}{\hat{s}}\,\mathcal{C}_7^* + Y + \hat{\lambda}_u^* Y_9^{(u)}}\,. \tag{3.109}$$

Both for vanishing strong phases (i.e.for $\mathrm{Im}\{Y_9\} = 0$) as well as for vanishing weak phases (i.e.for $\mathrm{Im}\{\mathcal{C}_i\} = 0,\ \mathrm{Im}\left\{\hat{\lambda}_u\right\} = 0$) we find $|\xi_{L(R)}| = 1$. In the SM, we find that $|\xi_{L(R)}| - 1 = \mathcal{O}\left((m_c^2/m_b^2)\,\mathrm{Im}\left\{\hat{\lambda}_u\right\}\right)$.

We now concentrate on how such mixing-induced CP violation can be measured in the experiments. For this, we recall that CP-odd observables allow measurement of CP asymmetries without tagging of the B meson, a quality which is known as *self-tagging*.

We note that self-tagging can be hampered by a nonzero production asymmetry of the B_s and $\bar{B}_s$ mesons. The angular distribution offers in principle four CP-odd angular observables $J_{5,6s,8,9}$ [79, 54], of which two ($J_{8,9}$) vanish at low recoil in the SM basis. We therefore construct in the following – schematically – two mixing-induced, self-tagging CP asymmetries. For J_5 we obtain at low recoil from Eq. (3.108):

$$\int_0^\infty \mathrm{d}t\, \mathrm{Re}\left\{ \bar{A}_0^L(t) \bar{A}_\perp^{L,*}(t) + A_0^L(t) A_\perp^{L,*}(t) - (L \to R) \right\} = f_0 f_\perp \times \frac{A_{\mathrm{mix}}}{\Gamma(1-y^2)} \tag{3.110}$$

with

$$A_{\mathrm{mix}} \equiv 2\rho_2(|\xi_L|^2 + |\xi_R|^2 - 2) + \rho_1(|\xi_R|^2 - |\xi_L|^2)\,. \tag{3.111}$$

The formula for J_{6s} is identical after changing the transversity index 0 to $\|$. Similar to $H_T^{(2,3)}$ we can now remove the form factors terms $f_0 f_\perp$ ($f_\| f_\perp$ in the case of J_{6s}). For this, we introduce the normalizing quantities

$$n_i \equiv \int_0^\infty \mathrm{d}t\ \left[|\bar{A}_i^L(t)|^2 + |A_i^L(t)|^2 + (L \to R) \right] = f_i^2 \times \frac{(B_{\mathrm{mix}} - 2\eta_i y\, C_{\mathrm{mix}})}{\Gamma(1-y^2)}\,, \tag{3.112}$$

which can be obtained from the angular observables $J_{1,2,3}$, see also Eqs. (3.89)-(3.90), where we use

$$B_{\mathrm{mix}} \equiv \rho_1(|\xi_L|^2 + |\xi_R|^2 + 2) + 2\rho_2(|\xi_R|^2 - |\xi_L|^2)\,, \tag{3.113}$$

$$C_{\mathrm{mix}} \equiv \rho_1 \mathrm{Re}\{\xi_L + \xi_R\} + 2\rho_2 \mathrm{Re}\{\xi_R - \xi_L\}\ . \tag{3.114}$$

We remark that C_{mix} is the only contribution dependent on the mixing phase Φ_M. By normalizing Eq. (3.110) to $\sqrt{n_\perp n_0}$ we obtain the mixing-induced CP asymmetry

$$a_{\mathrm{CP}}^{\mathrm{mix}} = \frac{A_{\mathrm{mix}}}{\sqrt{(B_{\mathrm{mix}})^2 - 4y^2\,(C_{\mathrm{mix}})^2}}\,, \tag{3.115}$$

and the same CP asymmetry can by obtained from the angular observable J_{6s} when normalized to $\sqrt{n_\| n_\perp}$. We remark $a_{\mathrm{CP}}^{\mathrm{mix}}$ is insensitive to the sign of the reduced decay width difference y, and simultaneously, the sensitivity to Φ_M is very low since it enters via C_{mix} only. We find that for $y \to 0$

$$a_{\mathrm{CP}}^{\mathrm{mix}} = \frac{A_{\mathrm{mix}}}{|B_{\mathrm{mix}}|} = -2\,\frac{(\rho_1^2 + 4\,\rho_2^2)\bar{\rho}_2 - 2\rho_1\rho_2\bar{\rho}_1 + (\bar{\rho}_1^2 - 4\,\bar{\rho}_2^2)\rho_2}{(\rho_1^2 + 4\,\rho_2^2)\bar{\rho}_1 - 8\rho_1\rho_2\bar{\rho}_2 + (\bar{\rho}_1^2 - 4\,\bar{\rho}_2^2)\rho_1}\,. \tag{3.116}$$

For $\Delta\rho_i \ll \rho_i, \bar{\rho}_i$ this simplifies further to

$$a_{\mathrm{CP}}^{\mathrm{mix}} = a_{\mathrm{CP}}^{(3)}\,. \tag{3.117}$$

We note that $a_{\mathrm{CP}}^{\mathrm{mix}}$ is insensitive to the B_s-mixing parameters y and Φ_M, especially when considering the most recent measurement $y = 0.094 \pm 0.033$ [43]. We find that $|\langle a_{\mathrm{CP}}^{\mathrm{mix}} \rangle / \langle a_{\mathrm{CP}}^{(3)} \rangle - 1| < 3\%$ after q^2-integration. Hence, the measurement of any difference between both asymmetries is highly unlikely, at least by current and currently planned experiments.

3.4.4. Including Chirality-Flipped Operators

As seen from Eqs. (3.58)-(3.60), the universal structure of the transversity amplitudes is broken by the inclusion of chirality-flipped operators within the SM′ basis. In this case, the relations Eqs. (3.82)-(3.84) are modified and now read

$$\frac{4}{3\beta_l^2}(2J_{2s}+J_3) = 2\,\rho_1^+ f_\perp^2, \quad \frac{4\sqrt{2}}{3\beta_l^2}J_4 = 2\,\rho_1^- f_0 f_\parallel, \quad J_7 = 0, \tag{3.118}$$

$$\frac{4}{3\beta_l^2}(2J_{2s}-J_3) = 2\,\rho_1^- f_\parallel^2, \quad \frac{2\sqrt{2}}{3\beta_l}J_5 = 4\,\mathrm{Re}(\rho_2) f_0 f_\perp, \quad \frac{4\sqrt{2}}{3\beta_l^2}J_8 = 4\,\mathrm{Im}(\rho_2) f_0 f_\perp,$$

$$-\frac{4}{3\beta_l^2}J_{2c} = 2\,\rho_1^- f_0^2, \quad \frac{2}{3\beta_l}J_{6s} = 4\,\mathrm{Re}(\rho_2) f_\parallel f_\perp, \quad -\frac{4}{3\beta_l^2}J_9 = 4\,\mathrm{Im}(\rho_2) f_\parallel f_\perp.$$

where ρ_1 and ρ_2 from Eqs. (3.80)-(3.81) have been generalized to

$$\rho_1^\pm \equiv \frac{1}{2}\left(|C_\pm^R|^2 + |C_\pm^L|^2\right), \qquad \rho_2 \equiv \frac{1}{4}\left(C_+^R C_-^{R*} - C_-^L C_+^{L*}\right). \tag{3.119}$$

We can observe that nonvanishing right-handed currents give rise to two major changes:

1. In the SM basis we have $J_{2c}, (2J_{2s} \pm J_3) \sim \rho_1$, whereas now we obtain $J_{2c}, (2J_{2s} - J_3) \sim \rho_1^-$, while $(2J_{2s} + J_3) \sim \rho_1^+$.
2. In the SM basis $J_{7,8,9} = 0$, whereas now only $J_7 = 0$ while $J_{8,9} \sim \mathrm{Im}(\rho_2) \neq 0$ in general.

As a consequence, in the presence of chirality-flipped operators the relations

$$H_T^{(1)} = \mathrm{sgn}\, f_0, \qquad J_7 = 0 \tag{3.120}$$

still hold, and a measurement of deviations would signal violations of the low recoil OPE. The previously defined low recoil observables $H_T^{(2,3)}$ now read

$$H_T^{(2,3)} = 2\,\frac{\mathrm{Re}(\rho_2)}{\sqrt{\rho_1^-\rho_1^+}}, \tag{3.121}$$

and remain free of hadronic input. Furthermore, we obtain two additional observables free of hadronic input,

$$H_T^{(4)} \equiv \frac{\sqrt{2}\,J_8}{\sqrt{-J_{2c}\,(2J_{2s}+J_3)}} = 2\,\frac{\mathrm{Im}(\rho_2)}{\sqrt{\rho_1^-\rho_1^+}}, \tag{3.122}$$

$$H_T^{(5)} \equiv \frac{-J_9}{\sqrt{(2J_{2s})^2 - J_3^2}} = 2\,\frac{\mathrm{Im}(\rho_2)}{\sqrt{\rho_1^-\rho_1^+}}. \tag{3.123}$$

From Eq. (3.121) and Eqs. (3.122)-(3.123) it follows that chirality flipped operators preserve the relations

$$H_T^{(2)} = H_T^{(3)}, \qquad H_T^{(4)} = H_T^{(5)}, \tag{3.124}$$

which had already been obtained within the SM operator basis [44], where $H_T^{(4,5)} = 0$. We conclude that a measurement of nonzero $H_T^{(4,5)}$ indicates the presence of nonvanishing Wilson coefficients for the chirality-flipped operators. In addition, the T-oddness of $J_{8,9}$ gives optimal access to CP violation in the presence of small strong phases [54]. Since both $J_{8,9}$ are also CP-odd, $H_T^{(4,5)}$ can be measured from B meson samples without tagging, and give rise to a fourth long-distance free CP asymmetry which reads

$$a_{\rm CP}^{(4)} = 2\,\frac{{\rm Im}(\rho_2 - \bar{\rho}_2)}{\sqrt{(\rho_1^+ - \bar{\rho}_1^+)(\rho_1^- - \bar{\rho}_1^-)}}\,. \tag{3.125}$$

In terms of the angular observables, it is defined as

$$a_{\rm CP}^{(4)} = \begin{cases} \dfrac{\sqrt{2}(J_8 - \bar{J}_8)}{\sqrt{-(J_{2c} + \bar{J}_{2c})\big[2(J_{2s} + \bar{J}_{2s}) + (J_3 + \bar{J}_3)\big]}} & \text{for } H_T^{(4)} \\ -\dfrac{J_9 - \bar{J}_9}{\sqrt{4\big(J_{2s} + \bar{J}_{2s}\big)^2 - \big(J_3 + \bar{J}_3\big)^2}} & \text{for } H_T^{(5)} \end{cases}. \tag{3.126}$$

Furthermore, the generalization of $a_{\rm CP}^{(3)}$ reads

$$a_{\rm CP}^{(3)} = 2\,\frac{{\rm Re}(\rho_2 - \bar{\rho}_2)}{\sqrt{(\rho_1^+ + \bar{\rho}_1^+)(\rho_1^- + \bar{\rho}_1^-)}}\,. \tag{3.127}$$

Due to the splitting $\rho_1 \to \rho_1^\pm$, the number of CP asymmetries is doubled and we generalize $a_{\rm CP}^{(1,2)}$ to

$$a_{\rm CP}^{(1,\pm)} \equiv \frac{\rho_1^\pm - \bar{\rho}_1^\pm}{\rho_1^\pm + \bar{\rho}_1^\pm}\,, \qquad\qquad a_{\rm CP}^{(2,\pm)} \equiv \frac{\frac{\rho_2}{\rho_1^\pm} - \frac{\bar{\rho}_2}{\bar{\rho}_1^\pm}}{\frac{\rho_2}{\rho_1^\pm} + \frac{\bar{\rho}_2}{\bar{\rho}_1^\pm}}\,. \tag{3.128}$$

In this case the rate asymmetry $A_{\rm CP}$ can neither be related to any of $a_{\rm CP}^{(1,\pm)}$, nor is it free of hadronic input. However, from Eq. (3.118) it is straightforward to read off strategies to relate these form factor free CP asymmetries to the angular observables J_i. In particular $a_{\rm CP}^{(1,-)}$ can be extracted from ratios involving $J_{2c}, (2J_{2s} - J_3), J_4$, whereas $a_{\rm CP}^{(1,+)}$ requires the use of $(2J_{2s} + J_3)$. Short-distance free ratios of form factors can still be formed for $f_0/f_\parallel$ in the presence of chirality-flipped operators as given in Eq. (3.92), and we obtain further

$$\frac{f_0}{f_\parallel} = \frac{\sqrt{2}J_8}{-J_9}. \tag{3.129}$$

However, due to $(2J_{2s} + J_3) \propto \rho_1^+$ there are no short-distance free ratios that involve $f_\perp$ in the SM′ basis.

3.4.5. Including Scalar and Pseudo-Scalar Operators

In the presence of (pseudo-) scalar operators, the angular observables receive unsuppressed contributions to J_{1c}. This leads to scalar contributions to the longitudinal polarization F_L of the K^* mesons, as defined in Eq. (3.70). Moreover, the relation $J_{1c} = -J_{2c}$

is broken, and thus the usual assumption is invalidated that F_L can be extracted in a combined fit to the distribution in $\cos\theta_\ell$, cf. Eq. (3.72). We remark that presently the latter is used in all experimental measurements. However, F_L and F_T can be model-independently extracted from the distribution in $\cos\theta_{K^*}$, cf. Eq. (3.71). Deviations between F_L as extracted from the distribution in $\cos\theta_\ell$, and F_L as extracted from the distribution in $\cos\theta_{K^*}$ would therefore indicate the presence of NP.

Furthermore, the presence of (pseudo-) scalar operators induces helicity suppressed interference terms between vector and scalar operators in $J_{5,6c,7}$. This means that the relation $H_T^{(2)} = H_T^{(3)}$, cf. Eq. (3.91), is broken. The magnitude of the breaking is controlled by $\mathcal{C}_S$ and the helicity suppression factor $m_\ell/\sqrt{q^2}$. Moreover, the relation $J_7 = 0$ is broken if additionally CPV beyond the SM is realized. However, since $J_{2s,2c,3,4,6s}$ are unaffected by the additional operators, we still find that $H_T^{(1,3)}$ remain free of hadronic input.

3.4.6. Including Tensor Operators

In the presence of tensor operators, cf. Eq. (2.29), the angular observables J_i receive (i) contributions which do not interfere with other operators in $J_{2s,2c,3,4,8,9}$, and (ii) interference terms suppressed by $m_\ell/\sqrt{q^2}$ in $J_{1s,1c,5,6s,6c,7}$. Both changes arise from the additional six tensor transversity amplitudes $A_{t0,\,\perp\parallel,\,t\perp,\,t\parallel,\,0\perp,\,0\parallel}$ introduced in Eq. (3.54).

The angular observables still factorize,

$$
\begin{aligned}
\frac{4}{3\beta_\ell^2}(2J_{2s}+J_3) &= 2\left(\rho_1 - \frac{M_B+M_{K^*}}{M_B-M_{K^*}}\rho_1^T\right) f_\perp^2\,, \\
\frac{4}{3\beta_\ell^2}(2J_{2s}-J_3) &= 2\left(\rho_1 - \frac{M_B-M_{K^*}}{M_B+M_{K^*}}\rho_1^T\right) f_\parallel^2\,, \\
-\frac{4}{3\beta_\ell^2}J_{2c} &= 2\left(\rho_1 - \frac{M_B+M_{K^*}}{M_B-M_{K^*}}\rho_1^T\right) f_0^2\,, \\
\frac{4\sqrt{2}}{3\beta_\ell^2}J_4 &= 2\left(\rho_1 - \rho_1^T\right) f_0 f_\parallel\,, \\
\frac{2\sqrt{2}}{3\beta_\ell}J_5 &= 4\,\mathrm{Re}\left\{\rho_2\right\} f_0 f_\perp + \mathcal{O}\left(\frac{m_\ell}{\sqrt{q^2}}\right)\,, \\
\frac{2}{3\beta_\ell}J_{6s} &= 4\,\mathrm{Re}\left\{\rho_2\right\} f_\parallel f_\perp + \mathcal{O}\left(\frac{m_\ell}{\sqrt{q^2}}\right)\,, \\
-\frac{4\sqrt{2}}{3\beta_\ell^2}J_8 &= 4\,\mathrm{Im}\left\{\rho_2 + \left(1+\frac{M_{K^*}}{M_B}\right)^2\rho_2^T\right\} f_0 f_\perp\,, \\
-\frac{4}{3\beta_\ell^2}J_9 &= 4\,\mathrm{Im}\left\{\rho_2 + \left(1-\frac{M_{K^*}^2}{M_B^2}\right)\rho_2^T\right\} f_\parallel f_\perp\,,
\end{aligned}
\tag{3.130}
$$

Scenario	$H_T^{(1)} = 1$	$\frac{H_T^{(2)}}{H_T^{(3)}} = 1$	$\frac{H_T^{(4)}}{H_T^{(5)}} = 1$	$J_7 = 0$	$J_{8,9} = 0$
SM	✓	✓	✓	✓	✓
SM $\otimes$ S $\otimes$ P	✓	$m_\ell/Q\,\mathrm{Re}\Big\{\mathcal{C}_-^{\mathrm{L,R}}\mathcal{C}_S^*\Big\}$	✓	$m_\ell/Q\,\mathrm{Im}\Big\{\mathcal{C}_+^{\mathrm{L,R}}\mathcal{C}_S^*\Big\}$	✓
SM $\otimes$ T	$m_{K^*}^2/Q^2\rho_1^T$	$m_\ell/Q\,\mathrm{Re}\{\rho_2^T\}$	$m_{K^*}/Q\mathrm{Im}\{\rho_2^T\}$	$m_\ell/Q\,\mathrm{Im}\{\mathcal{C}_i\mathcal{C}_{T5}^*\}$	$\mathrm{Im}\{\rho_2^T\}$
SM $\otimes$ S $\otimes$ P $\otimes$ T	$m_{K^*}^2/Q^2\rho_1^T$	$\mathrm{Re}\{\mathcal{C}_{T5}\mathcal{C}_S^*\}$	$m_{K^*}/Q\mathrm{Im}\{\rho_2^T\}$	$\mathrm{Im}\{\mathcal{C}_{T5}\mathcal{C}_S^*\}$	$\mathrm{Im}\{\rho_2^T\}$
SM′	✓	✓	✓	✓	$\mathrm{Im}\Big\{\mathcal{C}_i\mathcal{C}_j'^*\Big\}$
SM′ $\otimes$ S $\otimes$ P $\otimes$ T	$m_{K^*}^2/Q^2\rho_1^T$	$\mathrm{Re}\{\mathcal{C}_{T5}\mathcal{C}_S'^*\}$	$m_{K^*}/Q\,\mathrm{Im}\Big\{\rho_2^{(T)}\Big\}$	$\mathrm{Im}\{\mathcal{C}_{T5}\mathcal{C}_S^*\}$	$\mathrm{Im}\Big\{\mathcal{C}_i\mathcal{C}_j'^*\Big\}$

Table 3.1.: Overview of NP scenarios and corresponding theory predictions for the relations amongst the low recoil observables, and the terms that break these relations. Here S,P,T stand for scalar, pseudoscalar and tensor operators, respectively. A ✓ denotes at most corrections of order α_s/m_b and $\mathcal{C}_7/(\mathcal{C}_9 m_b)$. We use the shorthand notation $Q \in \Big\{m_b, \sqrt{q^2}\Big\}$.

where the tensor operators introduce the additional short-distance coefficients

$$\rho_1^T \equiv 16\,\kappa^2 \frac{M_B^2 - M_{K^*}^2}{q^2}\Big(|\mathcal{C}_T|^2 + |\mathcal{C}_{T5}|^2\Big)\,, \tag{3.131}$$

$$\rho_2^T \equiv 16\,\kappa^2 \frac{M_B^2}{q^2}\mathcal{C}_T\,\mathcal{C}_{T5}^*\,. \tag{3.132}$$

In the presence of the tensor operators $H_T^{(1)}$ reads

$$H_T^{(1)} = \mathrm{sgn}(f_0)\,\mathrm{sgn}(\rho_1^- - \rho_1^T)\left(1 - \frac{4M_B^2 M_{K^*}^2}{M_B^2 - M_{K^*}^2}\frac{\rho_1^-\rho_1^T}{\left(\rho_1^- - \rho_1^T\right)^2}\right)^{-1/2} \tag{3.133}$$

$$\approx \mathrm{sgn}(f_0)\,\mathrm{sgn}(\rho_1^- - \rho_1^T) + \mathcal{O}\left(\frac{M_{K^*}^2}{M_B^2}\right)\,. \tag{3.134}$$

As for the case without tensor operators, form factors cancel, i.e., $H_T^{(1)}$ is free of hadronic input. Additionally, $|H_T^{(1)}| = 1$ holds in the OPE up to kinematically suppressed terms of $\mathcal{O}\left(M_{K^*}^2/M_B^2\right) \approx 0.03$. Furthermore, $H_T^{(2,3)}$ remain free of hadronic input, and $H_T^{(2)} = H_T^{(3)}$ still holds up to helicity suppressed terms $m_\ell/Q\mathrm{Re}\Big\{\mathcal{C}_i\mathcal{C}_j^*\Big\}$.

3.4.7. Performance of Low Recoil Observables

When considering the complete set of operators, all of the previously presented relations are broken to varying degree. A complete overview of how the individual relations are broken is presented in Tab. 3.1 for all scenarios considered in this thesis. We emphasize that ratios of the low recoil designer observables $H_T^{(i)}$ are broken only by kinematically or helicity suppressed terms. However, the angular coefficients $J_{7,8,9}$ gain contributions

Scenario	$H_T^{(1)}$	$H_T^{(2)}$	$H_T^{(3)}$	$H_T^{(4)}$	$H_T^{(5)}$
SM	✓	✓	✓	—	—
SM $\otimes$ S $\otimes$ P	✓	A_0	✓	—	—
SM $\otimes$ T	✓	✓	✓	—	—
SM′	✓	✓	✓	✓	✓
SM′ $\otimes$ S $\otimes$ P $\otimes$ T	✓	A_0	✓	✓	✓

Table 3.2.: Overview of NP scenarios and which of the low recoil designer observables remain free of hadronic input. A ✓denotes at most corrections of order α_s/m_b and $\mathcal{C}_7/(\mathcal{C}_9 m_b)$, while A_0 denotes breaking through terms involving the corresponding $B \to K^*$ form factor. Observables marked with — vanish in the considered scenario.

which are generically unsuppressed. The factorization of the angular observables

$$J_i \sim \rho_i f_k f_l^* \tag{3.135}$$

into short-distance terms ρ_i and form factor terms $f_{k,l}$, cf. Eqs. (3.29)-(3.31), can also be affected when extending the operator basis. An overview is presented in Tab. 3.2. In particular, we find that factorization is broken by the emergence of operators S and P, and by interference terms (S,P) $\times$ (SM,T,T5). The former only affect J_{1c} and J_{6c}, while the latter break factorization only in J_5 and J_7. Exemplary, we find that

$$J_{1c} = \frac{3}{2}(\rho_1 - \rho_1^T) f_0^2 + 4\left|\mathcal{C}_S - \mathcal{C}_S'\right|^2 \frac{\lambda}{m_b^2} A_0^2 + \mathcal{O}\left(M_{K^*}/M_B\right) . \tag{3.136}$$

However, the angular observables $J_{2s,2c,3,4,6s,8,9}$ still factorize. We therefore conclude that $H_T^{(1,3,4,5)}$ remain free of hadronic inputs, even when considering the complete set of operators. This conclusively shows the model-independent merits of the low recoil observables $H_T^{(i)}$. $|H_T^{(1)}| = 1$ proves to be a very stable relation in all possible extensions of the basis of local operators. Hence it presents itself as a reliable tool to probe the performance of the OPE. We present an evaluation of $H_T^{(1)}$ in the SM for both the large and the low recoil region in Fig. 3.3.

The decay $\bar{B} \to \bar{K}^*\ell^+\ell^-$ at low recoil exposes only a limited number of independent short-distance couplings ($\rho_1^\pm - \rho_1^T, \rho_2, \rho_2^T, |\mathcal{C}_{S,P}^{(\prime)}|^2$ and interference terms), while it offers a large amount of observables. This allows model-independent analyses to over constrain the parameter space of the Wilson coefficients $\mathcal{C}_{9,10}^{(\prime)}$, see e.g. [44, 45, 80, 81]. However, recent experimental results from LHCb [82] indicate that NP effects in (semi)leptonic $|\Delta B| = 1$ processes appear to be small in comparison to the SM contributions. We therefore study how sensitive the low recoil observables $H_T^{(2,3)}$ are to NP effects in the Wilson coefficients $\mathcal{C}_{9,10}$ within the SM basis of operators, especially in comparison to A_{FB}, which is sensitive to these. At low recoil and in the SM basis, $H_T^{(2,3)}$ and A_{FB}

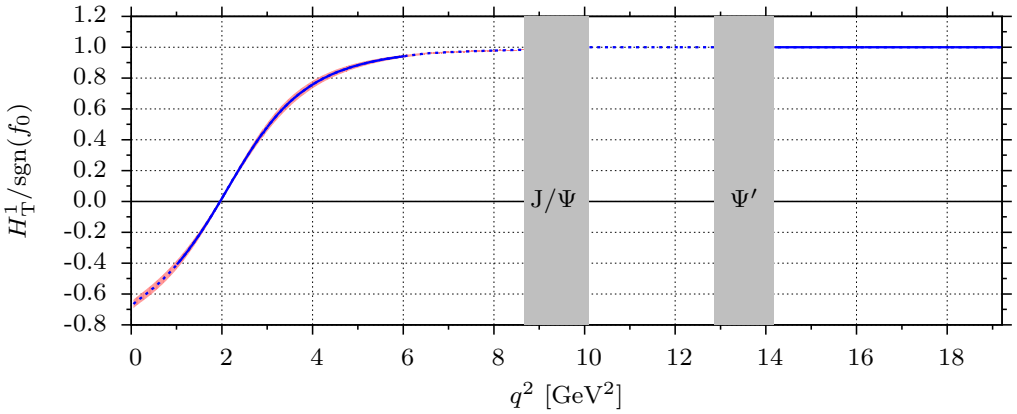

Figure 3.3.: $H_T^{(1)}$ in the SM basis, including theory uncertainties (shaded red bands) from subleading contributions and form factor inputs, as a function of q^2 in both the large and the low recoil region (blue, solid lines). We extrapolate our results beyond the respective regions of validity (blue, dashed lines).

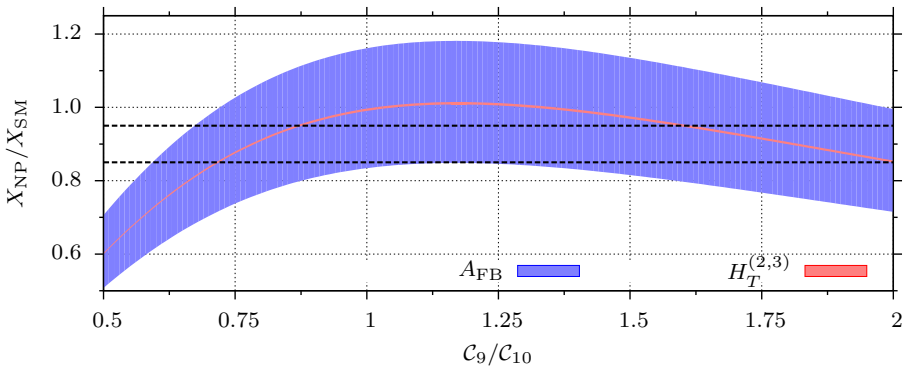

Figure 3.4.: The theory uncertainty of the binned observables A_{FB} (blue shaded band) and $H_T^{(2,3)}$ (red shaded band) normalized to their respective SM values versus $\mathcal{C}_9/\mathcal{C}_{10}$. The bin covers the complete low recoil region $q^2 \geq 14\,\mathrm{GeV}^2$. In addition, a hypothetical measurement of the respective observables at $(90 \pm 5)\%$ is drawn (black dashed lines).

depend only on the ratio

$$\frac{\rho_2}{\rho_1} \sim \frac{r}{1+|r|^2}\,, \quad \text{with } r = \frac{\mathcal{C}_9}{\mathcal{C}_{10}}\,, \tag{3.137}$$

where we understand the Wilson coefficients to be evaluated at the scale $\mu_b = 4.2\,\mathrm{GeV}$. We show the behavior of $\langle H_T^{(2,3)}\rangle_{14,19.21}$ and $\langle A_{\mathrm{FB}}\rangle_{14,19.21}$ as functions of the ratio $\mathcal{C}_9/\mathcal{C}_{10}$, normalized to their SM values, and including their respective theory uncertainties in Fig. 3.4. In order to probe the sensitivity, we compare the SM results with hypothetical measurements of the observables which correspond to $(90 \pm 5)\%$ of their SM central values. We find for the forward-backward asymmetry that such a measurement is indistinguishable from the SM result within its theory uncertainty. Within the latter, by far the biggest offender is the lack of knowledge of the hadronic matrix elements, which only partially cancel. Moreover, we find that, given the current understanding of the hadronic form factors for $B \to K^*$ transitions, any experimental measurement must exclude values larger that $0.85 \times A_{\mathrm{FB}}^{\mathrm{SM}}$ in the low recoil region to conclusively indicate any deviation from the SM. However, a similar measurement of either of $H_T^{(2,3)}$ is a clear indication of NP, as can be inferred from Fig. 3.4. In particular, the 10% deviation in the central value would correspond to two disjoint solutions $r \simeq 0.8$ and $r \simeq 1.8$, respectively, which is a sizable deviation from the SM value $r^{\mathrm{SM}} \simeq 1.03$.

3.5. The Decay $\bar{B} \to \bar{K}\ell^+\ell^-$

We study the angular distribution of $\bar{B} \to \bar{K}\ell^+\ell^-$ decays in Section 3.5.1. The observables, which arise from the angular distribution, are explored for both massless ($\ell = e, \mu$) and massive ($\ell = \tau$) final states in Section 3.5.2.

3.5.1. Angular Distribution

Using the kinematic variables as defined in Section 3.1, the fully differential decay width of the decay $\bar{B} \to \bar{K}\ell^+\ell^-$ can be parametrized [38] as

$$\frac{\mathrm{d}^2\Gamma_\ell[\bar{B} \to \bar{K}\ell^+\ell^-]}{\mathrm{d}q^2\,\mathrm{d}\cos\theta_\ell} = a_\ell(q^2) + b_\ell(q^2)\cos\theta_\ell + c_\ell(q^2)\cos^2\theta_\ell\,, \tag{3.138}$$

with angular observables a_ℓ, b_ℓ and c_ℓ. Within the SM operator basis one finds $b_\ell = 0$ up to small QED corrections [38, 83]. The remaining angular observables read

$$\begin{aligned}\frac{a_\ell}{\Gamma_0\sqrt{\lambda}\beta_\ell f_+^2} &= \frac{\lambda}{4}\left(|F_A|^2 + |F_V|^2\right) \\ &\quad + 2m_\ell(m_B^2 - m_K^2 + q^2)\mathrm{Re}(F_P F_A^*) + 4\,m_\ell^2\,m_B^2|F_A|^2 + q^2|F_P|^2\,, \\ \frac{c_\ell}{\Gamma_0\sqrt{\lambda}\beta_\ell (f_+^{BK})^2} &= -\beta_\ell^2\,\frac{\lambda}{4}\left(|F_A|^2 + |F_V|^2\right)\end{aligned} \tag{3.139}$$

where we make use of $\lambda \equiv \lambda(M_B^2, M_K^2, q^2)$ and

$$\Gamma_0 = \frac{G_\mathrm{F}^2\alpha_e^2|V_{tb}V_{ts}^*|^2}{2^9\pi^5 m_B^3}\,, \tag{3.140}$$

Here, the coefficients $F_{A,V,P}$ parametrize the hadronic matrix element [38]

$$i\mathcal{M} = i\frac{G_\mathrm{F}\alpha_\mathrm{e}}{\sqrt{2}\pi}V_{tb}V_{ts}^* f_+\left[F_V p^\mu(\bar{\ell}\gamma_\mu\ell) + F_A p^\mu(\bar{\ell}\gamma_\mu\gamma_5\ell) + F_P(\bar{\ell}\gamma_5\ell)\right]\,. \tag{3.141}$$

At low recoil and after application of both the low recoil OPE and the improved Isgur-Wise relation, cf. Eq. (3.24), we find [45]

$$F_V = \mathcal{C}_9^\mathrm{eff} + \kappa\frac{2m_b M_B}{q^2}\mathcal{C}_7^\mathrm{eff}\,, \tag{3.142}$$

$$F_P = -m_\ell\left(1 + \frac{M_B^2 - M_K^2}{q^2}\left(1 - \frac{f_0^{BK}}{f_+^{BK}}\right)\right)\mathcal{C}_{10}\,, \tag{3.143}$$

$$F_A = \mathcal{C}_{10}\,. \tag{3.144}$$

We obtain for $\ell = e, \mu$ – i.e.for negligible lepton masses m_ℓ –

$$a_\ell = \Gamma_0\frac{\sqrt{\lambda}^3}{4}f_+^2\,\rho_1\,, \qquad\qquad c_\ell = -a_\ell\,, \tag{3.145}$$

with ρ_1, the only emerging combination of short-distance coefficients, identical to the one obtained for $\bar{B} \to \bar{K}^*\ell^+\ell^-$ decays in Eq. (3.80) [45]. This fact leads to heightened

statistical power when combining the constraints on the Wilson coefficients $\mathcal{C}_{9,10}$ as obtained from both decays and at low recoil. For the massive case of $\ell = \tau$ the angular observables read

$$a_\tau = \frac{\Gamma_0}{4}(\sqrt{\lambda})^3\,\beta_\tau f_+^2\left[\rho_1 - \frac{4\,m_\tau^2}{q^2}|\mathcal{C}_{10}|^2\mathcal{F}_0\right], \qquad c_\tau = -\frac{\Gamma_0}{4}(\sqrt{\lambda})^3\,\beta_\tau^3 f_+^2\,\rho_1\,, \tag{3.146}$$

where we use the shorthand notation

$$\mathcal{F}_0 \equiv 1 - \frac{(M_B^2 - M_K^2)^2}{\lambda}\frac{f_0^2}{f_+^2}\,, \tag{3.147}$$

As the helicity factor m_τ^2/q^2 is bounded by

$$0.6 \lesssim 4\,m_\tau^2/q^2 \lesssim 0.9 \tag{3.148}$$

for $q^2 \in [14,\,23]$ GeV^2, the additional contributions $\propto |\mathcal{C}_{10}|^2$ are not suppressed within decays to τ final states. This allows – in principle – to constrain the magnitude of $\mathcal{C}_{10}$ from comparison of $\bar{B} \to \bar{K}\tau^+\tau^-$ and $\bar{B} \to \bar{K}\ell^+\ell^-$, $\ell = e, \mu$ decays [84].

3.5.2. Observables

Compared to the decay $\bar{B} \to \bar{K}^*\ell^+\ell^-$, the decay $\bar{B} \to \bar{K}\ell^+\ell^-$ has fewer angular observables and thus correspondingly lower potential for probing $|\Delta B| = 1$ FCNCs. As far as CP conserving observables are concerned, one finds [38] for $\ell = e, \mu$ the single-differential decay width

$$\frac{\mathrm{d}\Gamma_\ell[\bar{B} \to \bar{K}\ell^+\ell^-]}{\mathrm{d}q^2} = 2\left[a_\ell(q^2) + \frac{1}{3}c_\ell(q^2)\right]. \tag{3.149}$$

The double-differential decay width can expressed as [85, 86]

$$\frac{1}{\Gamma_\ell}\frac{\mathrm{d}^2\Gamma_\ell}{\mathrm{d}\cos\theta_\ell\,\mathrm{d}q^2} = \frac{3}{4}\left(1 - F_H^\ell\right)\sin^2\theta_\ell + \frac{1}{2}F_H^\ell + A_{\mathrm{FB}}^\ell\cos\theta_\ell\,. \tag{3.150}$$

Here, the forward-backward asymmetry reads

$$A_{\mathrm{FB}}^\ell(q^2) = \frac{b_\ell(q^2)}{\mathrm{d}\Gamma/\mathrm{d}q^2}\,, \tag{3.151}$$

and for the flat-term we one obtains

$$F_H^\ell = \frac{2a_\ell(q^2) + 2c_\ell(q^2)}{\mathrm{d}\Gamma/\mathrm{d}q^2}\,. \tag{3.152}$$

which can be obtained experimentally be means of an angular analysis. Using the earlier results for the angular observables in Eq. (3.145) we obtain for the decay rate into massless leptons $\ell = e, \mu$

$$\frac{\mathrm{d}\Gamma_\ell[\bar{B} \to \bar{K}\ell^+\ell^-]}{\mathrm{d}q^2} = \Gamma_0\frac{\sqrt{\lambda}^3}{3}f_+^2\rho_1\,, \tag{3.153}$$

and the forward-backward asymmetries $A_{\rm FB}^\ell$ and the flat-term F_H^e vanish. Moreover, we obtain the CP asymmetry of the decay rate, $A_{\rm CP}^\ell$, as

$$A_{\rm CP}^\ell[\bar{B} \to \bar{K}\ell^+\ell^-] = \frac{\mathrm{d}\Gamma_\ell/\mathrm{d}q^2 - \mathrm{d}\bar{\Gamma}_\ell/\mathrm{d}q^2}{\mathrm{d}\Gamma_\ell/\mathrm{d}q^2 + \mathrm{d}\bar{\Gamma}_\ell/\mathrm{d}q^2} = \frac{\rho_1 - \bar{\rho}_1}{\rho_1 + \bar{\rho}_1} = a_{\rm CP}^{(1)}[\bar{B} \to \bar{K}^*\ell^+\ell^-]\,. \tag{3.154}$$

The CP asymmetry $a_{\rm CP}^{(1)}$ was identified in Eq. (3.101) as a form factor free quantity in $\bar{B} \to \bar{K}^*\ell^+\ell^-$ decays [60], and the results and discussion of the strong phase δ_s within Section 3.4.3 apply here likewise. In addition to decays into massless leptons $\ell = e, \mu$, we study the flat term for massive leptons $\ell = \tau$. In terms of the short-distance coefficients we obtain

$$F_H^\tau(q^2) = \frac{6m_\tau^2}{q^2} \times \frac{\rho_1 - |\mathcal{C}_{10}|^2\mathcal{F}_0}{\rho_1 + \frac{2m_\tau^2}{q^2}(\rho_1 - 3|\mathcal{C}_{10}|^2\mathcal{F}_0)}\,. \tag{3.155}$$

Thus, for $\ell = \tau$ the flat term can become sizable. We remark that both ρ_1 and $|\mathcal{C}_{10}|^2$ could in principle be extracted through a global fit to $\bar{B} \to \bar{K}\mu^+\mu^-$ and $\bar{B} \to \bar{K}\tau^+\tau^-$ data, cf. Ref. [84]. However, the quality of the fit results will crucially depend on the theory control of the ratio f_0/f_+, which dominates the theory uncertainty of the flat term F_H^τ.

We present SM results for both the decay rate and the flat term in Chapter 4. However, we abstain from providing results for the forward-backward asymmetry since it vanishes in the SM operator basis, cf. also earlier comments on b_ℓ in Section 3.5.1.

4. Standard Model Results

In this chapter we present the SM results for $\bar{B} \to \bar{K}^{(*)}\ell^+\ell^-$ decays. We start by describing all necessary components for the precision calculation of the observables. Our results are obtained by means of EOS [89], a high energy physics program for the calculation of flavor observables. We specifically use the `eos-evaluate` client to calculate all results within this chapter.

First, we evaluate the $|\Delta B| = 1$ Wilson coefficients at NNLO in the SM [35] numerically at an initial (high) scale μ_0. We decide to use $\mu_0^{(t)} = 120\,\mathrm{GeV}$ for the top sector Wilson coefficients, and $\mu_0^{(c,u)} = 80\,\mathrm{GeV}$ for the charm and up sector Wilson coefficients in order to minimize emerging logarithms $\ln(\mu_0/M_W)$ and $\ln(\mu_0/m_t)$. Further input parameters are the mass M_W of the W bosons and the sine square of the Weinberg angle $\sin^2\theta_W$. By means of unitarity the Wilson coefficients as defined in Eq. (2.26) are independent of any CKM matrix elements. Next, the Wilson coefficients are run down to the low scale $\mu_b = 4.2\,\mathrm{GeV}$ as governed by Eq. (2.33). For this step we use the NNLO results for the anomalous mass dimension matrix as given in [35]. Hence, large logarithms are resummed to NNLL. As an intermediate result, we present the numerical values of the Wilson coefficients of the SM basis at the low scale μ_b in Tab. 4.1.

In addition to the low recoil framework for $\bar{B} \to \bar{K}^{(*)}\ell^+\ell^-$ decays, we have also implemented the QCDF results [49, 51, 38] for the angular observables of both decays. With regard to the nonfactorizing contributions, we implement all the leading order terms as well as the numerically significant subleading terms. These nonfactorizing contributions contain isospin breaking spectator effects, which play a crucial role in the differences between the neutral and charged decay modes. QCDF is assumed to be valid within the kinematical range $1\,\mathrm{GeV}^2 \leq q^2 \leq 6\,\mathrm{GeV}^2$. However, we give results beyond this range, which are to be understood as extrapolations only. Differences between our numerical results and the results in Ref. [45] stem from an analytic implementation of the QCDF

$\mathcal{C}_1$	$\mathcal{C}_2$	$\mathcal{C}_3$	$\mathcal{C}_4$	$\mathcal{C}_5$
-0.288	$+1.010$	-0.006	-0.086	$<10^{-3}$
$\mathcal{C}_6$	$\mathcal{C}_7$	$\mathcal{C}_8$	$\mathcal{C}_9$	$\mathcal{C}_{10}$
$+0.001$	-0.327	-0.177	$+4.276$	-4.151

Table 4.1.: The numerical SM values of the Wilson coefficients $\mathcal{C}_{1\ldots10}$ in the NDR scheme and for $\mu_b = 4.2\,\mathrm{GeV}$, $\mu_0^{(t)} = 120\,\mathrm{GeV}$ and $\mu_0^{(c,u)} = 80\,\mathrm{GeV}$. The numerical input is listed in Tab. 4.2.

A	$0.812^{+0.013}_{-0.027}$	[87]	λ	0.22543 ± 0.00077	[87]
$\bar{\rho}$	0.144 ± 0.025	[87]	$\bar{\eta}$	$0.342^{+0.016}_{-0.015}$	[87]
$\alpha_s(M_Z)$	0.11762		τ_{B^+}	1.638 ps	[22]
$\alpha_e(m_b)$	1/133		τ_{B^0}	1.525 ps	[22]
$m_c(m_c)$	$(1.27^{+0.07}_{-0.09})$ GeV	[22]	M_{B^+}	5.2792 GeV	[22]
$m_b(m_b)$	$(4.19^{+0.18}_{-0.06})$ GeV	[22]	M_{B^0}	5.2795 GeV	[22]
m_t^{pole}	(173.3 ± 1.1) GeV	[88]	M_{K^+}	0.494 GeV	[22]
m_e	0.511 MeV	[22]	M_{K^0}	0.498 GeV	[22]
m_μ	0.106 GeV	[22]	$M_{K^{*+}}$	0.89166 GeV	[22]
m_τ	1.777 GeV	[22]	$M_{K^{*0}}$	0.89594 GeV	[22]
M_W	(80.399 ± 0.023) GeV	[22]			
$\sin^2\theta_W$	0.23116 ± 0.00013	[22]			

Table 4.2.: The numerical input used in our analysis. We neglect the mass of the strange quark. τ_{B^0} (τ_{B^+}) denotes the lifetime of the neutral (charged) B meson.

convolution integrals, as well as a switch from the $\overline{\text{MS}}$ to the pole mass scheme for the c quark mass. For the latter, see also earlier comments on the charm quark mass scheme in Section 2.4. We note that the implementation yields numerically more stable results than the previous one. We remark also that the convolution integral $X_\perp(q^2)$ – see Ref. [52] for the definition – is regulated by a cutoff for the entire large recoil region. We follow Ref. [52] closely and regularize only the potentially divergent part of $X_\perp(q^2)$. The procedure of regularizing $X_\perp$ for the entire region of large recoil ensures that observables such as the isospin asymmetry $A_I(q^2)$ exhibit a smooth transition from $B \to K^*\ell^+\ell^-$ to $B \to K^*\gamma$, i.e., in the limit $q^2 \to 0$.

With regard to $B \to K$ form factors, we use extrapolations of LCSR results as given in Ref. [48]. The results there have the virtue of stating explicit uncertainties for each of the form factors f_+ and f_0. The latter are directly used in the computation of the theory uncertainties.

While the authors of Ref. [48] also give results for $B \to K^*$ form factors, we abstain from using these. Our decision is based on the fact that Khodjamirian *et al.* employ a different ansatz for the calculation of the $B \to K^*$ form factors than usually found in the literature. Instead of interpolating the B meson by a heavy-light quark current, they choose to interpolate the light K^* meson. While this calculation is an important cross check against previous LCSR calculations of $B \to K^*$ form factors, their results exhibit a considerably larger theory uncertainty that, e.g., the results obtained by Ball and Zwicky [63]. We therefore choose to use the latter results in our evaluation of $\bar{B} \to \bar{K}^*\ell^+\ell^-$ observables.

We present SM predictions for a subset of the observables that were previously discussed in Section 3.4 and Section 3.5. The same binning as used by Belle [46] is employed in order to achieve comparability with the experimental measurements. The numerical input used for our results are given in Tab. 4.2. We give the binned results

Observable	Bin $[\,\mathrm{GeV}^2]$	$\bar{B}^0 \to \bar{K}^0\ell^+\ell^-$	$B^- \to K^-\ell^+\ell^-$
$10^7 \times \langle\mathcal{B}\rangle$	$4m_\mu^2 - 2.0$	$0.64^{+0.21}_{-0.11}$	$0.69^{+0.22}_{-0.11}$
	$2.0 - 4.3$	$0.75^{+0.26}_{-0.13}$	$0.81^{+0.28}_{-0.14}$
	$4.3 - 8.68$	$1.37^{+0.51}_{-0.25}$	$1.48^{+0.55}_{-0.27}$
	$1.0 - 6.0$	$1.62^{+0.56}_{-0.27}$	$1.75^{+0.60}_{-0.29}$
	$14.18 - 16.0$	$0.34^{+0.18}_{-0.08}$	$0.37^{+0.19}_{-0.09}$
	$16.0 - q^2_{\mathrm{max}}$	$0.63^{+0.38}_{-0.18}$	$0.68^{+0.41}_{-0.19}$
$\langle F_H\rangle$	$4m_\mu^2..2.0$	$0.103^{+0.006}_{-0.012}$	$0.103^{+0.006}_{-0.12}$
	$2.0..4.3$	$0.024^{+0.002}_{-0.003}$	$0.024^{+0.002}_{-0.003}$
	$4.3..8.68$	$0.012^{+0.001}_{-0.002}$	$0.012^{+0.001}_{-0.002}$
	$1.0..6.0$	$0.025^{+0.002}_{-0.004}$	$0.025^{+0.002}_{-0.004}$
	$14.18..16.0$	$0.007^{+0.001}_{-0.002}$	$0.007^{+0.001}_{-0.002}$
	$16.0..q^2_{\mathrm{max}}$	$0.008^{+0.002}_{-0.003}$	$0.008^{+0.002}_{-0.003}$

Table 4.3.: SM predictions for $\bar{B}^0 \to \bar{K}^0\ell^+\ell^-$ and $B^- \to K^-\ell^+\ell^-$ decays in q^2 bins which are compatible with existing measurements. For the large recoil region $q^2 \leq 8.68\,\mathrm{GeV}^2$, we use the QCDF results [49, 38], and include all known power-suppressed contributions [51], see text. For the low recoil region $14.18\,\mathrm{GeV}^2 \leq q^2 \leq q^2_{\mathrm{max}} = (M_B - M_{K^*})^2$ we use the low recoil framework [45]. In both cases we use extrapolations of the $B \to K$ form factors [48].

for $B \to K\ell^+\ell^-$ decays in Tab. 4.3, while results for $B \to K^*\ell^+\ell^-$ decays can be found in Tab. 4.4. In the latter case we give the results for $A_T^{(2)}$ only for the low recoil region, since at large recoil $A_T^{(2)} \simeq 0$ in the SM up to small corrections, and the relative theory uncertainties are very large. In both cases we present CP averaged observables for both isospin modes of the respective decays. In addition, we present the differential observables in Figures 4.1 to 4.3. All given theory uncertainties are part of one of the following uncertainty budgets:

CKM The CKM budget encompasses the input uncertainties of the Wolfenstein CKM parameters $\lambda, A, \bar{\rho}$ and $\bar{\eta}$.

FF The form factor budget consists of uncertainties that arise from the extrapolation of the respective LCSR results. For the results from [48], we use the given (asymmetric) uncertainty ranges. For the results from [63], we vary the input parameters by $\pm 15\%$ as suggested there.

SD The short-distance budget includes uncertainties that arise from the measurement of the top pole mass m_t, the sine squared of the weak mixing angle $\sin^2\theta_W$, the mass of the W bosons M_W, and the variation of the low scale $m_b/2 \leq \mu_b \leq 2m_b$.

SL This budget estimates the influence of contributions to the $B \to K^{(*)}$ decay amplitudes which are subleading in the $1/m_b$ expansion.

We obtain an overall theory uncertainty by adding all of the above budgets in quadrature.

Due to the strong dependence on the strong phase δ_s and its associated model-dependent uncertainty (cf. Section 3.4.2), we deliberately abstain from providing SM results for the low recoil CP asymmetries $a_{\rm CP}^{(1,2,3)}$ in the same manner as for the CP conserving observables. However, we are able to provide approximate results. In the SM, CP violating effects only arise from the small weak phase of the terms $\propto V_{ub}V_{us}^*$. From Eq. (3.10) one can infer, that the leading order CP violating contributions arise only at the order $m_c^2/q^2\hat{\lambda}_u \sim 10^{-3}$. Furthermore, in the SM only T-even CP asymmetries appear, which are further suppressed by the sine of the small strong phase $\sin\delta_s \approx \delta_s$. We therefore estimate that at low recoil

$$\left|A_{\rm CP}^{(1,2,3)}\right| \leq 10^{-4}\,. \tag{4.1}$$

In addition to the tabulated results, we also provide an update to the QCDF results [51] for the zero-crossing point $q_{0,n}^2$ of the forward-backward asymmetry $A_{\rm FB}$ for the neutral decay channel $\bar{B}^0 \to \bar{K}^{*0}\ell^+\ell^-$. We quickly summarize the changes to EOS [89] and the consequent changes to the numerical value for the neutral decay. First, we change the numeric input for the $\bar{B}^0$ decay constants $f_{\bar{B}^0}$ to $0.212\,\text{GeV}$, according to recent lattice results [90], which increases the value of $q_{0,n}^2$ by 1.7%. Second, we now include the subleading HSA terms [51] which additionally affect the zero-crossing point by 0.3%. Lastly, we switch to using the charm mass in the pole mass scheme (cf. also Section 2.4), which increases the $q_{0,n}^2$ even further by 0.3%. In the end, we obtain for the neutral decay mode a zero-crossing point of

$$q_{0,\rm n}^2 = \left(4.07^{+0.25}_{-0.25}\right)\ \text{GeV}^2\,, \tag{4.2}$$

which corresponds to a shift from the previous result [45] of 2.3%. Furthermore, due to the inclusion of the weak annihilation contributions [51] which only affect the charged decay mode $B^- \to K^{*-}\ell^+\ell^-$, we can calculate its zero-crossing point

$$q_{0,\rm c}^2 = \left(4.01^{+0.24}_{-0.22}\right)\ \text{GeV}^2\,. \tag{4.3}$$

The budget that contributes most to the overall theory uncertainties is SD, to which the renormalization scale μ contributes dominantly.

LHCb has recently measured the zero-crossing point $q_{0,n}^2$ for the first time [91], and their result

$$q_{0,n,\rm LHCb}^2 = (4.9^{+1.1}_{-1.3})\,\text{GeV}^2 \tag{4.4}$$

is still affected by a considerable error. Since the precision of this measurement will improve over time, controlling the theory uncertainty of the SM prediction becomes very important. Here one might be able to reduce the large residual dependence on the renormalization scale by computing the NNLO $\alpha_{\rm s}$ contributions.

Since we use the inclusive branching ratio for $\bar{B} \to X_s \mu^+ \mu^-$ for our model independent analysis in Chapter 5, we also provide the corresponding SM result. The latter is obtained from the EOS [89] implementation of the NNLO calculation [92], and the central value reads

$$\int_{1\ \mathrm{GeV}^2}^{6\ \mathrm{GeV}^2} \mathrm{d}q^2 \frac{\mathrm{d}\mathcal{B}^{\mathrm{SM}}\left(\bar{B} \to X_s \mu^+ \mu^-\right)}{\mathrm{d}q^2} = (1.55 \pm 0.11) \times 10^6 \,. \tag{4.5}$$

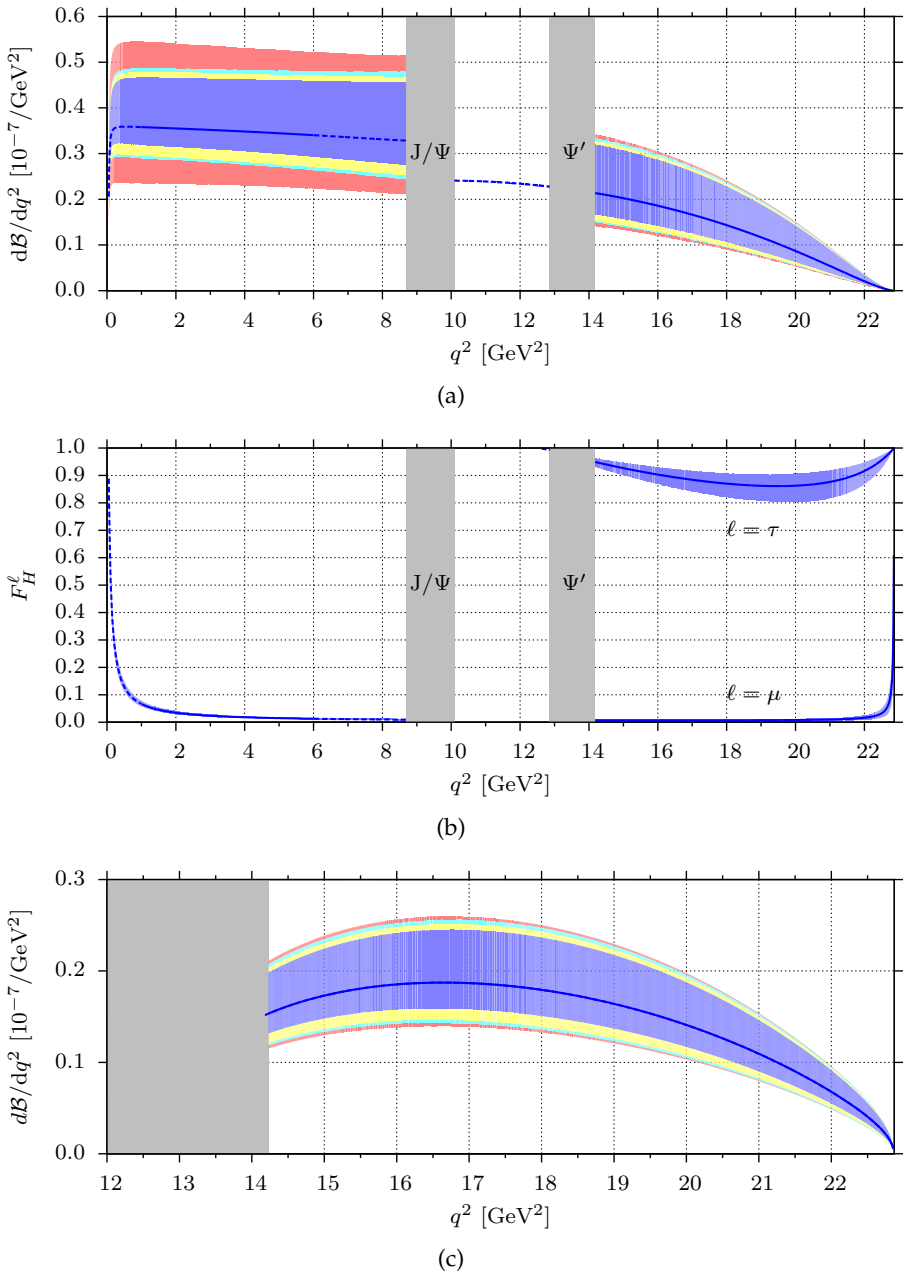

Figure 4.1.: (a) The differential branching ratio $\mathrm{d}\mathcal{B}/\mathrm{d}q^2$ for $\ell = \mu$, (b) the flat term F_H^ℓ for $\ell = \mu, \tau$ and (c) the branching ratio $\mathrm{d}\,\mathcal{B}/\mathrm{d}\,q^2$ for $\ell = \tau$ for the decay $B^+ \to K^+\mu^+\mu^-$ in both the large and the low recoil region using extrapolations of the form factors according to Khodjamirian *et al.* [48] (blue solid and dashed lines). In (a) and (c) the color coded uncertainties arise from the budgets CKM (yellow), FF (blue), SD (cyan) and SL (red), see text. In (b) the theoretical uncertainties from all budgets are added in quadrature. The vertical gray bands are the experimental veto regions to remove contributions from $\bar{B} \to \bar{K}J/\psi(\to \mu^+\mu^-)$ (left-hand band) and $\bar{B} \to \bar{K}\psi'(\to \mu^+\mu^-)$ (right-hand band) in (a) and (b). The vertical gray band in (c) is the experimental cut as used in a recent BaBar search [93]. Figure adapted from Ref. [45].

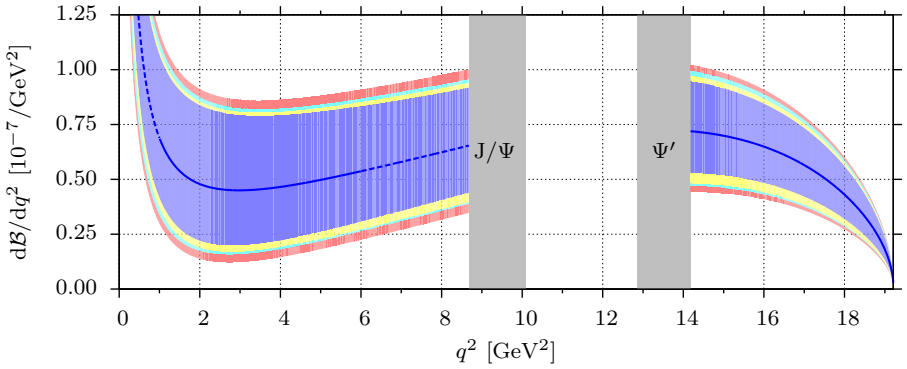

(a)

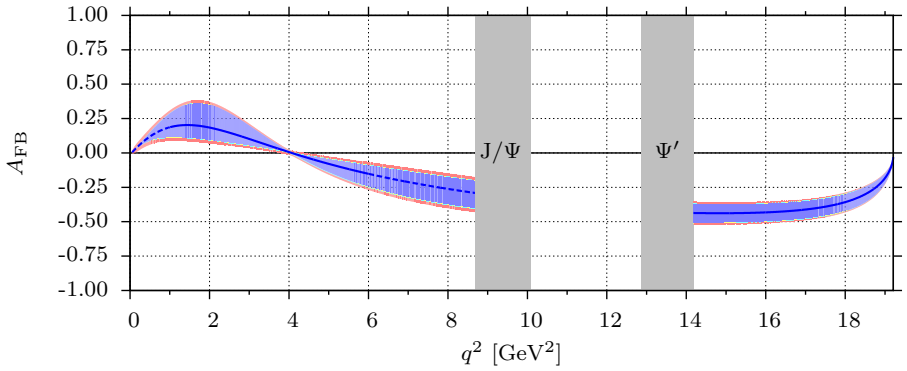

(b)

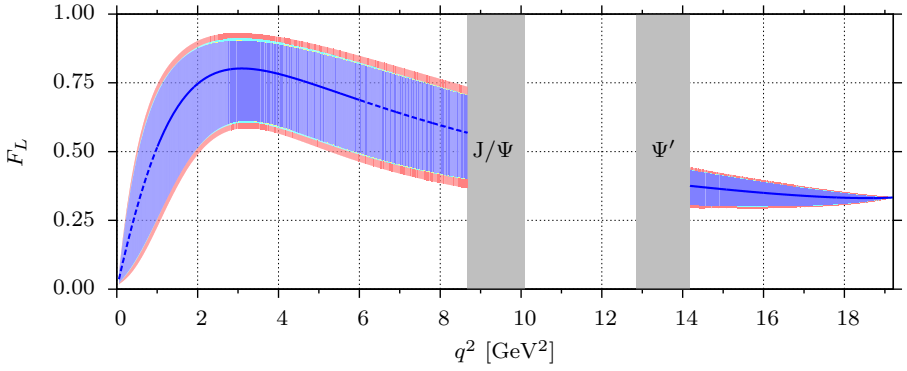

(c)

Figure 4.2.: (a) The differential branching ratio $d\mathcal{B}/dq^2$, (b) the forward-backward asymmetry A_{FB} and (c) the fraction F_L of longitudinally polarized kaons for the decay $\bar{B}^0 \to \bar{K}^{*0}\mu^+\mu^-$ in both the large and the low recoil region using extrapolations of the form factors according to Ball and Zwicky [63] (blue solid and dashed lines). The color coding for the theory uncertainties is the same as in Fig. 4.1. The vertical gray bands are the experimental veto regions to remove contributions from $\bar{B} \to \bar{K}^* J/\psi(\to \mu^+\mu^-)$ (left-hand band) and $\bar{B} \to \bar{K}^* \psi'(\to \mu^+\mu^-)$ (right-hand band). Figure adapted from Ref. [44].

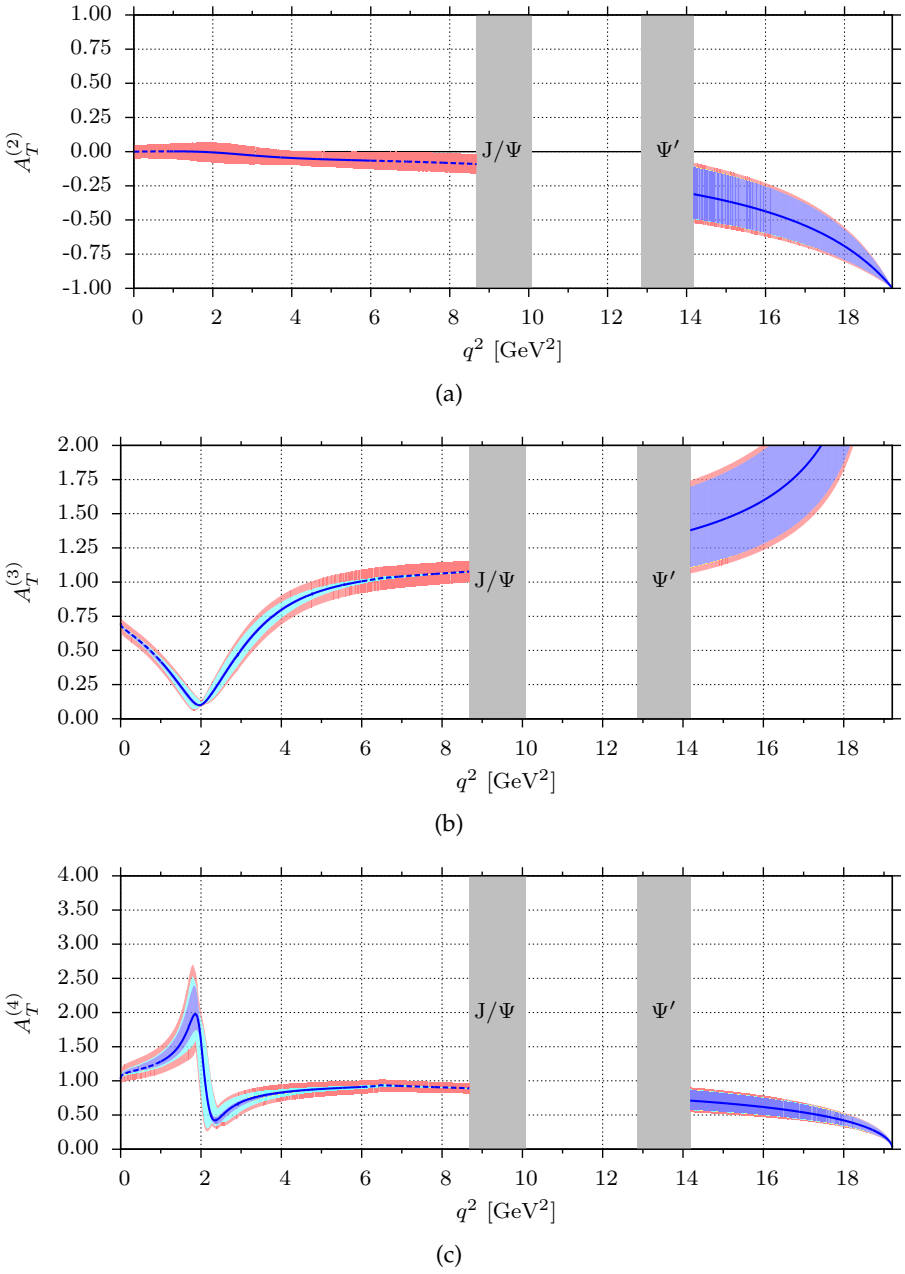

Figure 4.3.: (cont. of Fig. 4.2) The transverse asymmetries (a)-(c) $A_T^{(2,3,4)}$ in both the large and the low recoil region. All further remarks in Fig. 4.2 apply likewise to this figure. Figure adapted from Ref. [44].

Observable	Bin $[\,\mathrm{GeV}^2]$	$\bar{B}^0 \to \bar{K}^{*0}\ell^+\ell^-$	$B^- \to K^{*-}\ell^+\ell^-$
$10^7 \times \langle\mathcal{B}\rangle$	$4m_\mu^2 - 2.0$	$2.16^{+0.44}_{-0.39}$	$2.26^{+0.45}_{-0.41}$
	$2.0 - 4.3$	$1.05^{+0.25}_{-0.23}$	$1.15^{+0.27}_{-0.25}$
	$4.3 - 8.68$	$2.45^{+0.52}_{-0.49}$	$2.66^{+0.56}_{-0.53}$
	$1.0 - 6.0$	$2.46^{+0.55}_{-0.51}$	$2.68^{+0.60}_{-0.56}$
	$14.18 - 16.0$	$1.26^{+0.40}_{-0.34}$	$1.35^{+0.43}_{-0.37}$
	$16.0 - q^2_{\rm max}$	$1.46^{+0.45}_{-0.39}$	$1.57^{+0.48}_{-0.42}$
$\langle A_{\rm FB}\rangle$	$4m_\mu^2 - 2.0$	$+0.11^{+0.02}_{-0.02}$	$+0.11^{+0.02}_{-0.02}$
	$2.0 - 4.3$	$+0.09^{+0.03}_{-0.03}$	$+0.08^{+0.03}_{-0.03}$
	$4.3 - 8.68$	$-0.18^{+0.05}_{-0.05}$	$-0.18^{+0.04}_{-0.05}$
	$1.0 - 6.0$	$+0.05^{+0.03}_{-0.03}$	$+0.04^{+0.03}_{-0.02}$
	$14.18 - 16.0$	$-0.44^{+0.07}_{-0.07}$	$-0.44^{+0.07}_{-0.07}$
	$16.0 - q^2_{\rm max}$	$-0.38^{+0.06}_{-0.07}$	$-0.38^{+0.06}_{-0.07}$
$\langle F_L\rangle$	$4m_\mu^2 - 2.0$	$0.36^{+0.07}_{-0.07}$	$0.380^{+0.07}_{-0.07}$
	$2.0 - 4.3$	$0.78^{+0.05}_{-0.06}$	$0.786^{+0.05}_{-0.06}$
	$4.3 - 8.68$	$0.66^{+0.07}_{-0.08}$	$0.660^{+0.07}_{-0.07}$
	$1.0 - 6.0$	$0.73^{+0.06}_{-0.07}$	$0.736^{+0.06}_{-0.07}$
	$14.18 - 16.0$	$0.36^{+0.05}_{-0.06}$	$0.362^{+0.05}_{-0.06}$
	$16.0 - q^2_{\rm max}$	$0.34^{+0.03}_{-0.03}$	$0.338^{+0.03}_{-0.03}$
$\langle F_T\rangle$	$4m_\mu^2 - 2.0$	$0.64^{+0.07}_{-0.07}$	$0.620^{+0.07}_{-0.07}$
	$2.0 - 4.3$	$0.22^{+0.06}_{-0.05}$	$0.214^{+0.06}_{-0.05}$
	$4.3 - 8.68$	$0.34^{+0.08}_{-0.07}$	$0.340^{+0.07}_{-0.07}$
	$1.0 - 6.0$	$0.27^{+0.07}_{-0.06}$	$0.264^{+0.07}_{-0.06}$
	$14.18 - 16.0$	$0.64^{+0.06}_{-0.05}$	$0.638^{+0.06}_{-0.05}$
	$16.0 - q^2_{\rm max}$	$0.66^{+0.03}_{-0.03}$	$0.662^{+0.03}_{-0.03}$
$\langle A_T^{(2)}\rangle$	$14.18 - 16.0$	$-0.37^{+0.20}_{-0.18}$	$-0.37^{+0.20}_{-0.18}$
	$16.0 - q^2_{\rm max}$	$-0.60^{+0.15}_{-0.13}$	$-0.60^{+0.15}_{-0.13}$

Table 4.4.: SM predictions for $\bar{B}^0 \to \bar{K}^{*0}\ell^+\ell^-$ and $B^- \to K^{*-}\ell^+\ell^-$ decays in q^2 bins which are compatible with existing measurements. For the large recoil region $q^2 \leq 8.68\,\mathrm{GeV}^2$, we use the QCDF results [49], and include all known power-suppressed contributions [51], see text. For the low recoil region $14.18\,\mathrm{GeV}^2 \leq q^2 \leq q^2_{\rm max} = (M_B - M_{K^*})^2$ we use the low recoil framework [55, 44]. In both cases we use extrapolations of the $B \to K^*$ form factors [63].

5. Model Independent Analysis

We confront the available experimental data on $B \to \{X_s, K, K^*\}\,\ell^+\ell^-$ decays with the SM by performing a model independent analysis, i.e., we treat the Wilson coefficient $\mathcal{C}_{7,9,10}$ as free parameters and scan over the complete parameter space. In the following, we find that $B \to K^*\ell^+\ell^-$ observables in the low recoil region play a crucial role in constraining the parameter space. Our analysis uses EOS [89], a HEP flavor program which was created by the author for this very use case. Specifically, we use the client programs `eos-scan-polynomial`, `eos-find-cr` and `eos-marginalise` to obtain all results within this chapter. For an introduction to EOS we refer the reader to Appendix D

The experimental data on $B \to K^{(*)}\ell^+\ell^-$ decays as used in this analysis is compiled in Tab. 5.1[1]. In addition to this data, we use the inclusive branching ratio $\mathcal{B}\left(\bar{B} \to X_s\ell^+\ell^-\right)$ as measured by both BaBar [96] and Belle [97],

$$\int_{1\ \mathrm{GeV}^2}^{6\ \mathrm{GeV}^2} \mathrm{d}q^2 \frac{\mathrm{d}\mathcal{B}^{\mathrm{BaBar}}\left(\bar{B} \to X_s\ell^+\ell^-\right)}{\mathrm{d}q^2} = (1.8 \pm 1.2) \times 10^{-6}\,, \tag{5.1}$$

$$\int_{1\ \mathrm{GeV}^2}^{6\ \mathrm{GeV}^2} \mathrm{d}q^2 \frac{\mathrm{d}\mathcal{B}^{\mathrm{Belle}}\left(\bar{B} \to X_s\ell^+\ell^-\right)}{\mathrm{d}q^2} = \left(1.49^{+0.92}_{-0.83}\right) \times 10^{-6}\,. \tag{5.2}$$

To constrain the parameter space we perform a scan over the moduli and phases of the Wilson coefficients $\mathcal{C}_{7,9,10}$. The inclusion of complex phases allows us to model-independently account for generic CP violation beyond the SM. The $\mathcal{B}(\bar{B} \to X_s\gamma)$ data strongly constrain the magnitude $|\mathcal{C}_7|$ to a narrow range of values around $|\mathcal{C}_7^{\mathrm{SM}}| \approx 0.33$, however, they do not constrain the phase of $\mathcal{C}_7$. We therefore restrict both the scan interval and granularity of $|\mathcal{C}_7|$ accordingly. In particular, we perform the scan on the six-dimensional grid

$$\begin{aligned}
|\mathcal{C}_7| &\in [0.30, 0.40] \quad \Delta|\mathcal{C}_7| = 0.02\,, & \phi_7 &\in [0, 2\pi) \quad \Delta\phi_7 = \frac{\pi}{16}\,,\\
|\mathcal{C}_9| &\in [0, 15] \quad \Delta|\mathcal{C}_9| = 0.25\,, & \phi_9 &\in [0, 2\pi) \quad \Delta\phi_9 = \frac{\pi}{16}\,,\\
|\mathcal{C}_{10}| &\in [0, 15] \quad \Delta|\mathcal{C}_{10}| = 0.25\,, & \phi_{10} &\in [0, 2\pi) \quad \Delta\phi_{10} = \frac{\pi}{16}\,,
\end{aligned} \tag{5.3}$$

which necessitates approximately 6×10^8 evaluations of all observables. In order to shorten the computation time, we make use of that fact that all observables considered in this analysis are polynomials of degree two in the Wilson coefficients. We can therefore

[1] We remark that the Belle data on $B \to K^{(*)}\ell^+\ell^-$ stems from an unknown admixture of B^+ and B^0 decay modes. However, we explicitly test that the interpretation of the data as pure either B^+ or B^0 modes affect the scan results only by the order of the scan resolution. We note that with improving statistical significance of the LHCb results this ambiguity will become even less important. In this work, our results are always presented for the B^+ hypothesis.

Observable	Bin [GeV^2]	Belle [46]	CDF [47, 94]	LHCb [42]
		$\bar{B} \to \bar{K}^* \ell^+ \ell^-$		
$10^7 \times \langle \mathcal{B} \rangle$	$1.00 - 6.00$	$1.49^{+0.45}_{-0.40} \pm 0.12$	$1.42 \pm 0.41 \pm 0.12$	$0.39 \pm 0.06 \pm 0.02$
	$14.18 - 16.00$	$1.05^{+0.29}_{-0.26} \pm 0.08$	$1.34 \pm 0.26 \pm 0.08$	$0.59 \pm 0.10 \pm 0.03$
	$16.00 - 19.21$	$2.04^{+0.27}_{-0.24} \pm 0.16$	$0.97 \pm 0.26 \pm 0.07$	$0.48 \pm 0.08 \pm 0.03^\dagger$
$\langle A_{\mathrm{FB}} \rangle^\ddagger$	$1.00 - 6.00$	$-0.26^{+0.30}_{-0.27} \pm 0.07$	$-0.43^{+0.37}_{-0.36} \pm 0.06$	$+0.10^{+0.14}_{-0.14} \pm 0.05$
	$14.18 - 16.00$	$-0.70^{+0.22}_{-0.16} \pm 0.10$	$-0.42^{+0.16}_{-0.16} \pm 0.09$	$-0.50^{+0.09}_{-0.06} \pm 0.03$
	$16.00 - 19.21$	$-0.66^{+0.16}_{-0.11} \pm 0.04$	$-0.70^{+0.25}_{-0.16} \pm 0.10$	$-0.10^{+0.13}_{-0.13} \pm 0.06^\dagger$
$\langle F_L \rangle$	$1.00 - 6.00$	$0.67^{+0.23}_{-0.23} \pm 0.05$	$0.50^{+0.27}_{-0.30} \pm 0.03$	$0.57^{+0.11}_{-0.10} \pm 0.03$
	$14.18 - 16.00$	$-0.15^{+0.27}_{-0.23} \pm 0.07$	$0.55^{+0.17}_{-0.18} \pm 0.02$	$0.33^{+0.11}_{-0.08} \pm 0.04$
	$16.00 - 19.21$	$0.12^{+0.15}_{-0.13} \pm 0.02$	$0.09^{+0.18}_{-0.14} \pm 0.03$	$0.28^{+0.10}_{-0.09} \pm 0.04^\dagger$
		$B^+ \to K^+ \ell^+ \ell^-$		
$10^7 \times \langle \mathcal{B} \rangle$	$1.00 - 6.00$	$1.36^{+0.23}_{-0.21} \pm 0.08$	$1.41 \pm 0.20 \pm 0.10$	-
	$14.18 - 16.00$	$0.38^{+0.19}_{-0.12} \pm 0.02$	$0.53 \pm 0.10 \pm 0.03$	-
	$16.00 - 19.21$	$0.98^{+0.20}_{-0.18} \pm 0.06$	$0.48 \pm 0.11 \pm 0.03$	-

Table 5.1.: Experimental data for $B \to K^{(*)} \ell^+ \ell^-$ decays in both the large and low recoil regions which are used in the analysis. †: The max. q^2 for these bins is $19.0\,\mathrm{GeV}^2$ and used accordingly in the scans. ‡: The experimental convention for A_{FB} differs from our convention by a sign.

compute the polynomial coefficients for arbitrary input parameters from a few evaluations of the observables. This procedure is implemented within EOS as part of the client program `eos-scan-polynomial` [89].

The numerical results, as obtained for the scanning process, are naturally subject to theory uncertainties. Most of these uncertainties stem from incomplete knowledge of the input parameters, such as for example the Wolfenstein parameters of the CKM matrix, the form factor parameters, or the bottom and charm quark masses m_b and m_c. Furthermore, theory uncertainties can arise from unknown subleading contributions, which need to be estimated. For the treatment of the subleading contributions to $\bar{B} \to \bar{K}^{(*)} \ell^+ \ell^-$ decays at low recoil, we use the fact that subleading terms only arise from the OPE, where they are additionally suppressed by at least one power of $\alpha_s(\mu_b)/\pi \sim 0.07$, or from the improved Isgur-Wise relations, where they are additionally suppressed by a factor $\mathcal{C}_7/\mathcal{C}_9 \sim 0.1$. This suppression of subleading contributions makes the low recoil observables superior to those at large recoil with regard to theory uncertainties. For the large recoil region, we follow [71] closely for the parametrization of unknown subleading terms.

In order to determine the theory uncertainty of a given observable X, we set each of the variable input parameters to its maximally and minimally allowed value, thereby collecting deviations from the central value of X. By $\left(\Delta^{+(-)}\right)^2$, we denote the sum of

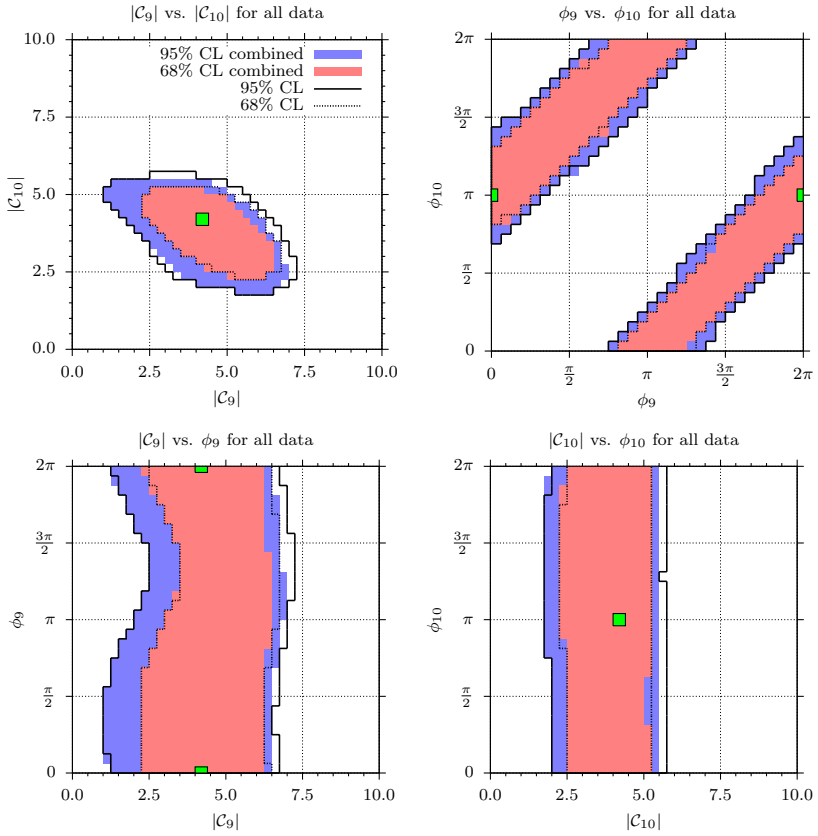

Figure 5.1.: Constraints on the complex-valued Wilson coefficients $\mathcal{C}_{9,10}$. The red (blue) shaded areas correspond to the 68% CL (95% CL) regions when using all available data. The dotted (solid) contours show the 68% CL (95% CL) regions without the available data on $B \to K\ell^+\ell^-$ observables. The green square marks the SM. Plots taken from Refs. [45] and [95].

the squares of these deviations towards larger (smaller) values, respectively. In order to calculate the goodness of fit in each parameter point, we define the following χ^2 function,

$$\chi_i\left(\{\mathcal{C}_j\}\right) \equiv \begin{cases} \frac{|X_i - E_i| - \Delta_i^+}{\sigma_i} & E_i \geq X_i + \Delta_i^+ \\ \frac{|X_i - E_i| - \Delta_i^-}{\sigma_i} & E_i \leq X_i - \Delta_i^- \\ 0 & \text{otherwise} \end{cases}, \tag{5.4}$$

$$\chi^2 \equiv \sum_i \chi_i^2\,, \tag{5.5}$$

where the index i iterates over the available observables and their respective measurements, and E and σ are the experimental result and the associated experimental uncertainty, respectively. We then obtain the (unnormalized) likelihood function

$$-2\ln\mathcal{L} = \chi^2\,, \tag{5.6}$$

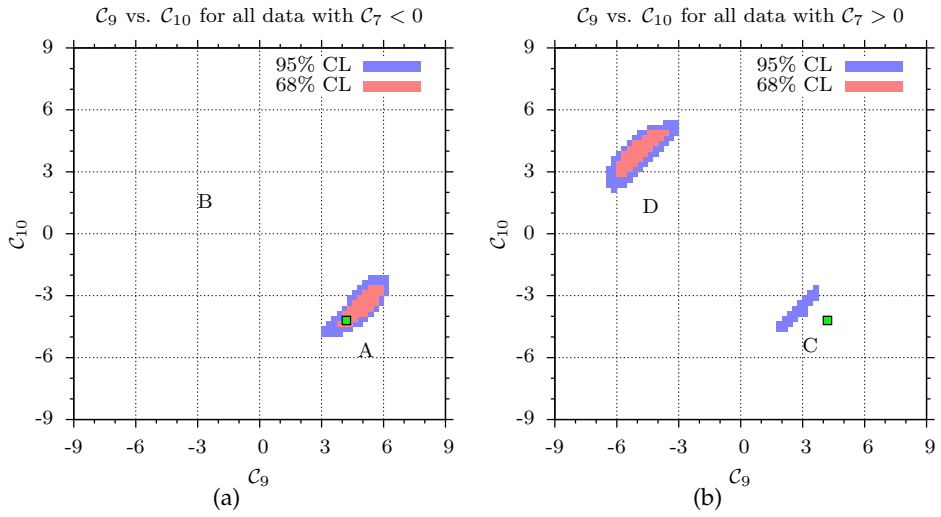

Figure 5.2.: Constraints on the real-valued Wilson coefficients $\mathcal{C}_{9,10}$ for (a) an SM-like sign of $\mathcal{C}_7$ and (b) for a flipped sign of $\mathcal{C}_7$ with respect to the SMvalue. The red (blue) shaded areas correspond to the 68% CL (95% CL) regions when using all available data. The letters A through D denote the four principal solutions, of which solution B has been disfavored at the 99% CL by recent LHCb data [42]. The green square marks the SM. Plots taken from Ref. [45].

on the full six-dimensional parameter space. This method was introduced in Ref. [98] under the name Range Fit (Rfit).

The scans presented here allow us to constrain the values of the coefficients $\mathcal{C}_9$ and $\mathcal{C}_{10}$ under the assumption that there are neither right-handed, scalar nor tensor contributions, and that the Wilson coefficients $\mathcal{C}_{1\ldots6,8}$ retain their respective SM values. In order to visualize the constraints, we first find the 68% and 95% confidence regions within the six-dimensional parameter space by means of numerical integration of the likelihood. The points $P_{68,95}$ that comprise the confidence regions are found by solving

$$\sum_{x\in P_{68\%}} \mathcal{L}(x) = 0.68 \times \sum_{\text{all } x} \mathcal{L}(x)\,, \qquad \sum_{x\in P_{95\%}} \mathcal{L}(x) = 0.95 \times \sum_{\text{all } x} \mathcal{L}(x)\,. \tag{5.7}$$

We obtain

$$2.3 \leq |\mathcal{C}_9| \leq 6.5 \qquad (1.0 \leq |\mathcal{C}_9| \leq 7.0)\,, \tag{5.8}$$

$$2.3 \leq |\mathcal{C}_{10}| \leq 5.3 \qquad (1.8 \leq |\mathcal{C}_{10}| \leq 5.5) \tag{5.9}$$

as allowed ranges at 68% CL (95% CL). In a further step, we then project these regions onto the planes $|\mathcal{C}_9|$–$|\mathcal{C}_{10}|$, $|\mathcal{C}_9|$–ϕ_9, $|\mathcal{C}_{10}|$-ϕ_{10} and ϕ_9–ϕ_{10}. The results of our scan are shown as these projections in Fig. 5.1. We remark that the constraints from $\bar{B} \to \bar{K}^*\ell^+\ell^-$ in the low recoil regions are presently much more powerful than all other constraints [44]. Furthermore, the first LHCb measurements [42] provide the most constraining power when compared with all other experimental inputs. Unfortunately, at the time of this

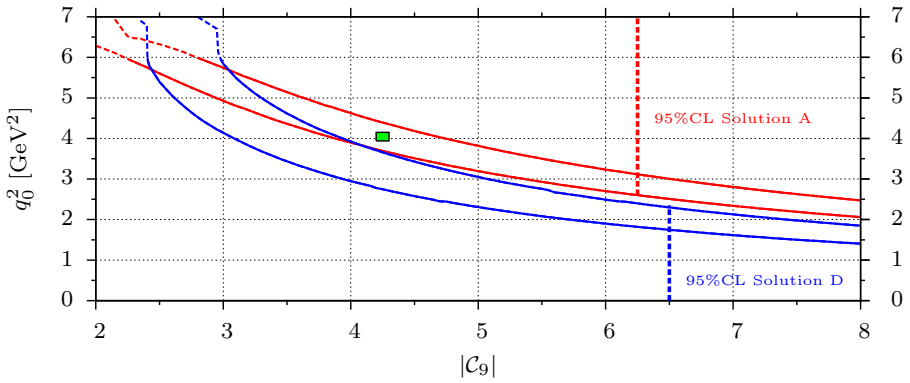

Figure 5.3.: Zero-crossing of the forward-backward asymmetry in $\bar{B}^0 \to \bar{K}^{*0}\ell^+\ell^-$ decays as a function of $|\mathcal{C}_9|$ for both signs of $\mathcal{C}_7$. The green rectangle marks the SM value. Plot taken from Ref. [45].

writing there have been no LHCb results on $B \to K\ell^+\ell^-$ decays. We expect that with the inclusion of the latter, the global constraints on $\mathcal{C}_{9,10}$ will grow considerably stronger.

Building on top of our scan results for complex-valued Wilson coefficients, we can derive results for real-valued Wilson coefficients by discarding all parameter points which do not fulfill $\phi_{7,9,10} = 0, \pi$. We present these results for both signs of $\mathcal{C}_7$ in Fig. 5.2. We find three disjoint solutions which are labeled A, C and D. The disappearance of the previously allowed solution B [44, 69] can be traced back to the inclusion of recent LHCb measurements, in particular the measurements of both the branching ratio and the forward-backward asymmetry at large recoil. Here, the fact that the very precise LHCb data are compatible with a zero-crossing within $A_{\rm FB}$ disfavors solution B and C strongly. With the first (preliminary) measurement of the zero-crossing by LHCb [91] we can now exclude solution C. However, differentiating between solutions A and D is a more complicated task. One possible approach would be to conduct precision measurements at a level where the observables become sensitive to the differences $\mathcal{C}_{7(9)}^{\rm eff} - \mathcal{C}_{7(9)}$ [44]. While the difference for $\mathcal{C}_9$ can be accessed through observables in both kinematical regions, the sensitivity to the difference for $\mathcal{C}_7$ is highest in the large recoil region and in $\bar{B} \to \bar{K}^*\gamma$ decays.

The solutions A and D both exhibit a zero-crossing in the forward-backward asymmetry $A_{\rm FB}$, which allows us to derive a lower bound on the crossing point [99, 45]. We obtain for $\mu_b = 4.2\,\text{GeV}$

$$q_0^2 > 2.6\,\text{GeV}^2 \qquad (q_0^2 > 1.7\,\text{GeV}^2) \tag{5.10}$$

for an SM-like (flipped) sign of $\mathcal{C}_{7,9,10}$ when using the 95% CL bound on $|\mathcal{C}_9|$. We note that our bounds are consistent with the recent (preliminary) data on, cf. Eq. (4.4). Moreover, the functional dependence of the lower bound on $|\mathcal{C}_9|$ is given in Fig. 5.3.

6. Conclusion

In this thesis we have studied for the first time the importance and the benefits in the phenomenology of $B \to K^{(*)}\ell^+\ell^-$ decays at low hadronic recoil. Thanks to the existence of an OPE this kinematic region is under good theory control. The strong suppression of subleading power corrections reduces the theory uncertainties in the low recoil region to a level below the uncertainties for the large recoil region. The factorization of short-distance and hadronic terms at low recoil offers many phenomenological opportunities, such as precision fits of the Wilson coefficients $\mathcal{C}_{9,10}$ and the measurement of form factor ratios. In the light of the former, we introduce a number of designer observables $H_T^{(1,2,3,4,5)}$ for the low recoil region, of which $H_T^{(1,3,4,5)}$ are free of hadronic input in all conceivable extensions of the operator basis. We have shown that $|H_T^{(1)}| = 1$ even beyond the SM, unless tensor operators are involved. Any deviation from this relation therefore indicates breaking of the low recoil OPE. Furthermore, we have shown that probing the short-distance couplings with $H_T^{(2,3)}$ is superior to using the forward-backward asymmetry A_{FB}, especially when BSM physics effects are very small in comparison with the SM results.

In addition to the analytic work on the decays $\bar{B} \to \bar{K}^*\ell^+\ell^-$ and $\bar{B} \to \bar{K}\ell^+\ell^-$, we have performed a global, model-independent analysis of both inclusive and exclusive semileptonic and radiative rare b decays. Our analysis yields strong constraints on the Wilson coefficients $\mathcal{C}_9$ and $\mathcal{C}_{10}$. Three solutions arise, which correspond to one SM-like solution (A), one solution for which the signs of $\mathcal{C}_{7,9,10}$ are flipped (D) and a further, disfavored solution with $\mathcal{C}_{9,10}$ SM-like and the sign of $\mathcal{C}_7$ flipped (C). The latter solution has recently been excluded by a preliminary LHCb measurement [91] at the time when this thesis was completed. The obtained constraints provide valuable input for further model-dependent studies.

In order to constrain the parameter space even further, more and more precise data is needed. We find that with one nominal year run time, i.e., using the 2010 and 2011 data set, LHCb has already surpassed the precision and constraining power of BaBar, Belle and CDF. Preliminary results by LHCb provide a strong indication that the zero-crossing of the forward-backward asymmetry exists [91], and solution (C) would therefore be excluded. Future works should rather concentrate on distinguishing between solutions (A) and (D). For this, both precision measurements and precision calculations will be needed. With regard to exclusive measurements, LHCb is already the leader of the field after over-taking the first generation B factory experiments BaBar and Belle. However, estimations of how LHCb will improve on the existing data are notoriously uncertain, as they depend on the overall performance of the LHC before the year-long technical stop in 2013 and the planned LHCb upgrade in 2017. Furthermore, the theoretical calculations of the exclusive decays is still hampered by the necessary hadronic

input. Inclusive decays, on the other hand, do not suffer from this problem but cannot be studied at hadron colliders. Here, the upcoming Belle II experiment will be able to contribute after the first collisions, expected at the end of 2015 [10]. With an integrated luminosity of 5ab^{-1} after the first year, the statistical error will be reduced[1] by a factor of six compared to the current Belle measurements [97]. It will be interesting to observe what will come first: Sufficient reduction of the theory uncertainties in exclusive decays, or improved measurements on the inclusive decays. Beyond this race for precision measurements and calculations, however, data is needed which is complementary to the existing measurements. Here, we have shown that the exclusive decays clearly have their benefits, since they provide powerful new types of constraints from observables which have severely reduced theoretical uncertainties. However, all currently measured observables restrict almost exclusively the magnitudes of the short-distance couplings. The phases of the Wilson coefficients, however, are only weakly constrained. To remedy that situation measurements of the CP asymmetries such as in $B \to K^{(*)}\ell^+\ell^-$ decays will be needed.

[1] Estimation based on the most precise measurement to date with 140fb^{-1} integrated luminosity.

A. $\bar{B} \to \bar{K}^*(\to \bar{K}\pi)\,\ell^+\ell^-$ Matrix Element

In this Appendix we present our choice of parametrization of the hadronic matrix element for the decay $\bar{B} \to \bar{K}^*(\to \bar{K}\pi)\,\ell^+\ell^-$

$$\mathcal{M}[\bar{B} \to \bar{K}^*(\to \bar{K}\pi)\bar{\ell}\ell] = \mathcal{F}\Big(X_S \left[\bar{\ell}\ell\right] + X_P \left[\bar{\ell}\gamma_5\ell\right] + X_V^\mu \left[\bar{\ell}\gamma_\mu\ell\right] + X_A^\mu \left[\bar{\ell}\gamma_\mu\gamma_5\ell\right] + X_T^{\mu\nu} \left[\bar{\ell}\sigma_{\mu\nu}\ell\right] \Big). \tag{A.1}$$

Here we collect all prefactors in $\mathcal{F}$,

$$\mathcal{F} = i\frac{G_{\rm F}\alpha_e}{\sqrt{2}\pi}\, V_{tb}V_{ts}^*\; g_{K^*K\pi} D_V\, 2|\vec{p}_K|\,, \tag{A.2}$$

with $\vec{p}_K$, the three-momentum of the $\bar{K}$ meson in the $\bar{K}\pi$ c.m.s.,

$$|\vec{p}_K| = \frac{\sqrt{\lambda\left(M_{K^*}^2, M_K^2, M_\pi^2\right)}}{2\,M_{K^*}}\,. \tag{A.3}$$

The hadronic tensors read

$$X_S = -\frac{i}{4}\cos\theta_K\, A_S, \tag{A.4}$$

$$X_P = +\frac{i}{2}\cos\theta_K\, \frac{m_\ell}{\sqrt{q^2}}\, A_t, \tag{A.5}$$

$$\begin{aligned} X_{V,A}^\mu = {} & +\frac{i}{4}\cos\theta_K\, \varepsilon^\mu(0)\,(A_0^R \pm A_0^L) \\ & + \frac{i}{8}\sin\theta_K \Big(\varepsilon^\mu(+)\, e^{+i\phi}\left[(A_\parallel^R + A_\perp^R) \pm (A_\parallel^L + A_\perp^L)\right] \\ & \qquad + \varepsilon^\mu(-)\, e^{-i\phi}\left[(A_\parallel^R - A_\perp^R) \pm (A_\parallel^L - A_\perp^L)\right] \Big), \end{aligned} \tag{A.6}$$

$$\begin{aligned} X_T^{\mu\nu} = {} & \cos\theta_K \left[A_{t0}\, \varepsilon^\mu(t)\, \varepsilon^\nu(0) - A_{\parallel\perp}\, \varepsilon^\mu(+)\, \varepsilon^\nu(-)\right] \\ & + \frac{\sin\theta_K}{\sqrt{2}}\, \varepsilon^\mu(t) \left[\varepsilon^\nu(+)\, e^{i\phi}\,(A_{t\parallel} + A_{t\perp}) + \varepsilon^\nu(-)\, e^{-i\phi}\,(A_{t\parallel} - A_{t\perp})\right] \\ & - \frac{\sin\theta_K}{\sqrt{2}}\, \varepsilon^\mu(0) \left[\varepsilon^\nu(+)\, e^{i\phi}(A_{0\parallel} + A_{0\perp}) + \varepsilon^\nu(-)\, e^{-i\phi}(A_{0\parallel} - A_{0\perp})\right], \end{aligned} \tag{A.7}$$

where we use the following explicit representation of the polarization vectors $\varepsilon^\mu(n)$ [69]

$$\varepsilon^\mu(\pm) = \frac{1}{\sqrt{2}}(0, 1, \mp i, 0), \qquad \varepsilon^\mu(0) = \frac{1}{\sqrt{q^2}}(-q_z, 0, 0, -q_0), \tag{A.8}$$
$$\varepsilon^\mu(t) = \frac{1}{\sqrt{q^2}}(q_0, 0, 0, q_z)$$

in the $\bar{B}$ meson rest frame. Here q_0 (q_z) denotes the timelike (spacelike) component of four-momentum q^μ and the polarization vectors fulfill

$$\varepsilon_\mu^\dagger(n)\,\varepsilon^\mu(n') = g_{nn'}, \qquad \sum_{n,n'} \varepsilon_\mu^\dagger(n)\,\varepsilon_\nu(n')\,g_{nn'} = g_{\mu\nu} \tag{A.9}$$

with $g_{nn'} = \text{diag}(+,-,-,-)$ for $n, n' = t, 0, \pm$. We use the orthonormality relation to insert the full set of polarization vectors $\varepsilon^\mu(n)$ between the hadronic and leptonic currents – see for example [100] for more details. The polarization vectors of the intermediate on-shell $\bar{K}^*$ read

$$\eta^\mu(\pm) = \frac{1}{\sqrt{2}}(0,1,\pm i,0), \qquad \eta^\mu(0) = \frac{1}{\sqrt{M_{K^*}}}(-q_z,0,0,M_B - q_0)\,, \tag{A.10}$$

where the z-axis in the $\bar{B}$ meson rest frame has been chosen along the $\bar{K}^*$ momentum and q^μ in the opposite direction.

The definition $\gamma_5 = -i/(4\,!)\,\varepsilon^{\alpha\beta\mu\nu}\gamma_\alpha\gamma_\beta\gamma_\mu\gamma_\nu$ is used, such that

$$\text{Tr}[\gamma^\alpha\gamma^\beta\gamma^\mu\gamma^\nu\gamma_5] = -4\,i\,\varepsilon^{\alpha\beta\mu\nu}, \qquad \sigma^{\alpha\beta}\gamma_5 = \frac{i}{2}\,\varepsilon^{\alpha\beta\mu\nu}\sigma_{\mu\nu} \tag{A.11}$$

with the usual anti-symmetric $\sigma_{\mu\nu} = i/2\,[\gamma_\mu, \gamma_\nu]$. The convention $\varepsilon_{0123} = -\varepsilon^{0123} = 1$ is adopted when evaluating the squared matrix element (A.1) using the explicit representation (A.8) and (A.10) of the polarization vectors.

B. $\bar{B} \to \bar{K}^*$ Form Factors

In this Appendix we discuss the state of nonperturbative calculations of the hadronic matrix elements in $\bar{B} \to \bar{K}^* \ell^+ \ell^-$ decays. These matrix elements can be parametrized in terms of seven q^2-dependent form factors $V, A_{0,1,2}, T_{1,2,3}$, which are define in Eqs. (3.17)-(3.21). In the following, we will consider results for the form factors which stem from two different, nonperturbative approaches.

First, we consider LCSR results as presented in Ref. [63]. This technique yields analytic results which are valid for large recoil of the final state kaon. In terms of the dilepton mass square, the region of validity is approximately $q^2 \lesssim 14\,\mathrm{GeV}^2$ [63]. In order to access the low recoil region, the authors of Ref. [63] fit their analytic results to q^2-dependent functions that exhibit either one or two poles within the physical region, i.e., for $q^2 \leq (M_B - M_{K^*})^2$. While these functions successfully reproduce the LCSR results in the large recoil region, their use for the low recoil region constitutes an extrapolation. For completeness, we give here the parametrization of the form factors $V, A_{1,2}$ from Ref. [63],

$$V(q^2) = \frac{r_1}{1 - q^2/m_R^2} + \frac{r_2}{1 - q^2/m_{\text{fit}}^2}, \tag{B.1}$$

$$A_1(q^2) = \frac{r_2}{1 - q^2/m_{\text{fit}}^2}, \tag{B.2}$$

$$A_2(q^2) = \frac{r_1}{1 - q^2/m_{\text{fit}}^2} + \frac{r_2}{(1 - q^2/m_{\text{fit}}^2)^2}, \tag{B.3}$$

which we use at both low and large recoil. The fit parameters $r_{1,2}, m_R^2$ and m_{fit}^2 are given in Tab. B.1. The resulting form factors are shown in Fig. B.1. We assume an overall, uncorrelated theory uncertainty of 15% for each of the above form factors, as suggested in Ref. [63]. We are compelled to remark that this treatment of the theory uncertainty is very conservative, and most likely overestimates the overall theory uncertainty of $\bar{B} \to \bar{K}^* \ell^+ \ell^-$ observables.

	r_1	r_2	$m_R^2\,[\mathrm{GeV}^2]$	$m_{\text{fit}}^2\,[\mathrm{GeV}^2]$
V	0.923	-0.511	5.32^2	49.40
A_1	–	0.290	–	40.38
A_2	-0.084	0.343	–	52.00

Table B.1.: The parameters of the form factors $V, A_{1,2}$ taken from Ref. [63]. Figure taken from Ref. [44].

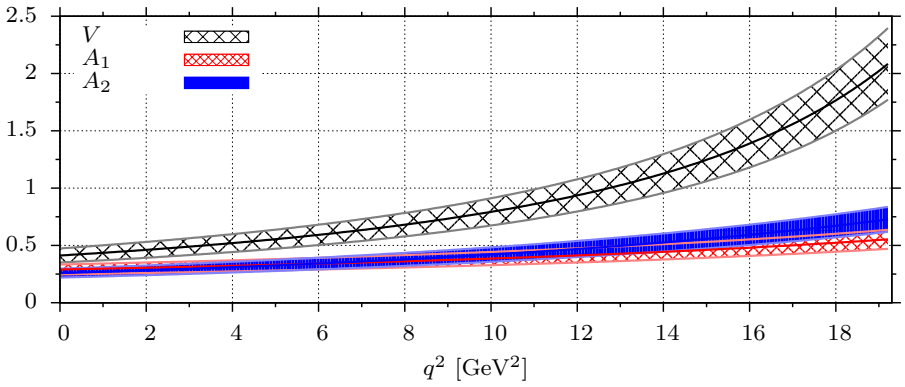

Figure B.1.: The $B \to K^*$ form factors V, A_1 and A_2 from Ref. [63]. Figure taken from Ref. [44].

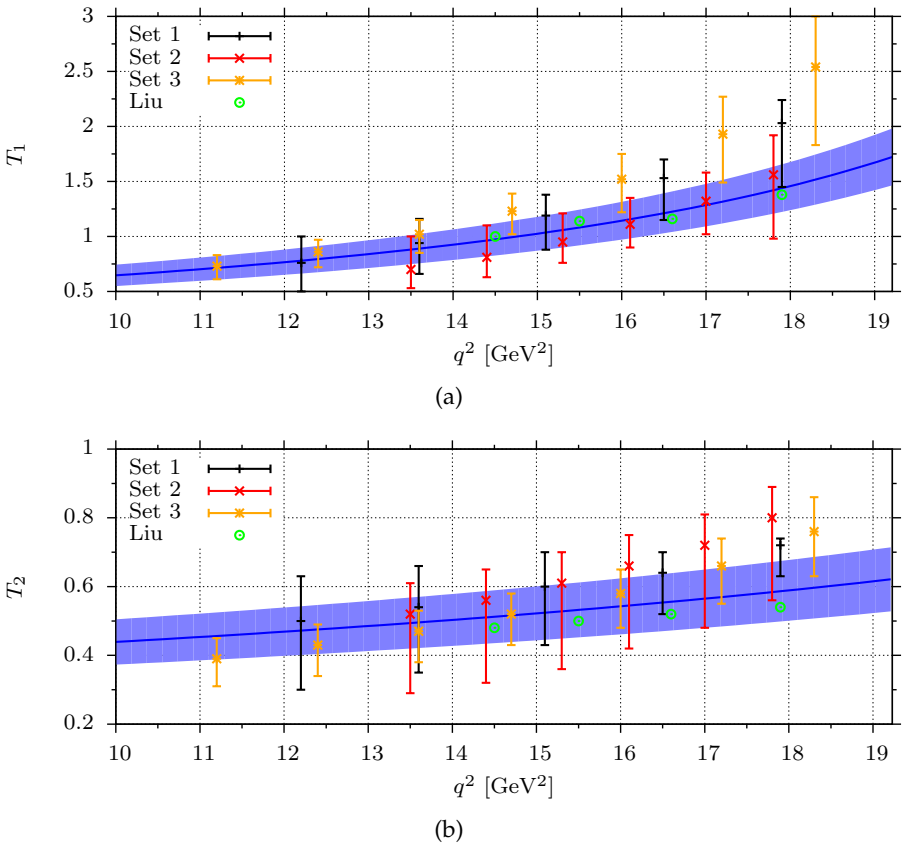

Figure B.2.: The form factors T_1 (a) and T_2 (b) for $B \to K^*$ transitions from Ref. [63] (blue bands) and LQCD results (3 data sets) [101]. Figure taken from Ref. [44].

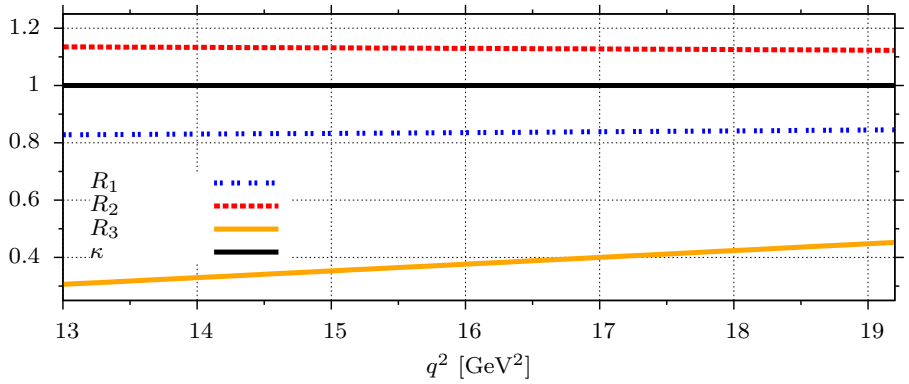

Figure B.3.: Comparison of the extrapolated LCSR form factors from [63] to the improved Isgur-Wise relations in Eq. (3.23). Shown are R_1 (blue dotted line), R_2 (red dashed line) and R_3 (golden solid line) as given in Eq. (B.4) and $\kappa = 1 + \mathcal{O}(\alpha_s^2)$ for $\mu = m_b(m_b)$ (black thick line). Figure taken from Ref. [44].

Second, we consider quenched LQCD results, which are currently only available for the form factors $T_{1,2}$ [101]. We use their data sets for a variety of points with $q^2 \geq 11\,\mathrm{GeV}^2$, and compare them in Fig. B.2 with extrapolations of the aforementioned LCSR results. In light of considerable uncertainties of both LCSR extrapolation and LQCD results, we find agreement between both nonperturbative approaches. We explicitly check that the preliminary results from unquenched calculations in Ref. [102] agree with the LCSR extrapolations as well. We therefore decide to use the LCSR extrapolations for the evaluation of $\bar{B} \to \bar{K}^* \ell^+ \ell^-$ observables at both large and low recoil.

We probe the performance of the improved Isgur-Wise relations in Eq. (3.23) with three ratios

$$R_1 = \frac{T_1(q^2)}{V(q^2)}\,, \qquad R_2 = \frac{T_2(q^2)}{A_1(q^2)}\,, \qquad R_3 = \frac{q^2}{M_B^2}\frac{T_3(q^2)}{A_2(q^2)}\,, \tag{B.4}$$

which should all be compatible with $\kappa(\mu = m_b) = 1 + \mathcal{O}\left(\alpha_s^2\right)$ if the relations hold. Both the R_i as functions of q^2, and κ are shown in Fig. B.3. We remark that similar relations hold in the large recoil region. There $R_{1,2} = 1 + \mathcal{O}(m_{K^*}/m_B)$ and $T_3/A_2 = 1 + \mathcal{O}(m_{K^*}/m_B)$ [103, 64]. We find that the improved Isgur-Wise relations hold reasonably well for $T_{1,2}$. The relation R_3, however, exhibits a considerable q^2 dependence and shows deviations from κ by $\sim 50\%$ for $q^2 = 14\,\mathrm{GeV}^2$. While replacement of the factor q^2/M_B^2 in both the respective Isgur-Wise relation and R_3 remedies this deviation, we still keep it. This decision is justified by the fact that the dipole form factors $T_{1,2,3}$ always enter $B \to K^* \ell^+ \ell^-$ observables with a suppression factor of $\mathcal{C}_7/\mathcal{C}_9 \simeq 0.1$.

B. $\bar{B} \to \bar{K}^*$ Form Factors

For the low q^2 form factors we employ a factorization scheme within QCDF where the universal soft form factors $\xi_{\perp,\parallel}$ are expressed in terms of the full QCD form factors $V, A_{1,2}$ [51]. They read

$$\xi_\perp = \frac{M_B}{M_B + M_{K^*}} V, \qquad \xi_\parallel = \frac{M_B + M_{K^*}}{2E_{K^*}} A_1 - \frac{M_B - M_{K^*}}{M_B} A_2 \,. \tag{B.5}$$

C. $\bar{B} \to \bar{K}$ Form Factors

In this Appendix we discuss the state of nonperturbative calculations of the hadronic matrix elements in $\bar{B} \to \bar{K}\ell^+\ell^-$ decays. These matrix elements can be parametrized in terms of three q^2-dependent form factors $f_+^{BK}, f_0^{BK}, f_T^{BK}$. We drop the superscript BK for the remainder of this appendix. For the concrete parametrization, we refer to Eqs. (3.13)-(3.15). In addition to these three QCD form factors, we also define the subleading HQET form factors $\delta_\pm^{(0)}(q^2)$ via

$$\left\langle \bar{K}(k)\right| \bar{s}\, i \overleftarrow{D}_\mu h_v \left|\bar{B}(p)\right\rangle = \delta_+^{(0)}(q^2)(p+k)_\mu + \delta_-^{(0)}(q^2) q_\mu \,, \tag{C.1}$$

with the HQET heavy quark field h_ν of the b quark. In the following, we will study results for the form factors which stem from several different, nonperturbative approaches.

As for the discussion of $\bar{B} \to \bar{K}^*$ form factors in Appendix B we use LCSR results for the form factors. For $\bar{B} \to \bar{K}$ transitions, we rely on the findings of Ref. [48] for large hadronic recoil. In the same work the results are also extrapolated to the region of low hadronic recoil by means of the parametrization [104]

$$F(q^2) = \frac{F(0)}{1 - q^2/M_{B_s(J^P)}^2} \left\{ 1 + b_1 \left(z(q^2) - z(0) + \frac{1}{2}\left[z(q^2) - z(0) \right] \right) \right\} , \tag{C.2}$$

with

$$z(\tau) = \frac{\sqrt{\tau_+ - \tau} - \sqrt{\tau_+ - \tau_0}}{\sqrt{\tau_+ - \tau} + \sqrt{\tau_+ - \tau_0}} \tag{C.3}$$

$$\tau_\pm = \left(M_B \pm M_K\right)^2 , \tag{C.4}$$

$$\tau_0 = \tau_+ - \sqrt{\tau_+ - \tau_-}\sqrt{\tau_+} \,. \tag{C.5}$$

The poles of $F(q^2)$ at $M_{B_s(J^P)}^2$ correspond to the resonances with quark content $\bar{s}b$ that match the angular momentum and parity eigenvalue of the interpolating currents. This is $B_s^*(1^-)$ for the form factors f_+ and f_T, while for f_0 no resonance exists below $q^2 = \tau_-$. For the parameters b_1^i and $F_i(0)$ as well as their uncertainties we refer the reader to [48]. The q^2 dependence of the form factors is shown in Fig. C.1.

We follow the procedure of Appendix B and define the quantity

$$R_T(q^2) = \frac{q^2}{M_B(M_B + M_K)} \frac{f_T(q^2)}{f_+(q^2)} \tag{C.6}$$

to probe the performance of the improved Isgur-Wise relation Eq. (3.24) to its lowest order. Here $R_T \simeq \kappa = 1 + \mathcal{O}\left(\alpha_s^2\right)$ indicates a good performance of the relation. We find

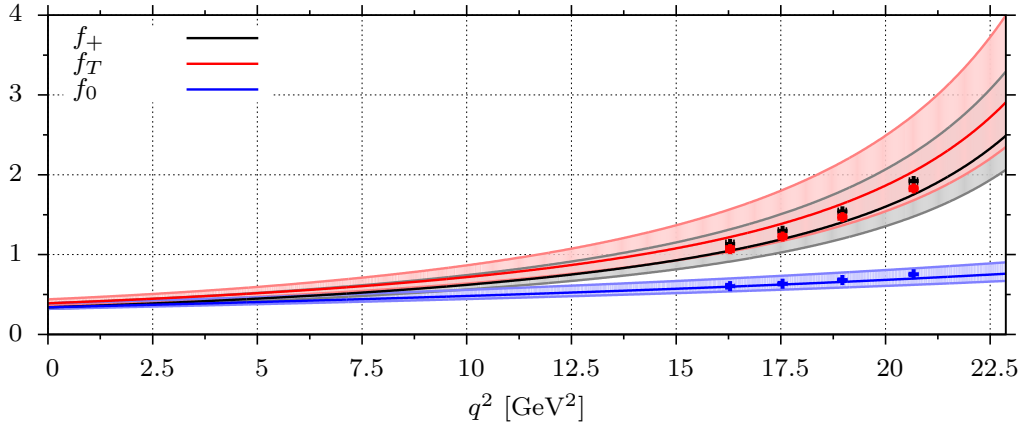

Figure C.1.: Extrapolation to high-q^2 of the form factors f_+, f_T and f_0 for $\bar{B} \to \bar{K}$ transitions as given by [48]. The shaded bands show the respective form factor uncertainties. Figure taken from Ref. [45].

that R_T agrees well with κ close to the zero recoil point. However, for $q^2 \simeq 14\,\mathrm{GeV}^2$, the deviations from κ of both the LCSR results as well as preliminary LQCD points [65] approach 50%. R_T is shown within the low recoil region in Fig. C.2. When we include the subleading form factors $\delta_+^{(0)}$ the situation grows worse [45]. However, the apparent breaking of the improved Isgur-Wise relation does not surprise when we study the nature of the parametrizations of the involved form factors f_+ and f_T. Schematically, one has an expansion in powers of $z \equiv z(q^2)$ which reads

$$f_+(q^2) = \frac{\sum_n a_n z^n}{q^2 - M_{B_s^*}^2} \tag{C.7}$$

$$f_T(q^2) = \frac{\sum_n b_n z^n}{q^2 - M_{B_s^*}^2} \tag{C.8}$$

with the coefficients a_n, b_n determined by fits to, e.g., the LCSR results. When plugged into Eq. (C.6), one finds naturally

$$R_T(q^2) = \frac{q^2}{M_B(M_B + M_K)} \frac{b_0}{a_0} + \mathcal{O}(z)\,, \tag{C.9}$$

and thus a strong q^2 dependence with R_T. Unfortunately, we cannot extract the shape of f_T from experimental data, since in all observables f_T only enters with a numerically small factors $\mathcal{C}_7/\mathcal{C}_9$. Further input from, e.g., LQCD is needed to determine the best choice of form factor parametrization [45]. On the other hand, the low sensitivity to f_T allows us to apply the improved Isgur-Wise relation to our model-independent analysis without adverse effects. Furthermore, choosing the form factors from Ref. [48] appears justified, since they match the preliminary LQCD results in the low recoil region, further LCSR results [62] in the large recoil region, and results from relativistic quark model [100] for the both kinematic regions. We show a comparison of the individual form factors results in Fig. C.3.

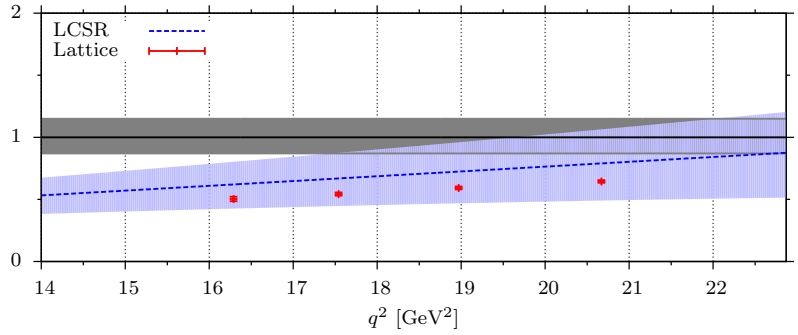

Figure C.2.: The relation R_T as a function of q^2 in the low recoil region. The blue band shows the form factor relation as obtained from light cone sum rule (LCSR) calculations by Khodjamirian et al [48]. Preliminary results from the lattice (with only statistical uncertainties) by Liu et al [65] are presented as red points. The prediction of R_T to leading order in α_s for the range $\frac{m_b}{2} \leq \mu \leq 2m_b$ is shown by the gray band. Figure taken from Ref. [45].

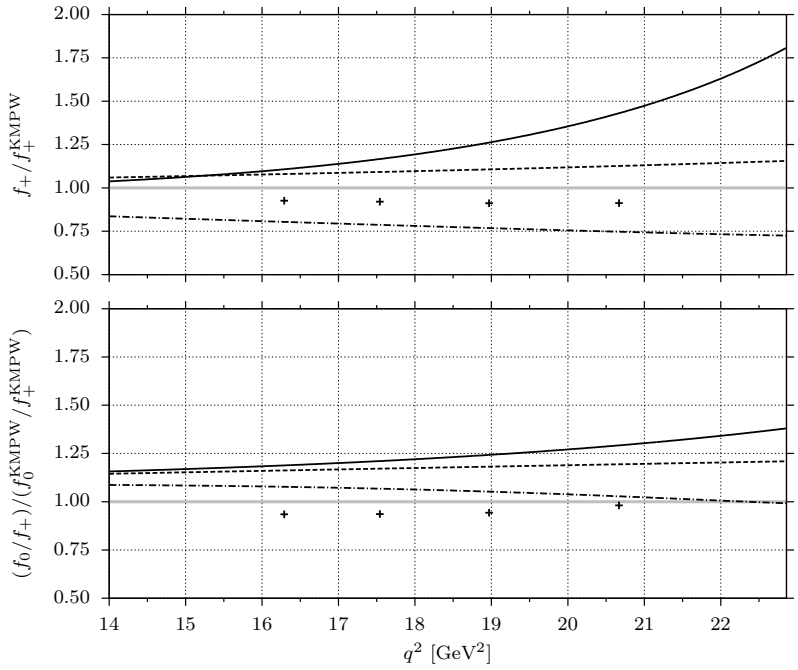

Figure C.3.: The form factor f_+ and the ratio f_0/f_+ from extrapolated LCSRs by [62] (solid lines), extrapolated LCSRs with simplified series expansion [67] (dashed), a relativistic quark model [100] (dash-dotted) and unquenched lattice calculations [65] (points), normalized to the corresponding quantities derived from Ref. [48] and as used in this work. Figure taken from Ref. [45].

D. Introduction to EOS

The development of EOS [89], a framework for the evaluation of flavor observables, was instrumental to the work presented in this thesis. The most recent source code can be downloaded from `http://project.het.physik.tu-dortmund.de/eos/source`. In this Appendix we would like to present an overview of this framework. For this overview, we expect the reader to have a working knowledge in object oriented programming with the `C++` programming language. The EOS source code makes heavy use of `C++` features, some of which have only been introduced in the recently enacted `C++2011` standard. Readers interested in the development of EOS should further be familiar with software design patterns. We start our tour with EOS' use cases in Section D.1. After that, we give insights into the nomenclature and concepts of the source code in Section D.2. We conclude the chapter in Section D.3 with a brief description how extensions to EOS can be developed by interested users.

D.1. Use Cases

EOS has been developed with two distinct use cases in mind. First, it is meant to numerically evaluate flavor observables of several processes, for a large number of input parameters and for varying kinematic variables. All these evaluations are intended to be possible via a UNIX-like command line and within shell scripts. This use case is achieved by means of the client `eos-evaluate`. It accepts a list of observables, their associated kinematics and input parameters, and outputs the numerical values and associated theory uncertainties. Input parameters whose numerical values shall be varied can be grouped into uncertainty budgets. An example on how to invoke this client for one observable and with two uncertainty budgets, including the generated output, is listed in Fig. D.1. We refer to Tab. D.1 for an overview of the set of flavor observables that have been implemented within EOS at the time of this writing.

Furthermore, EOS is meant to constrain input parameters based on existing experimental results. For this use case, the evaluation of observables needs to be reasonably fast. Moreover, in order to effectively store samples of the parameter space from a multi-threaded computation, a suitable storage backend is needed. For the latter, EOS uses the HDF5 library. This use case is handled by the `eos-scan` family of clients. For the scans presented in this thesis, the `eos-scan-polynomial` client has been used. Its usage is restricted to scanning the complex-valued Wilson coefficients $\mathcal{C}_{7,9,10}$, and it will be deprecated once development of the `eos-scan-mc` client has been completed. The latter client will be universally usable, i.e., it will allow to perform a Bayesian analysis by means of Monte Carlo sampling of the complete `Parameter` space. We abstain from listing examples on how to invoke the `eos-scan` or `eos-scan-polynomial` clients. However, the scripts used to generate the data as used in Chapter 5 can be obtained

```
$ eos-evaluate \
  --kinematics "s" "15.0" \
  --observable "B->Kˆ*ll::H_Tˆ3(s)@LowRecoil,model=SM,form-factors=KMPW2010" \
  --budget "FF" \
  --vary "B->Kˆ*::FˆV(0)@KMPW2010" \
  --vary "B->Kˆ*::FˆA1(0)@KMPW2010" \
  --vary "B->Kˆ*::FˆA2(0)@KMPW2010" \
  --vary "B->Kˆ*::bˆV_1@KMPW2010" \
  --vary "B->Kˆ*::bˆA1_1@KMPW2010" \
  --vary "B->Kˆ*::bˆA2_1@KMPW2010" \
  --budget "SD" \
  --vary "mu" \
  --vary "mass::t(pole)" \
  --vary "mass::W" \
  --vary "GSW::sinˆ2(theta)"
```

(a)

```
  # B->Kˆ*ll::H_Tˆ3(s)@LowRecoil:
  # s central FF_min  FF_max  SD_min  SD_max  delta_min delta_max
  15  -0.983845 8.59975e-16 1.11022e-16 0.00734327  0.00602218  0.00734327 \
    0.00602218   (-0.746386% / +0.612107%)
```

(b)

Figure D.1.: Example (a) invocation and (b) output of the `eos-evaluate` client to numerically evaluate the observable $H_T^{(3)}$ for the decay $\bar{B}^0 \to \bar{K}^{*0}\mu^+\mu^-$ for $s \equiv q^2 = 15.0\,\mathrm{GeV}^2$. For the theory uncertainty, two budgets are defined, each of which contains a number of input parameters that are varied within their respective uncertainty regions.

from the author upon request.

Common to both use cases is the computation of running masses, couplings and the underlying physical observables, as well utilities such as numerical integration, multi-threaded computations and file storage. These common features are bundled in a set of libraries and form the core of the EOS framework.

D.2. Concepts and Implementation

At the core of EOS' design stands the concept of an `Observable`, which does not fully coincide with the physical definition. For EOS, every quantity that is meant to be numerically evaluated and presented to the user is an `Observable`. This includes, among others, physical observables such as branching ratios and angular observables, but beyond those also form factors and short-distance couplings, e.g., $\rho_{1,2}(q^2)$. EOS constructs `Observables` at run time from an `ObservableName` via an abstract factory. For the construction the factory further needs a set of `Parameters`, a set of `Kinematics` and a set of `Options`. After construction, the `Observable` itself is immutable, and it can evaluated. Changes to the `Parameters` object that was used in the `Observables` construction will affect the evaluation. This enables EOS to efficiently accomplish both of

the aforementioned use cases.

ObservableName is a standard `C++` string with a fixed format. It consists of four parts,

```
PROCESS::NAME@SUFFIX,KEYVALUELIST
```
(D.1)

of which `PROCESS` and `NAME` are mandatory, `SUFFIX` can be used depending on the `PROCESS` and `KEYVALUELIST` is always optional. As examples consider

```
B->K^*gamma::S_K^*gamma,
```

referring to a time-dependent CP asymmetry in $B, \bar{B} \to K^{*0}(\to K_s\pi^0)\gamma$ decays, and

```
B->K^*ll::A_FB@LowRecoil,
B->K^*ll::A_FB@LargeRecoil.
```

as the forward-backward asymmetry in $\bar{B} \to \bar{K}^*\ell^+\ell^-$ decays at low and large recoil, respectively. The `SUFFIX` is used to distinguish between observables for the same process, e.g., when several kinematic regions demand different approaches to the calculation, or when a switch to the next order is made for perturbative calculations.

Kinematics represents the set of kinematic variables, which are organized as a string key and a double-precision floating-point value. All EOS clients allow building of the `Kinematics` from the command line interface by preceding each `--observable` command by zero or more `--kinematics` commands. The syntax for the latter reads `--kinematic NAME VALUE`. Note that the kinematics can only be used once for the next `--observable` command. For repeated use of the same kinematics we recommend using a shell script.

Options represents a set of key-value pairs: the key is a string with a (per Process) unique identifier, and the value is also a string. Options are used as multi-value switches, to select for instance form factor results, as well as lepton and quark flavors. The semileptonic $|\Delta B| = 1$ `Observable`s all recognize the following `Options`:

`model` Selects the `Model` class which shall be used for the evaluation. Valid values are `SM` and `WilsonScan`.

`form-factors` Selects the form factor class which shall be used for the evaluation. Valid values depend on the concrete `Observable`.

`q` Selects the final state quark flavor. Valid values are `s` and `d`.

`l` Selects the final state lepton flavor. Valid values are `e`, `mu` and `tau`.

Parameters represents a set of key-value pairs, which are organized as a string key and a three-tuple of double-precision floating-point values. By default, each parameter is initialized with a minimal, a central and a maximal value. The default `Parameters` can be obtained from the named constructor `Parameters::Default()`. For a complete list of `Parameters` we refer the reader to the `eos-list-parameters` client. The latter accepts `--kinematics` / `--observable` commands, which restricts the list of parameters to only those which are used by the `Observable`(s) at hand.

Model represents a physical model for which an observable is evaluated. It provides access to the running quark masses, CKM matrix elements and $|\Delta B| = 1$ Wilson coefficients. By default, all observables are created with the `SM Model`. However, for the determination of the $|\Delta B| = 1$ Wilson coefficients, the `WilsonScan Model` should be used.

D.3. Development

EOS is meant to be expanded by interested parties, and its design reflects the wish to reduce the amount of work needed for such expansions. An interested developer might most likely want to add further `Observable`s to EOS.

The requirements for adding a further `Observable` are few. First, one needs to implement the numerical evaluation of the underlying process within a new class[1], named `NewProcess` in the following. Each exported `Observable` should correspond to one `public const` method of `NewProcess`. All input parameters used in the evaluation must be `UsedParameter` members of `NewProcess`'s implementation. In a last step, the `Observable` factory within `eos/observable.cc` needs to be made aware of the new `Observables` by linking the class' methods to its unique `ObservableName`. The kinematic variables must be provided to the methods as `const double` references, and they are associated by name and order through a list of unique identifiers. A hypothetical example for the cross section of a process $AB \to CD$, as a function of s, the center of mass energy squared, is given in Fig. D.2. Once the above steps are completed, all EOS clients that accept `--observable` as a command line argument will be able to use the newly introduced `Observable`.

[1] For details on the class structure, we refer to the EOS source code. The source file `eos/rare-b-decays/exclusive-b-to-dilepton.cc` and its eponymous header file should be a good start for a relatively simply-structured decay. For processes with a larger number of observables, see `eos/rare-b-decays/exclusive-b-to-s-dilepton-low-recoil.cc` for instance. Readers of the source code should be advised that EOS makes extensive use of the private implementation design pattern.

```
#include <eos/utils/parameters.hh>

class ABToCD
{
    UsedParameter g;
    ABToCD();
    double diff2_sigma(const double & s, const double & theta) const;
    double diff1_sigma(const double & s) const;
};
```

(a) New file `eos/a-b-to-c-d.hh`

```
#include <eos/a-b-to-c-d.hh>

class ABToCD
{
    UsedParameter g;

    ABToCD(...) :
      g(p["g"], u)
    {
    }

    double diff2_sigma(const double & s, const double & theta) const
    {
        return g * g / (4.0 * M_PI) / s * std::sin(theta);
    }

    double diff1_sigma(const double & s) const
    {
        return g * g / (3.0 * M_PI) / s;
    }
}
```

(b) New file `eos/a-b-to-c-d.cc`

```
// At the top of the file
#include <eos/a-b-to-c-d.hh>
...

// Inside the std::map's initializer list within Observable::make()
make_observable("AB->CD::sigma(s,theta)", &ABToCD::diff2_sigma,
    std::make_tuple("s", "theta")),
make_observable("AB->CD::sigma(s)", &ABToCD::diff1_sigma,
    std::make_tuple("s")),
```

(c) Within `eos/observable.cc`

```
// Within the std::initializer_list inside Parameters::Defaults()
Parameter::Template{ "g",   -1.0, +0.1, +1.0 },
```

(d) Within `eos/utils/parameters.cc`

Figure D.2.: Example on how to add two observables (a double-differential and a single-differential cross section) for a hypothetical process $AB \to CD$ to EOS. For any yet undeclared parameter used by the new process, an addition similar to (d) must be made.

EOS Name	Suffixes	Kinematics	Symbol	Ref
`B->K^*gamma::BR`	—		$\mathcal{B}(\bar{B} \to \bar{K}^*\gamma)$	[51]
`B->K^*gamma::S_K^*gamma`	—		$S_{K^*\gamma}$	[51]
`B->K^*gamma::C_K^*gamma`	—		$C_{K^*\gamma}$	[51]
`B->K^*gamma::A_I`	—		A_I	[52, 51]
`B->K^*ll::BR`	`LargeRecoil`, `LowRecoil`	$s_{\min}, s_{\max}$	$\mathcal{B}(\bar{B} \to \bar{K}^*\ell^+\ell^-)$	[51, 44]
`B->K^*ll::A_FB`	`LargeRecoil`, `LowRecoil`	$s_{\min}, s_{\max}$	$A_{\rm FB}$	[51, 44]
`B->K^*ll::F_L`	`LargeRecoil`, `LowRecoil`	$s_{\min}, s_{\max}$	F_L	[51, 44]
`B->K^*ll::A_T^i`	`LargeRecoil`, `LowRecoil`	$s_{\min}, s_{\max}$	$A_T^{(i)}$	[51, 44]
`B->K^*ll::H_T^i`	`LargeRecoil`, `LowRecoil`	$s_{\min}, s_{\max}$	$H_T^{(i)}$	[51, 44]
`B->K^*ll::a_CP^i`	`LowRecoil`	$s_{\min}, s_{\max}$	$a_{\rm CP}^{(i)}$	[60]
`B->K^*ll::A_I`	`LargeRecoil`	$s_{\min}, s_{\max}$	A_I	[52, 51]
`B->Kll::BR`	`LargeRecoil`, `LowRecoil`	$s_{\min}, s_{\max}$	$\mathcal{B}(\bar{B} \to \bar{K}\ell^+\ell^-)$	[38, 45]
`B->Kll::F_H`	`LargeRecoil`, `LowRecoil`	$s_{\min}, s_{\max}$	F_H^ℓ	[38, 45]
`B->Kll::R_K`	`LargeRecoil`, `LowRecoil`	$s_{\min}, s_{\max}$	$R_K^{e,\mu}$	[38, 45]

Table D.1.: List of observables that are implemented within EOS at the time of this writing. We give the EOS base name, the applicable suffixes, the needed kinematic variables, as well as the usual symbolic representation and a reference for the numeric implementation (see also references therein) for each `observable`. In the case of $\bar{B} \to \bar{K}^{(*)}\ell^+\ell^-$ observables, we only list the (partially) $s \equiv q^2$ integrated observables. For the q^2 differential observables, the name must be appended by `(s)`, and the kinematic variable reads likewise.

Acknowledgments

First of all I wish to express gratitude and love for my parents Detlef and Bärbel, my sister Carolin and my grandmothers Erika and Maria, for their loving support throughout the last years.

Next I wish to thank my advisor Gudrun Hiller, who provided me with a fascinating topic. I am grateful to her and to my colleagues Christoph Bobeth and Christian Wacker for the opportunity to collaborate on several interesting projects in the course of my studies, and of course for constant support and help. Both Christian's and Christoph's eagle eyes saved the day more than once, and both of them were instrumental and of great help in developing EOS.

Moreover, I am indebted to Martin Gorbahn for making possible two trips to Munich, in order to collaborate with Christoph. During these trips I benefited hugely from discussions with Frederik Beaujean, whose contributions to EOS I hold in high esteem.

As users of EOS, both Ulrik Egede and Hideki Miyake uncovered numerical problems which originally went by me. I am very grateful for their input and helpful questions.

To m'colleague Hollenberg. Working with you has always been both an interesting and an amusing experience. That was a good journey, thank you for your support!

I am very grateful to Arnd Behring, Christoph Bobeth, Christian Hambrock, Gudrun Hiller, m'coll Hollenberg, Martin Jung and Christian Wacker for careful reading of the manuscript and of course for their very helpful and plentiful comments.

List of Acronyms

BSM Beyond the Standard Model

CKM Cabibbo-Kobayashi-Maskawa

FCNC Flavor Changing Neutral Current

HQET Heavy Quark Effective Theory

LHC Large Hadron Collider, not to be confused with a Large Hardon Colluder

LCSR Light Cone Sum Rules

LQCD Lattice QCD

NP New Physics

OPE Operator Production Expansion

QCD Quantum Chromo Dynamics

QCDF QCD Factorization

SCET Soft Collinear Effective Theory

SM Standard Model

Bibliography

[1] Kobayashi M. and Maskawa T. *CP Violation in the Renormalizable Theory of Weak Interaction*. Prog.Theor.Phys. **49**, (1973), 652–657.

[2] Herb S., Hom D., Lederman L., Sens J., Snyder H. et al. *Observation of a Dimuon Resonance at 9.5-GeV in 400-GeV Proton-Nucleus Collisions*. Phys.Rev.Lett. **39**, (1977), 252–255.

[3] Abachi S. et al. [D0 Collaboration]. *Search for high mass top quark production in $p\bar{p}$ collisions at $\sqrt{s} = 1.8$ TeV*. Phys.Rev.Lett. **74**, (1995), 2422–2426. arXiv:hep-ex/9411001.

[4] Abe F. et al. [CDF Collaboration]. *Observation of top quark production in $\bar{p}p$ collisions*. Phys.Rev.Lett. **74**, (1995), 2626–2631. arXiv:hep-ex/9503002.

[5] Cleveland B., Daily T., Davis R., Distel J.R., Lande K. et al. *Measurement of the solar electron neutrino flux with the Homestake chlorine detector*. Astrophys.J. **496**, (1998), 505–526.

[6] Zwicky F. *Spectral displacement of extra galactic nebulae*. Helv.Phys.Acta **6**, (1933), 110–127.

[7] Abe K. et al. [BELLE Collaboration]. *Observation of the decay $B \to K\ell^+\ell^-$*. Phys.Rev.Lett. **88**, (2002), 021801. arXiv:hep-ex/0109026.

[8] Aubert B. et al. [BABAR Collaboration]. *Evidence for the rare decay $B \to K^*\ell^+\ell^-$ and measurement of the $B \to K\ell^+\ell^-$ branching fraction*. Phys.Rev.Lett. **91**, (2003), 221802. arXiv:hep-ex/0308042.

[9] Aaltonen T. et al. [CDF Collaboration]. *Search for the Rare Decays $B^+ \to \mu^+\mu^- K^+$, $B^0 \to \mu^+\mu^- K^{*0}(892)$, and $B_s^0 \to \mu^+\mu^-\phi$ at CDF*. Phys.Rev. **D79**, (2009), 011104. arXiv:0804.3908.

[10] Moll A. *Belle II/SuperKEKB status*. Talk given at the Lake Louise Winter Institute 2012 (19-25 February 2012, Lake Louise, Canada).

[11] Glashow S., Iliopoulos J. and Maiani L. *Weak Interactions with Lepton-Hadron Symmetry*. Phys.Rev. **D2**, (1970), 1285–1292.

[12] Muta T. *Foundations of quantum chromodynamics. Second edition*. World Sci.Lect.Notes Phys. **57**, (1998), 1–409.

[13] Anderson P.W. *Plasmons, Gauge Invariance, and Mass*. Phys.Rev. **130**, (1963), 439–442.

[14] Higgs P.W. *Broken Symmetries and the Masses of Gauge Bosons*. Phys.Rev.Lett. **13**, (1964), 508–509.

[15] Englert F. and Brout R. *Broken Symmetry and the Mass of Gauge Vector Mesons*. Phys.Rev.Lett. **13**, (1964), 321–323.

[16] Guralnik G., Hagen C. and Kibble T. *Global Conservation Laws and Massless Particles*. Phys.Rev.Lett. **13**, (1964), 585–587.

[17] Dombey N. *Abdus Salam: A Reappraisal. PART I. How to Win the Nobel Prize*. ArXiv e-prints arXiv:1109.1972.

[18] Aad G. et al. [ATLAS Collaboration]. *Combined search for the Standard Model Higgs boson using up to 4.9 fb-1 of pp collision data at sqrt(s) = 7 TeV with the ATLAS detector at the LHC*. Phys.Lett. **B710**, (2012), 49–66. arXiv:1202.1408.

[19] Chatrchyan S. et al. [CMS Collaboration]. *Combined results of searches for the standard model Higgs boson in pp collisions at sqrt(s) = 7 TeV*. arXiv:1202.1488.

[20] [TEVNPH (Tevatron New Phenomina and Higgs Working Group), CDF and D0 Collaboration]. *Combined CDF and D0 Search for Standard Model Higgs Boson Production with up to 10.0 fb-1 of Data*. Preliminary results prepared for the Winter 2012 Conferences, arXiv:1203.3774.

[21] Barate R. et al. [LEP Working Group for Higgs boson searches, ALEPH Collaboration, DELPHI Collaboration, L3 Collaboration, OPAL Collaboration]. *Search for the standard model Higgs boson at LEP*. Phys.Lett. **B565**, (2003), 61–75. arXiv:hep-ex/0306033.

[22] Nakamura K. et al. [Particle Data Group]. *Review of particle physics*. J.Phys.G **G37**, (2010), 075021.

[23] Perl M.L., Abrams G., Boyarski A., Breidenbach M., Briggs D. et al. *Evidence for Anomalous Lepton Production in e^+e^- Annihilation*. Phys.Rev.Lett. **35**, (1975), 1489–1492.

[24] Aarnio P. et al. [Delphi Collaboration]. *Measurement of the Mass and Width of the Z^0 Particle from Multi - Hadronic Final States Produced in e^+e^- Annihilations*. Phys.Lett. **B231**, (1989), 539.

[25] Lee T. and Yang C.N. *Question of Parity Conservation in Weak Interactions*. Phys.Rev. **104**, (1956), 254–258.

[26] Wu C., Ambler E., Hayward R., Hoppes D. and Hudson R. *Experimental Test Of Parity Conservation In Beta Decay*. Phys.Rev. **105**, (1957), 1413–1414.

[27] Wolfenstein L. *Parametrization of the Kobayashi-Maskawa Matrix*. Phys.Rev.Lett. **51**, (1983), 1945.

[28] Buchalla G., Buras A.J. and Lautenbacher M.E. *Weak decays beyond leading logarithms*. Rev.Mod.Phys. **68**, (1996), 1125–1144. arXiv:hep-ph/9512380.

[29] Aguilar-Saavedra J. *Top flavor-changing neutral interactions: Theoretical expectations and experimental detection*. Acta Phys.Polon. **B35**, (2004), 2695–2710. arXiv:hep-ph/0409342.

[30] Behring, Arnd. *From bottom to top: Bounds on top FCNCs from B mixing in the MSSM*. Diploma Thesis, Lehrstuhl für Theoretische Physik III, Fakultät Physik, Technische Universität Dortmund (2011).

[31] Leutwyler H. *On the foundations of chiral perturbation theory*. Annals Phys. **235**, (1994), 165–203. arXiv:hep-ph/9311274.

[32] Manohar A.V. and Wise M.B. *Heavy quark physics*. Camb.Monogr.Part.Phys. Nucl.Phys.Cosmol. **10**, (2000), 1–191.

[33] Bauer C.W., Fleming S. and Luke M.E. *Summing Sudakov logarithms in $B \to X_s\gamma$ in effective field theory*. Phys.Rev. **D63**, (2000), 014006. arXiv:hep-ph/0005275.

[34] Chetyrkin K.G., Misiak M. and Munz M. *Weak radiative B meson decay beyond leading logarithms*. Phys.Lett. **B400**, (1997), 206–219. arXiv:hep-ph/9612313.

[35] Bobeth C., Misiak M. and Urban J. *Photonic penguins at two loops and $m(t)$ dependence of BR[$B \to X(s)\ell^+\ell^-$]*. Nucl.Phys. **B574**, (2000), 291–330. arXiv:hep-ph/9910220.

[36] Kim C. and Yoshikawa T. *Systematic analysis of $B \to K\pi\ell^+\ell^-$ decay through angular decomposition* arXiv:0711.3880.

[37] Alok A.K., Datta A., Dighe A., Duraisamy M., Ghosh D. et al. *New Physics in $b \to s\mu^+\mu^-$: CP-Conserving Observables*. JHEP **1111**, (2011), 121. arXiv:1008.2367.

[38] Bobeth C., Hiller G. and Piranishvili G. *Angular distributions of $\bar{B} \to \bar{K}\ell^+\ell^-$ decays*. JHEP **0712**, (2007), 040. arXiv:0709.4174.

[39] Misiak M., Asatrian H., Bieri K., Czakon M., Czarnecki A. et al. *Estimate of $\mathcal{B}(\bar{B} \to X_s\gamma)$ at $\mathcal{O}(\alpha_s^2)$*. Phys.Rev.Lett. **98**, (2007), 022002. arXiv:hep-ph/0609232.

[40] Abe T. et al. [Belle II Collaboration]. *Belle II Technical Design Report* arXiv:1011.0352.

[41] Neri N. *The SuperB project: status and the physics reach*. J.Phys.Conf.Ser. **347**, (20I2), 012007.

[42] [LHCb Collaboration]. *Angular analysis of $B^0 \to K^{*0}\mu^+\mu^-$* LHCb-CONF-2011-038.

[43] Aaij R. et al. [LHCb Collaboration]. *Measurement of the CP-violating phase ϕ_s in the decay $B_s \to J/\psi\phi$*. Phys.Rev.Lett. **108**, (2012), 101803. arXiv:1112.3183.

[44] Bobeth C., Hiller G. and van Dyk D. *The Benefits of $\bar{B} \to \bar{K}^*\ell^+\ell^-$ Decays at Low Recoil*. JHEP **1007**, (2010), 098. arXiv:1006.5013.

[45] Bobeth C., Hiller G., van Dyk D. and Wacker C. *The Decay $\bar{B} \to \bar{K}\ell^+\ell^-$ at Low Hadronic Recoil and Model-Independent $\Delta B = 1$ Constraints*. JHEP **1201**, (2012), 107. arXiv:1111.2558.

[46] Wei J.T. et al. [BELLE Collaboration]. *Measurement of the Differential Branching Fraction and Forward-Backword Asymmetry for $B \to K^{(*)}\ell^+\ell^-$*. Phys.Rev.Lett. **103**, (2009), 171801. arXiv:0904.0770.

[47] Aaltonen T. et al. [CDF Collaboration]. *Measurement of the Forward-Backward Asymmetry in the $B \to K^{(*)}\mu^+\mu^-$ Decay and First Observation of the $B_s^0 \to \phi\mu^+\mu^-$ Decay*. Phys.Rev.Lett. **106**, (2011), 161801. arXiv:1101.1028.

[48] Khodjamirian A., Mannel T., Pivovarov A. and Wang Y.M. *Charm-loop effect in $B \to K^{(*)}\ell^+\ell^-$ and $B \to K^*\gamma$*. JHEP **1009**, (2010), 089. arXiv:1006.4945.

[49] Beneke M., Feldmann T. and Seidel D. *Systematic approach to exclusive $B \to V\ell + \ell-, V\gamma$ decays*. Nucl.Phys. **B612**, (2001), 25–58. arXiv:hep-ph/0106067.

[50] Beneke M., Buchalla G., Neubert M. and Sachrajda C.T. *QCD factorization for exclusive, nonleptonic B meson decays: General arguments and the case of heavy light final states*. Nucl.Phys. **B591**, (2000), 313–418. arXiv:hep-ph/0006124.

[51] Beneke M., Feldmann T. and Seidel D. *Exclusive radiative and electroweak $b \to d$ and $b \to s$ penguin decays at NLO*. Eur.Phys.J. **C41**, (2005), 173–188. arXiv:hep-ph/0412400.

[52] Feldmann T. and Matias J. *Forward backward and isospin asymmetry for $B \to K^*\ell^+\ell^-$ decay in the standard model and in supersymmetry*. JHEP **0301**, (2003), 074. arXiv:hep-ph/0212158.

[53] Asatryan H., Asatrian H., Greub C. and Walker M. *Two loop virtual corrections to $\bar{B} \to X_s\ell^+\ell^-$ in the standard model*. Phys.Lett. **B507**, (2001), 162–172. arXiv:hep-ph/0103087.

[54] Bobeth C., Hiller G. and Piranishvili G. *CP Asymmetries in $\bar{B} \to \bar{K}^*(\to \bar{K}\pi)\bar{\ell}\ell$ and Untagged $\bar{B}_s$, $B_s \to \phi(\to K^+K^-)\bar{\ell}\ell$ Decays at NLO*. JHEP **0807**, (2008), 106. arXiv:0805.2525.

[55] Grinstein B. and Pirjol D. *Exclusive rare $B \to K^*\ell^+\ell^-$ decays at low recoil: Controlling the long-distance effects*. Phys.Rev. **D70**, (2004), 114005. arXiv:hep-ph/0404250.

[56] Bobeth C., Hiller G. and van Dyk D. *Angular analysis of $B \to V(\to P_1P_2)\ell^+\ell^-$ decays*. J.Phys.Conf.Ser. **335**, (2011), 012038. arXiv:1105.2659.

[57] Kruger F. and Matias J. *Probing new physics via the transverse amplitudes of $B^0 \to K^{*0}(\to K^-\pi^+)\ell^+\ell^-$ at large recoil*. Phys.Rev. **D71**, (2005), 094009. arXiv:hep-ph/0502060.

[58] Reya E. *Perturbative Quantum Chromodynamics*. Phys.Rept. **69**, (1981), 195. Updated lectures.

[59] Beylich M., Buchalla G. and Feldmann T. *Theory of $\bar{B} \to \bar{K}^{(*)}\ell^+\ell^-$ decays at high q^2: OPE and quark-hadron duality*. Eur.Phys.J. **C71**, (2011), 1635. arXiv:1101.5118.

[60] Bobeth C., Hiller G. and van Dyk D. *More Benefits of Semileptonic Rare B Decays at Low Recoil: CP Violation*. JHEP **1107**, (2011), 067. arXiv:1105.0376.

[61] Blok B., Shifman M.A. and Zhang D.X. *An Illustrative example of how quark hadron duality might work*. Phys.Rev. **D57**, (1998), 2691–2700. arXiv:hep-ph/9709333.

[62] Ball P. and Zwicky R. *New results on $B \to \pi, K, \eta$ decay formfactors from light-cone sum rules*. Phys.Rev. **D71**, (2005), 014015. arXiv:hep-ph/0406232.

[63] Ball P. and Zwicky R. *$B_{d,s} \to \rho, \omega, K^*, \phi$ decay form-factors from light-cone sum rules revisited*. Phys.Rev. **D71**, (2005), 014029. arXiv:hep-ph/0412079.

[64] Charles J., Le Yaouanc A., Oliver L., Pene O. and Raynal J. *Heavy to light form-factors in the heavy mass to large energy limit of QCD*. Phys.Rev. **D60**, (1999), 014001. arXiv:hep-ph/9812358.

[65] Liu Z., Meinel S., Hart A., Horgan R.R., Muller E.H. et al. *A Lattice calculation of $B \to K^{(*)}$ form factors*. To appear in the proceedings of the 6th International Workshop on the CKM Unitarity Triangle: CKM 2010, arXiv:1101.2726.

[66] Hurth T. and Wyler D. *Theoretical Prospects for $b \to s\bar{\nu}\nu$ and $B \to K(\pi)\bar{\nu}\nu$ Decays*. In Hewett J.L., Hitlin D.G. (Eds.) *The Discovery potential of a Super B Factory*, arXiv:hep-ph/0503261.

[67] Bharucha A., Feldmann T. and Wick M. *Theoretical and Phenomenological Constraints on Form Factors for Radiative and Semi-Leptonic B-Meson Decays*. JHEP **1009**, (2010), 090. arXiv:1004.3249.

[68] Lu C.D. and Wang W. *Analysis of $B \to K_J^*(\to K\pi)\mu^+\mu^-$ in the higher kaon resonance region*. Phys.Rev. **D85**, (2012), 034014. arXiv:1111.1513.

[69] Altmannshofer W., Ball P., Bharucha A., Buras A.J., Straub D.M. et al. *Symmetries and Asymmetries of $B \to K^*\mu^+\mu^-$ Decays in the Standard Model and Beyond*. JHEP **0901**, (2009), 019. arXiv:0811.1214.

[70] Bobeth C., Hiller G. and van Dyk D. *General Analysis and Optimal Observables in $\bar{B} \to \bar{K}^*(\to \bar{K}\pi)\ell^+\ell^-$ at Low Recoil*. To appear.

[71] Egede U., Hurth T., Matias J., Ramon M. and Reece W. *New physics reach of the decay mode $\bar{B} \to \bar{K}^{*0}\ell^+\ell^-$*. JHEP **1010**, (2010), 056. arXiv:1005.0571.

[72] Aubert B. et al. [BABAR Collaboration]. *Angular Distributions in the Decays $B \to K^*\ell^+\ell^-$*. Phys.Rev. **D79**, (2009), 031102. arXiv:0804.4412.

[73] Hambrock C. and Hiller G. *Extracting $B \to K^*$ Form Factors from Data* arXiv:1204.4444.

[74] Beaujean F., Bobeth C., van Dyk D. and Wacker C. *Bayesian Fit of Exclusive $b \to s\bar{\ell}\ell$ Decays: The Standard Model Operator Basis* arXiv:1205.1838.

[75] Kruger F. and Sehgal L. *Lepton polarization in the decays $B \to X_s\mu^+\mu^-$ and $B \to X_s\tau^+\tau^-$*. Phys.Lett. **B380**, (1996), 199–204. arXiv:hep-ph/9603237.

[76] Ligeti Z. and Wise M.B. *$|V_{ub}|$ from exclusive B and D decays*. Phys.Rev. **D53**, (1996), 4937–4945. arXiv:hep-ph/9512225.

[77] Fleischer R. and Dunietz I. *CP violation and CKM phases from angular distributions for B_s decays into admixtures of CP eigenstates*. Phys.Rev. **D55**, (1997), 259–267. arXiv:hep-ph/9605220.

[78] Barberio E. et al. [Heavy Flavor Averaging Group]. *Averages of $b-$hadron and $c-$hadron Properties at the End of 2007* arXiv:0808.1297.

[79] Kruger F., Sehgal L.M., Sinha N. and Sinha R. *Angular distribution and CP asymmetries in the decays $\bar{B} \to K^-\pi^+e^-e^+$ and $\bar{B} \to \pi^-\pi^+e^-e^+$*. Phys.Rev. **D61**, (2000), 114028. arXiv:hep-ph/9907386.

[80] Altmannshofer W., Paradisi P. and Straub D.M. *Model-Independent Constraints on New Physics in $b \to s$ Transitions*. JHEP **1204**, (2012), 008. arXiv:1111.1257.

[81] Descotes-Genon S., Ghosh D., Matias J. and Ramon M. *Exploring New Physics in the $C_7 - C_7'$ plane*. JHEP **1106**, (2011), 099. arXiv:1104.3342.

[82] Hernando Morata J.. *Rare decays in LHCb* Talk given at the 47th Rencontres de Moriond: Electroweak Interactions and Unified Theories 2012, (La Thuile), March 4th-10th, 2011.

[83] Demir D.A., Olive K.A. and Voloshin M. *The Forward backward asymmetry of $B \to (\pi, K)\ell^+\ell^-$: Supersymmetry at work*. Phys.Rev. **D66**, (2002), 034015. arXiv:hep-ph/0204119.

[84] Skands P.Z. *Branching ratios for $B_{d,s} \to J/\psi\eta$ and $B_{d,s} \to \eta\ell^+\ell^-$, extracting gamma from $B_{d,s} \to J/\psi\eta$, and possibilities for constraining C_{10A} in semileptonic B decays*. JHEP **0101**, (2001), 008. Erratum added online, Feb/14/2003, arXiv:hep-ph/0010115.

[85] Ali A., Ball P., Handoko L. and Hiller G. *A Comparative study of the decays $B \to (K, K^*)\ell^+\ell^-$ in standard model and supersymmetric theories*. Phys.Rev. **D61**, (2000), 074024. arXiv:hep-ph/9910221.

[86] Bobeth C., Ewerth T., Kruger F. and Urban J. *Analysis of neutral Higgs boson contributions to the decays $\bar{B}_s \to \ell^+\ell^-$ and $\bar{B} \to K\ell^+\ell^-$*. Phys.Rev. **D64**, (2001), 074014. arXiv:hep-ph/0104284.

[87] Charles J. et al. [CKMfitter Group]. *CP violation and the CKM matrix: Assessing the impact of the asymmetric B factories*. Eur.Phys.J. **C41**, (2005), 1–131. We use the numerical results as presented at ICHEP10, arXiv:hep-ph/0406184.

[88] Group T.E.W. [For the CDF and D0 Collaboration]. *Combination of CDF and D0 Results on the Mass of the Top Quark* arXiv:0903.2503.

[89] [EOS Collaboration]. *EOS: A HEP Program for Flavor Observables*. Available from `http://project.het.physik.tu-dortmund.de/eos`.

[90] Simone J. et al. [Fermilab Lattice and MILC Collaborations]. *The decay constants f(D/s), f(D+), f(B/s) and f(B) from lattice QCD*. PoS **LATTICE2010**, (2010), 317.

[91] [LHCb Collaboration]. *Differential branching fraction and angular analysis of the $B^0 \to K^{*0}\mu^+\mu^-$ decay* LHCb-CONF-2012-008, linked to LHCb-ANA-2011-089.

[92] Huber T., Lunghi E., Misiak M. and Wyler D. *Electromagnetic logarithms in $\bar{B} \to X_s\ell^+\ell^-$*. Nucl.Phys. **B740**, (2006), 105–137. arXiv:hep-ph/0512066.

[93] Walsh J. *Rare B and D Decays at BaBar*. Talk given at the 46th Rencontres de Moriond: Electroweak Interactions and Unified Theories 2011, (La Thuile), March 13th-20th, 2011.

[94] Aaltonen T. et al. [CDF Collaboration]. *Observation of the Baryonic Flavor-Changing Neutral Current Decay $\Lambda_b \to \Lambda\mu^+\mu^-$*. Phys.Rev.Lett. **107**, (2011), 201802. arXiv:1107.3753.

[95] Wacker, Christian. *Analysis of $B \to K\ell^+\ell^-$ at Low Hadronic Recoil*. Diploma Thesis, Lehrstuhl für Theoretische Physik III, Fakultät Physik, Technische Universität Dortmund (2011).

[96] Aubert B. et al. [BABAR Collaboration]. *Measurement of the $B \to X_s\ell^+\ell^-$ branching fraction with a sum over exclusive modes*. Phys.Rev.Lett. **93**, (2004), 081802. arXiv:hep-ex/0404006.

[97] Iwasaki M. et al. [Belle Collaboration]. *Improved measurement of the electroweak penguin process $B \to X_s\ell^+\ell^-$*. Phys.Rev. **D72**, (2005), 092005. arXiv:hep-ex/0503044.

[98] Hocker A., Lacker H., Laplace S. and Le Diberder F. *A New approach to a global fit of the CKM matrix*. Eur.Phys.J. **C21**, (2001), 225–259. arXiv:hep-ph/0104062.

[99] Hiller G. *The Pheno-analysis of $B \to K^{(*)}\mu^+\mu^-$ decays in 2011 plus* arXiv:1106.1547.

[100] Faessler A., Gutsche T., Ivanov M., Korner J. and Lyubovitskij V.E. *The Exclusive rare decays $B \to K(K^*)\,\bar{\ell}\ell$ and $B_c \to D(D^*)\,\bar{\ell}\ell$ in a relativistic quark model*. Eur.Phys.J.direct **C4**, (2002), 18. arXiv:hep-ph/0205287.

[101] Becirevic D., Lubicz V. and Mescia F. *An Estimate of the $B \to K^*\gamma$ form factor*. Nucl.Phys. **B769**, (2007), 31–43. arXiv:hep-ph/0611295.

[102] Liu Z., Meinel S., Hart A., Horgan R.R., Muller E.H. et al. *Form factors for rare B decays: Strategy, methodology, and numerical study*. PoS **LAT2009**, (2009), 242. arXiv:0911.2370.

[103] Burdman G. and Hiller G. *Semileptonic form-factors from $B \to K^*\gamma$ decays in the large energy limit*. Phys.Rev. **D63**, (2001), 113008. arXiv:hep-ph/0011266.

[104] Bourrely C., Caprini I. and Lellouch L. *Model-independent description of $B \to \pi\ell\nu$ decays and a determination of $|V_{ub}|$*. Phys.Rev. **D79**, (2009), 013008. arXiv:0807.2722.